

APPENDIX A

YANKEE NUCLEAR POWER STATION

INCORE DETECTION SYSTEM ANALYSIS

MARCH 1988

8804140031 880404
PDR ADOCK 05000029
P DCD

TABLE OF CONTENTS

	<u>Page</u>
1.0 INTRODUCTION/PURPOSE.....	A-1
2.0 STATUS OF CURRENT SYSTEM.....	A-3
3.0 FIXED DETECTORS - GENERAL DATA.....	A-9
4.0 CALIBRATION/NORMALIZATION OF FIXED DETECTOR DATA.....	A-14
5.0 STEADY-STATE POWER DISTRIBUTIONS.....	A-20
6.0 DETECTION OF POWER DISTRIBUTION ANOMALIES.....	A-88
7.0 DETERMINATION OF CONTROL ROD POSITIONING.....	A-90
8.0 INCORE DETECTION SYSTEM MEASUREMENT UNCERTAINTIES.....	A-94
9.0 FIXED DETECTOR OPERABILITY.....	A-95
10.0 CONCLUSIONS.....	A-101
11.0 REFERENCES.....	A-102

1.0 INTRODUCTION/PURPOSE

The Incore Detection System provides information on the neutron flux distribution at selected reactor core locations. The information obtained with the Incore Detection System, in conjunction with previously determined analytical data, can be used to determine the three-dimensional fission power distribution in the core at any time throughout the operating cycle. Once the fission power distribution has been established, the maximum power output can be determined, and confirmation of reactor core design parameters and calculated hot channel factors can be made.

The Incore Detection System for the Yankee plant provides three basic functions. The primary function is to provide the three-dimensional neutron flux and power distributions which are used to monitor the power peaking and hot channel factors versus established limits. Verification of the analytical core parameters assumed in the safety analyses is made as well. Comparisons of measured peaking factors, such as peak linear heat generation rate, F_q and $F_{\Delta H}$, to established limits are generally made via monthly surveillances utilizing the Incore Detection System. The secondary functions of the Incore Detection System are to detect anomalies in the core usually during core startup due to possible misloaded fuel assemblies or quadrant asymmetries and to aid in the determination of control rod positioning during loss of primary control rod position indications.

The purpose of this analysis is to show that the Incore Detection System with a combination of both movable U-235 fission chambers and fixed, self-powered, rhodium detectors can be used to accurately predict the core power distribution parameters with a monitoring capability which has increased measurement observability and consequently less measurement uncertainty. In addition, this combination system provides greater core coverage for detection of possible core anomalies and control rod malfunctions. The Fixed Incore Detector System (FIDS) can provide equivalent movable trace data which can be combined via analytical calibration to form one cohesive system with better monitoring capabilities than the Movable Incore Detection System (MIDS) alone. The fixed detectors, therefore, will be viable replacements for failed

movable detector paths and will help provide the greatest possible core coverage and system monitoring capabilities.

2.0 STATUS OF CURRENT SYSTEM

The original MIDS installed in the Yankee core in 1974 had provisions for monitoring 22 reactor core locations as shown in Figure 2-1. Since that time, there have been numerous thimble failures and subsequent attempts to repair inoperable thimbles. The thimble failures have led to various Technical Specification changes (References 1, 2, 3) regarding the operability of the Incore Detection System and application of uncertainties to the measured data. A number of these changes were made as contingencies to possible future thimble failures but were never exercised. Presently, provision (Reference 4) has been made for the current operating cycle, Cycle 19, to accommodate up to four additional thimble failures before operability requirements could not be met. During Cycle 18, 13 thimbles were available for access by the movable fission chambers as shown in Figure 2-2. After Cycle 19 startup, another thimble was declared inoperable due to restrictions in the thimble itself which would not permit a movable detector to be fully inserted into the reactor core. Therefore, there are 12 thimbles presently operable for meeting the operability requirement of the MIDS.

The FIDS installed in 1987 during the Cycle 18-19 refueling outage was originally scheduled to contain eight fixed detector strings in the core locations shown in Figure 2-3. However, two thimble locations, No. 9 and No. 15, had damaged tubes which would not allow insertion of the fixed strings; therefore, only six fixed strings were installed. Also, during plant heatup, three of the six fixed detector thimble locations were identified to be leaking a small amount of primary reactor coolant. Yankee plans to remove one of the fixed detector strings from a leaking thimble location for mechanical analysis during the next refueling outage and will attempt to replace it with one of the detectors originally scheduled to go into one of the damaged thimble locations. Therefore, Cycle 20 will have either five or six fixed detector strings for use in core monitoring. Once the mechanical analysis of the removed detector string is complete, Yankee plans to continue to install fixed detector strings in all the available locations during future refueling outages.

The analysis in this submittal is based on 12 movable detector locations and six fixed detector locations. This is the number of available locations expected for the remainder of Cycle 19 and during Cycle 20, the next operating cycle. These locations are shown in Figure 2-4.

FIGURE 2-1

INCORE INSTRUMENTATION LOCATIONS
AS ORIGINALLY INSTALLED

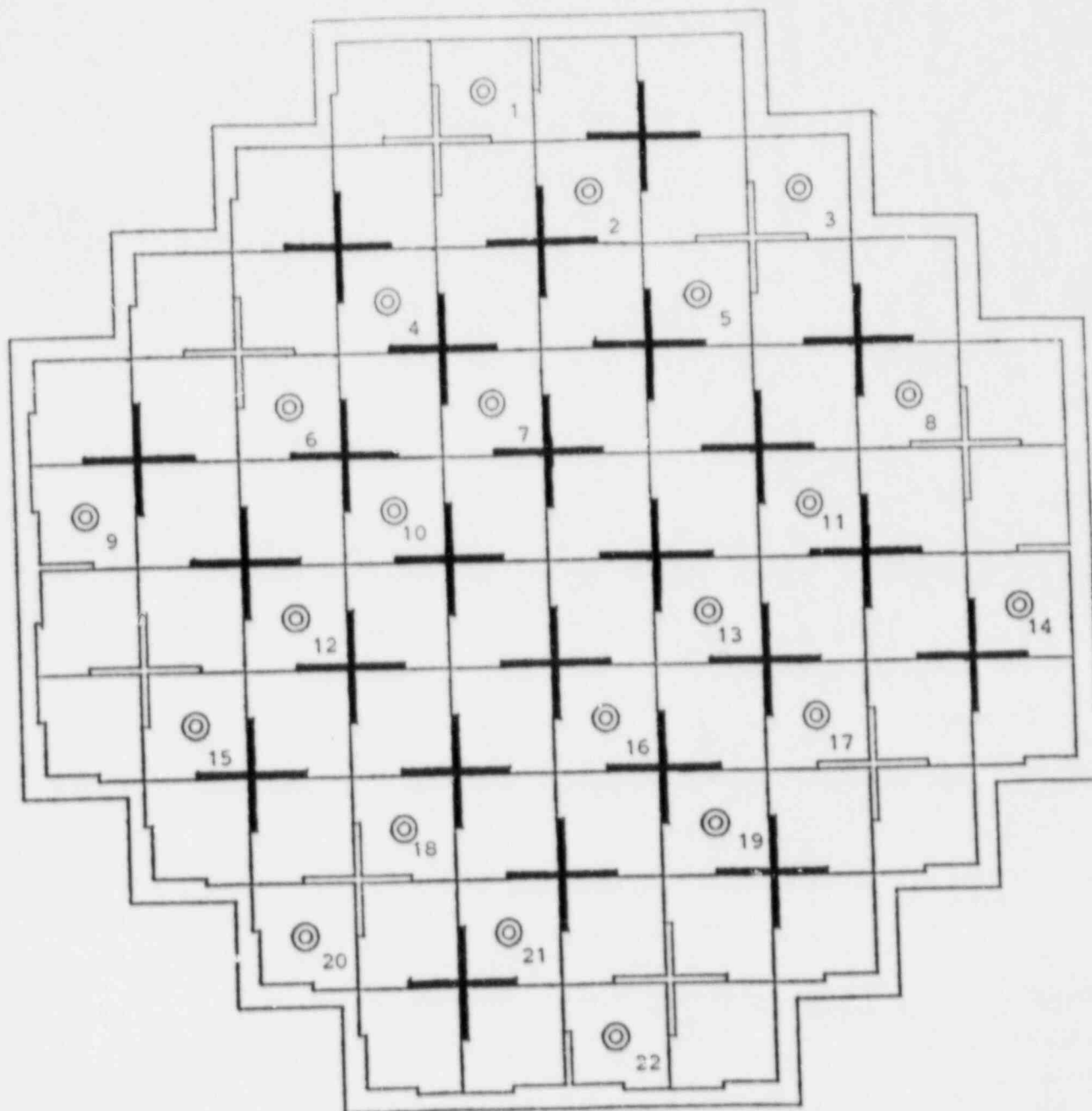


FIGURE 2-2

MOVABLE PATHS AVAILABLE
DURING CYCLE 18-19 REFUELING

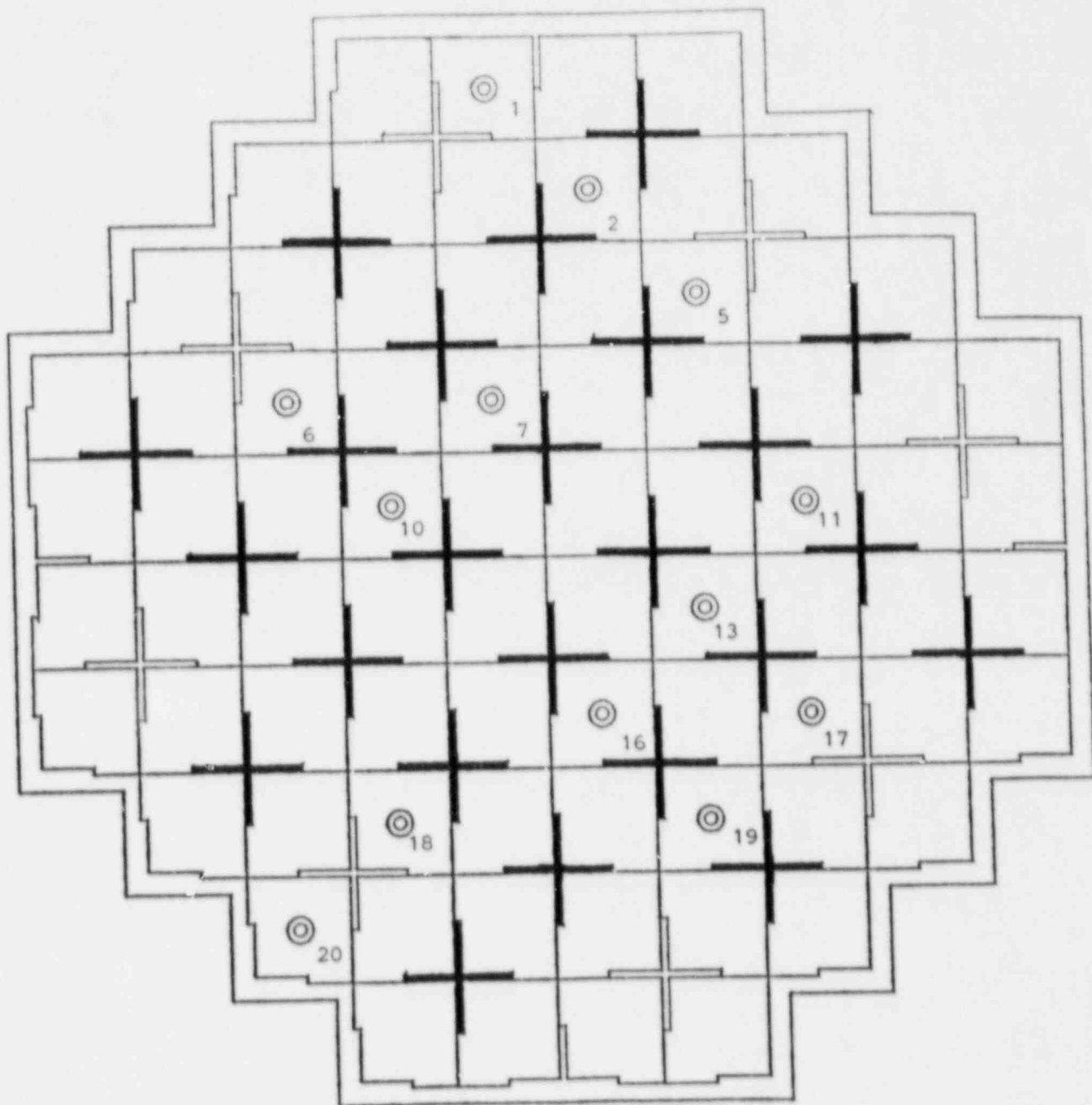


FIGURE 2-3

PROPOSED LOCATIONS OF
FIXED DETECTOR STRINGS

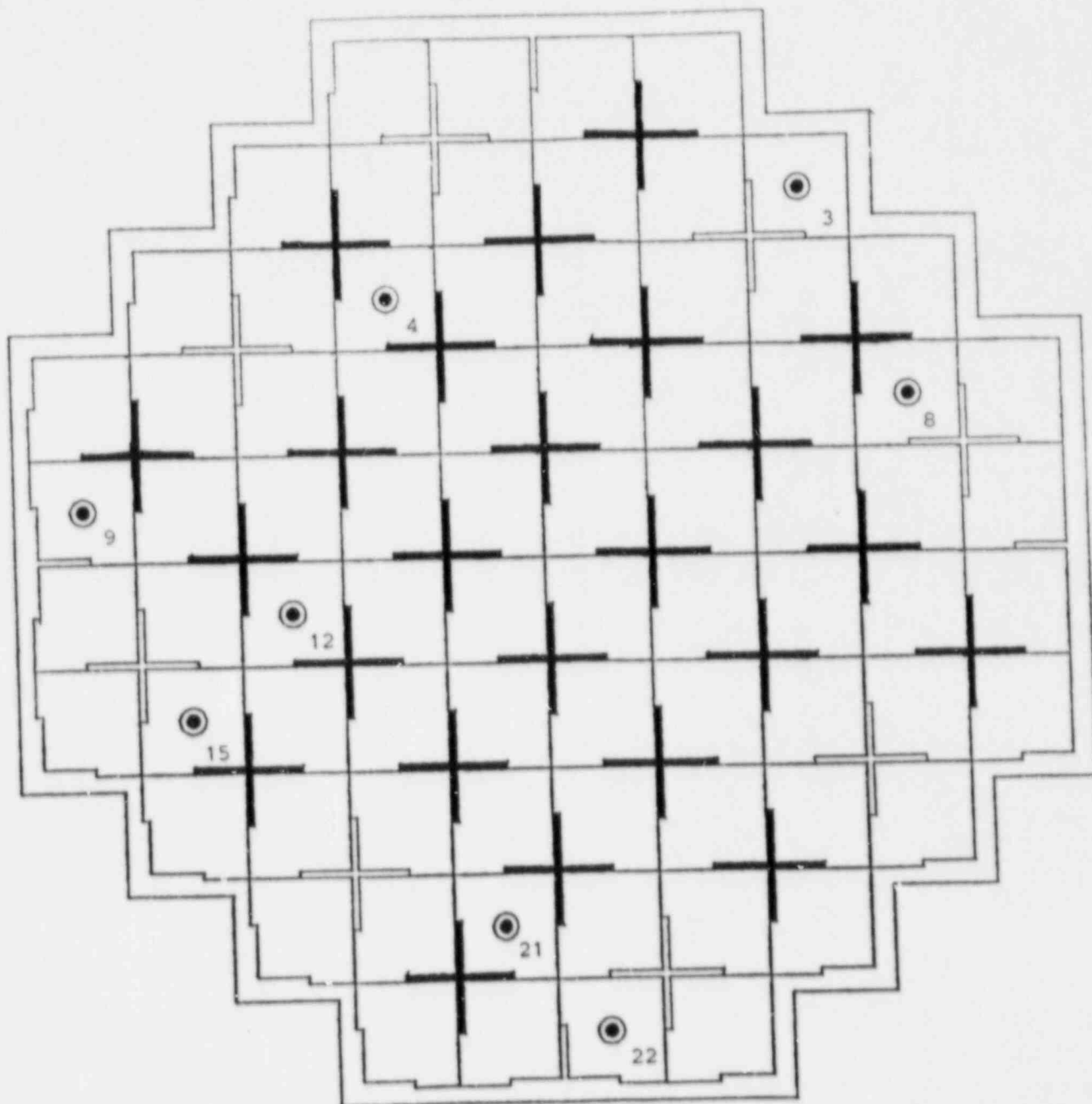
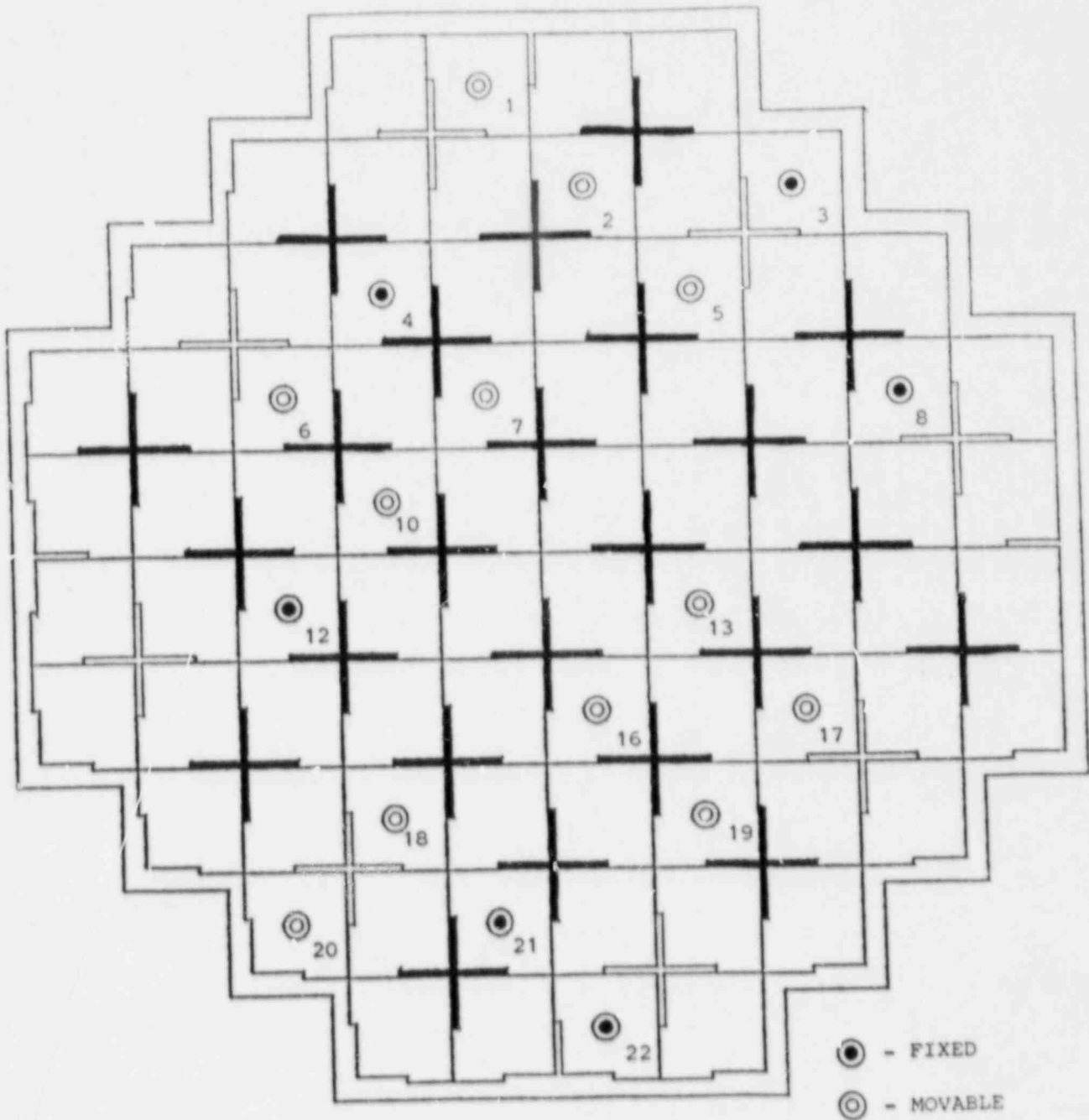


FIGURE 2-4

CURRENT LOCATIONS AVAILABLE
COMBINATION INCORE DETECTION SYSTEM



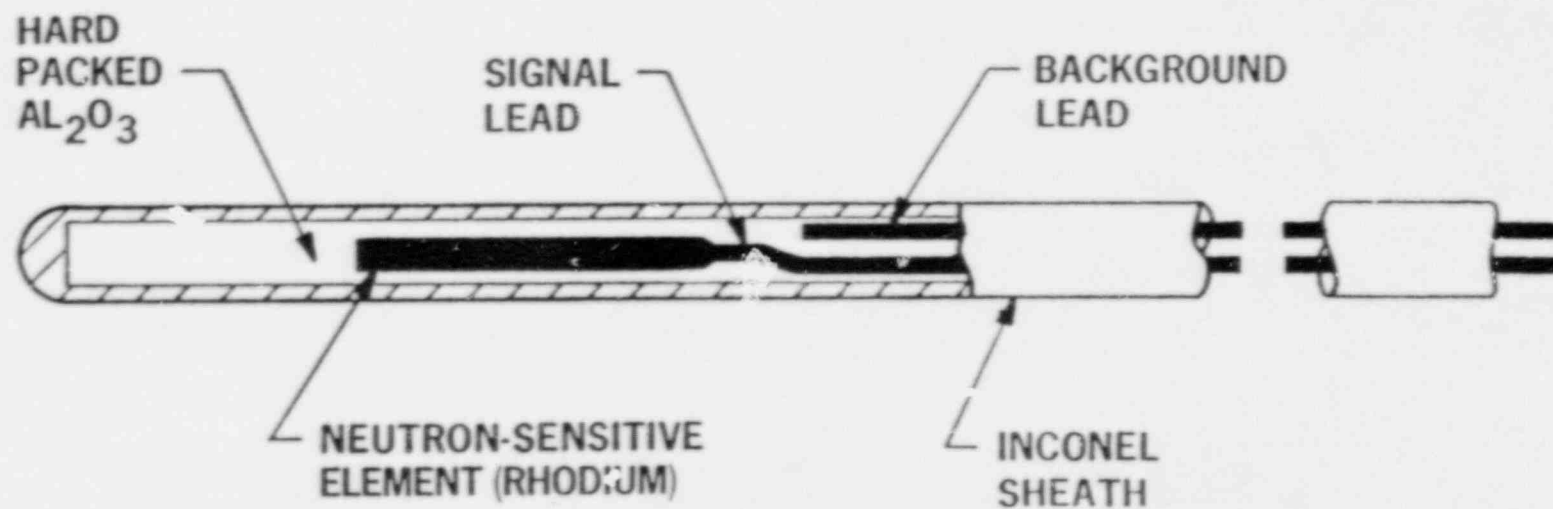
3.0 FIXED INCORE DETECTOR SYSTEM - GENERAL DATA

The Yankee plant FIDS consists of six strings each containing five self-powered rhodium neutron detectors manufactured by Babcock & Wilcox (B&W) and a Data Acquisition System (DAS). The detectors contain twin-leads which allow background-created signals to be subtracted from the raw rhodium detector signals. The Yankee design is .054" in diameter and consists of 10" rhodium emitters hard packed in a ceramic insulator of AL_2O_3 as shown in Figure 3-1 and cross-sectionally in Figure 3-2. The strings are designed so that the detectors are positioned axially 18.3" center-to-center as shown in Figure 3-3. The rhodium emitter absorbs thermal neutrons and, after a half-life of about 45 seconds, decays to palladium with the emission of a negatively-charged beta particle. As these beta particles leave the rhodium emitter, a small electrical current flows in the lead wire connected to the emitter. This current is proportional to the neutron flux present at the detector location.

The DAS is designed to collect, store, and process data from the fixed incore detectors. The DAS obtains signals once every five seconds from the fixed detectors and stores them in a file containing 24 hours worth of the latest five-second readings. In addition, files containing an 18-minute average, six-minute snapshots, and 12 effective full-power hours worth of data are stored by the DAS. The DAS updates the expended charges of each detector every 18 minutes and will recover expended charges and other integrated data from history files following a computer failure. The DAS software, supplied by B&W, identifies inoperable detectors, corrects the signals for depletion and sensitivity of the detectors, and will substitute for "failed" detector signals. Statistics on detector stability are calculated and stored by the DAS as well. The DAS software also provides an estimate of the total core power level based on input signal to power conversion factors.

Post-processing of the DAS data files is performed by Yankee's Nuclear Services Division in Framingham. The fixed detector data files are post-processed by spline fitting the five detector points plus two extrapolation points, normalizing the integrated curves to the movable

detectors, converting the curve to 46 axial points similar to the movable traces, and providing output in a format compatible for use in the INCORE (Reference 5) data analysis code. The INCORE code then determines the full core power distribution as it did before with only the movable data.



A-11

FIGURE 3-1

Twin-Leadwire Self-Powered Neutron Detector

Cross-Section of Yankee-Rowe Fixed Detector Assembly

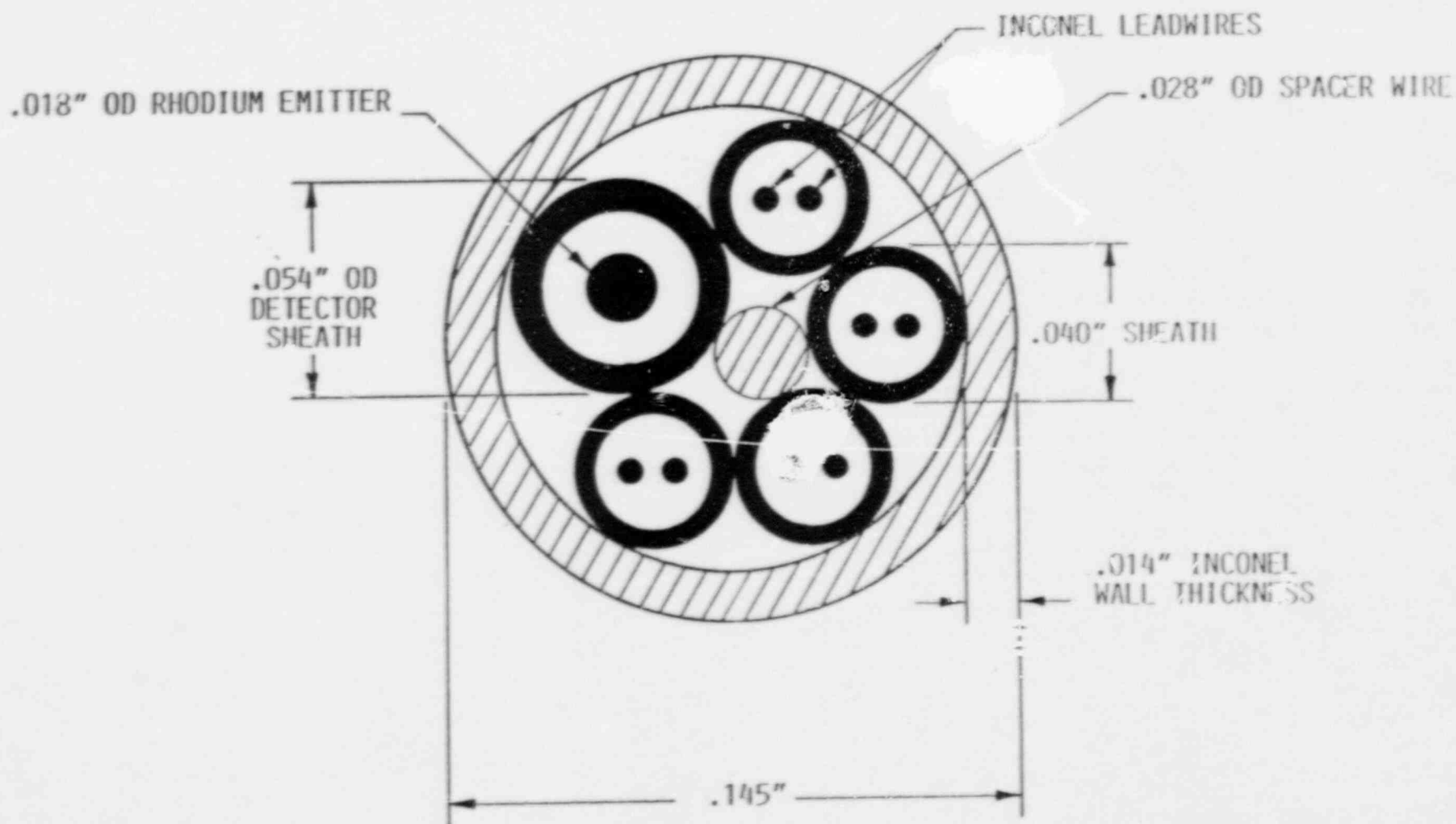
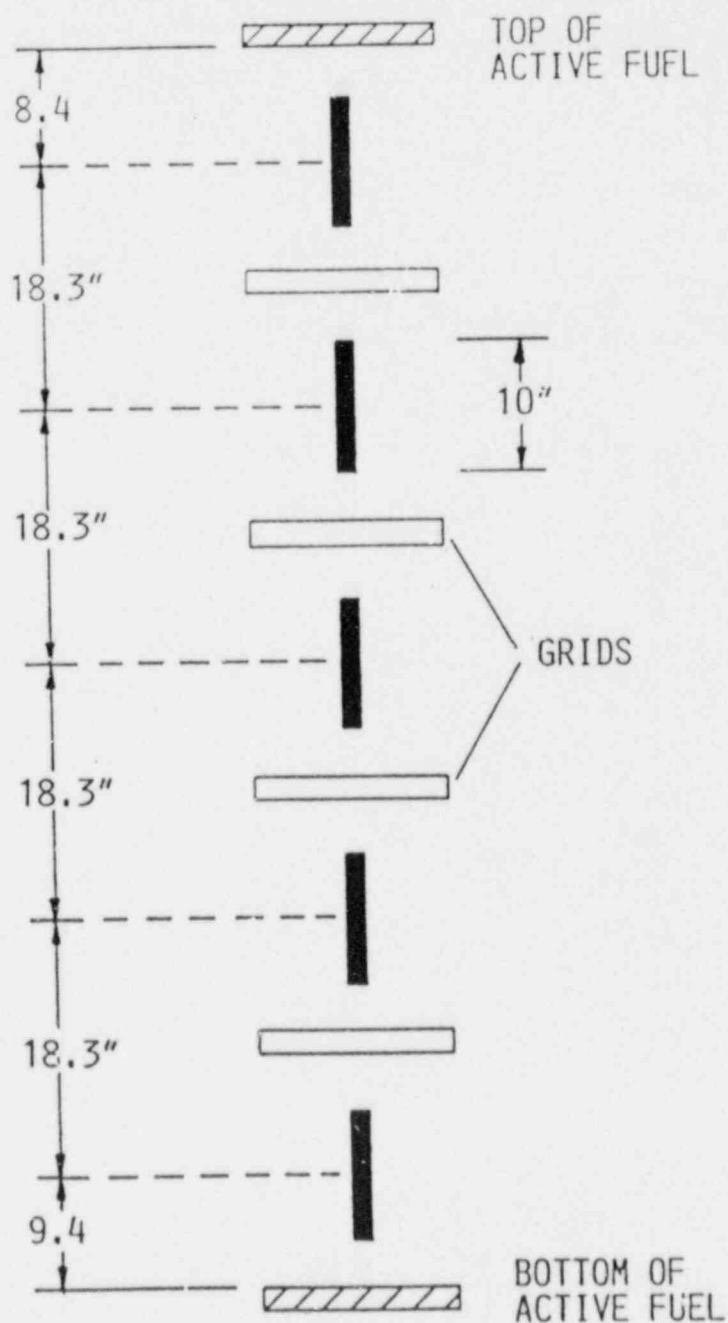


FIGURE 3-3

Position of Emitters Relative to Fuel Height



4.0 CALIBRATION/NORMALIZATION OF FIXED DETECTOR DATA

The sensitivity of the rhodium emitter in the fixed detectors to neutrons is a function of its geometry. Even though the emitter mass is the same for all rhodium detectors in the core, the relative sensitivity of the detectors will vary as a function of the emitter surface area. The neutron sensitivity of a given rhodium detector to a reference detector can be determined either by direct calibration in a known neutron flux or by accurately measuring the mass and length of the emitter and using an analytical formula to determine sensitivity. Babcock and Wilcox has shown (Reference 6) that the calculational method yields the same calibration results as the measured method, with a high degree of accuracy.

The sensitivity calibration of the fixed detectors used in the Yankee core is performed analytically based on the as-built lengths of the rhodium emitters. The neutron sensitivity of the rhodium detectors is proportional to the surface area of the emitter. Babcock and Wilcox manufactures the detector emitters with constant mass; therefore, the emitter surface area is directly proportional to the square root of the emitter length. The as-built emitter lengths supplied by the manufacturer can be measured quite accurately and is used as input in the DAS software.

The movable detectors are calibrated by insertion of the movable detectors into one or more common (calibration) thimbles. In the Yankee MIDS, two detectors are usually employed for power distribution mapping, and both detectors are inserted into two independent calibration paths. There are also situations where only one detector may be used for incore mapping, therefore, no movable detector calibration is needed. For Cycle 19 operation, the mappings to date have included both double and single detector mappings. As will be shown, provision has been made for both situations when used in combination with the fixed detector data.

Our analysis has shown that the fixed detector signals can be combined with the movable detector signals by using a single normalization factor for all fixed detector signals. For this combined system of fixed and movable

signals, normalization of the fixed signals was performed through comparisons with the movable data. The axial positions of the fixed strings in the core and extrapolation points were determined via comparison to symmetric movable traces. Radial normalization of the fixed data to the integrated movable flux traces was then performed empirically based on comparison of the measured-to-predicted reaction rates. Finally, a procedure was established to accommodate changes in the movable detector calibration that occurs in the monthly mapping surveillances.

The first step in the normalization process involved the determination of the axial shapes obtained from the fixed detectors. Axial positioning of the fixed strings in the core was originally designed as shown in Figure 3-3. However, actual positioning of the fixed strings in the various thimbles changed due to variances in the thimble tube lengths and axial positioning measurements. Prior to installation, eddy current techniques were used to determine reference core axial thimble positions in order to position the fixed strings. These fixed axial positions were used as the initial locations in the analytical processing of the fixed data. Fine tuning of these locations was subsequently made based on comparisons to the detailed movable symmetric traces. Once these positioning adjustments were made, extrapolation distances for the spline fitting routines were determined based on symmetric movable traces, and resulted in extrapolation distances of ± 8.65 ". These extrapolation distances have remained constant based on comparison to the mappings made to date in Cycle 19 and are expected to remain constant throughout the cycle based on discussions with Babcock and Wilcox on their experiences with fixed detector curve fitting techniques.

The normalization of the radial component of the fixed data was also determined using the movable trace data. There is no common thimble path which accommodates both a fixed and movable detector for cross-calibration analogous to the movable system. Adjustment of the fixed detector measured reaction rate integrals was based on a single empirical normalization factor to a reference movable detector. This factor was derived through the preservation of the movable reaction rate comparisons between the predicted and measured data. The movable signals are never adjusted in this process.

One constant factor was used for all fixed detector integrals throughout the present cycle, since the signals from the fixed detectors have been depletion corrected and represent fresh detector signals. The movable signals also represent fresh detector signals since depletion of the U-235 in the fission chambers is negligible.

A study was performed which evaluated the relationship between the movable and fixed signal responses as a function of assembly burnup. Using CASMO-3 (Reference 7), a transport theory assembly fuel depletion code, both detector types were modelled in the present Yankee assembly design. This design is a 3.8 w/o assembly manufactured by Combustion Engineering. For the fixed and movable detector types, the rhodium emitter and U-235 in the fission chamber were each modelled as unique regions within the instrument thimble. The fuel assemblies were depleted 50,000 MWd/Mtu, well past the expected burnup in Yankee discharge assemblies. The rhodium and U-235 number densities in the detector regions were held constant to simulate fresh detectors. From each CASMO-3 depletion, Y-factors were extracted and compared. The Y-factors are defined as follows:

$$Y_{\text{Fixed}} = \frac{\text{Fission Rate in Fuel}}{\text{Rh Absorption Rate}} = \frac{\Sigma_f \phi_{\text{fuel}}}{\Sigma_a^{\text{Rh}} \phi_{\text{Rh}}}$$

$$Y_{\text{Movable}} = \frac{\text{Fission Rate in Fuel}}{\text{U-235 Fission Rate}} = \frac{\Sigma_f \phi_{\text{fuel}}}{\Sigma_f^{\text{U-235}} \phi_{\text{U-235}}}$$

The Y-factor represents the relationship between the assembly power and the signal response of the fixed or movable detectors. These factors as a function of assembly burnup are shown for each detector in Figure 4-1. As can be seen, both curves follow similar trends and differ only by a proportionality constant. When the U-235 fission detector data is multiplied by a constant, as shown in Figure 4-2, the two curves compare remarkably well, implying no inconsistency in detector signal response as the flux spectrum changes in the assembly due to burnup. This is consistent with the data from

the two detector types seen to date. There has been no observed bias between the fixed signals located in the fresh assemblies with burnups ranging from 0 to 10,000 Mwd/Mtu versus the recycled fuel assemblies with burnups ranging from 15,000 to 25,000 Mwd/Mtu. Based on this study and observed data from Cycle 19, the one-factor normalization approach seems to be justified and should remain applicable for the remainder of the Yankee fuel cycle.

A procedure for normalization of the fixed detector data to equivalent movable data has been established. One movable map is needed to determine the constant of proportionality for a given fission chamber response. Thereafter, calibration of the fixed data is based on the initial normalization factor and the calibration factor calculated by the INCORE data analysis code for the two-detector Movable System. If a new detector is installed, once again, one movable map with that detector is needed to establish the normalization factor. The data presented in the following section is based on three different conditions: having two detectors initially, having only one detector when a detector failure occurred, and having a new detector as a replacement for a failed detector. The analysis shows that with our established calibration procedure, any combination of movable detector availability can be accommodated.

YANKEE NUCLEAR POWER STATION
COMPARISON OF Y-FACTORS FOR
FIXED RHODIUM EMITTER AND MOVABLE U-235 FISSION DETECTORS

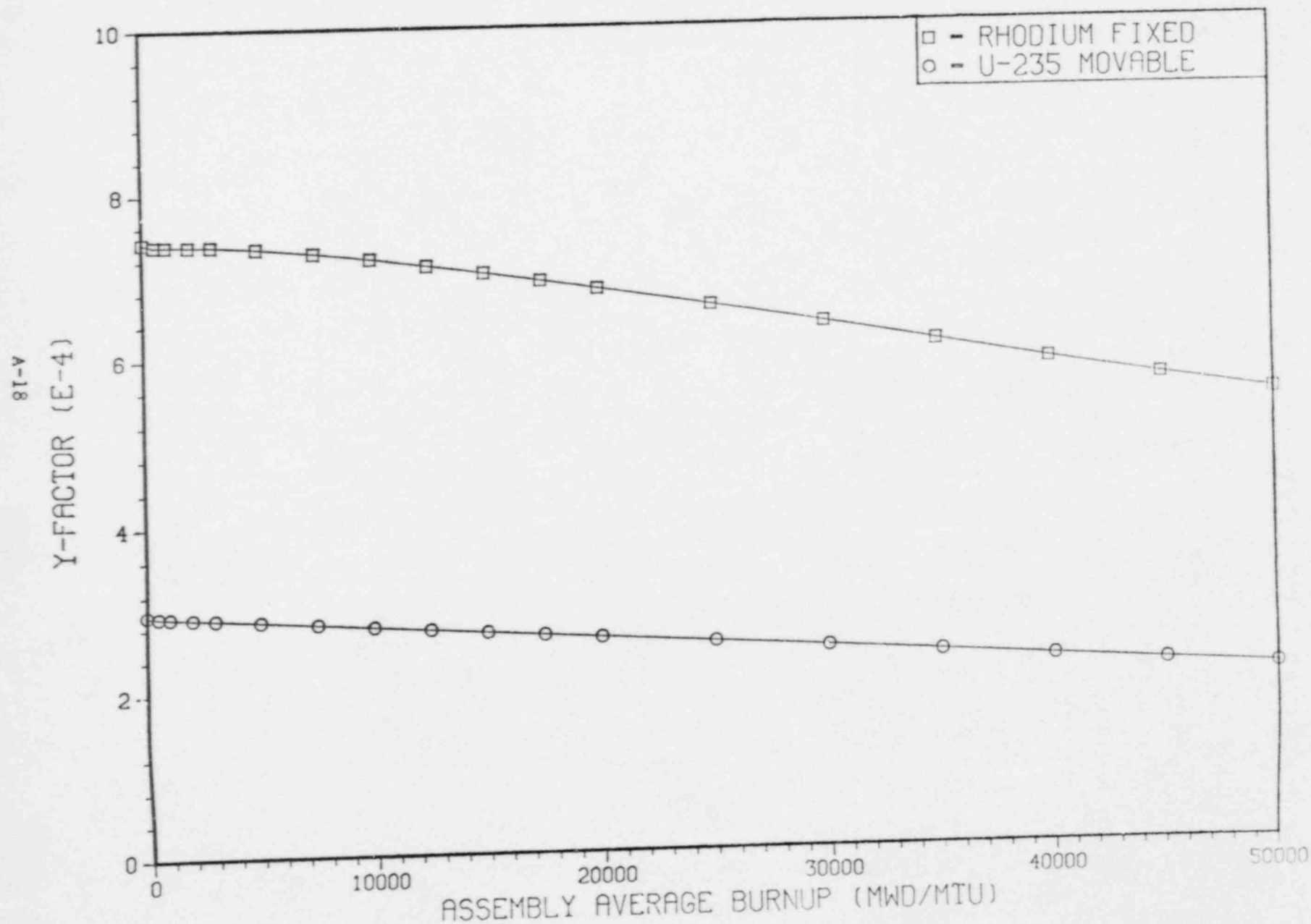


FIGURE 4-1

YANKEE NUCLEAR POWER STATION
COMPARISON OF NORMALIZED Y-FACTORS FOR
FIXED RHODIUM EMITTER AND U-235 FISSION DETECTORS

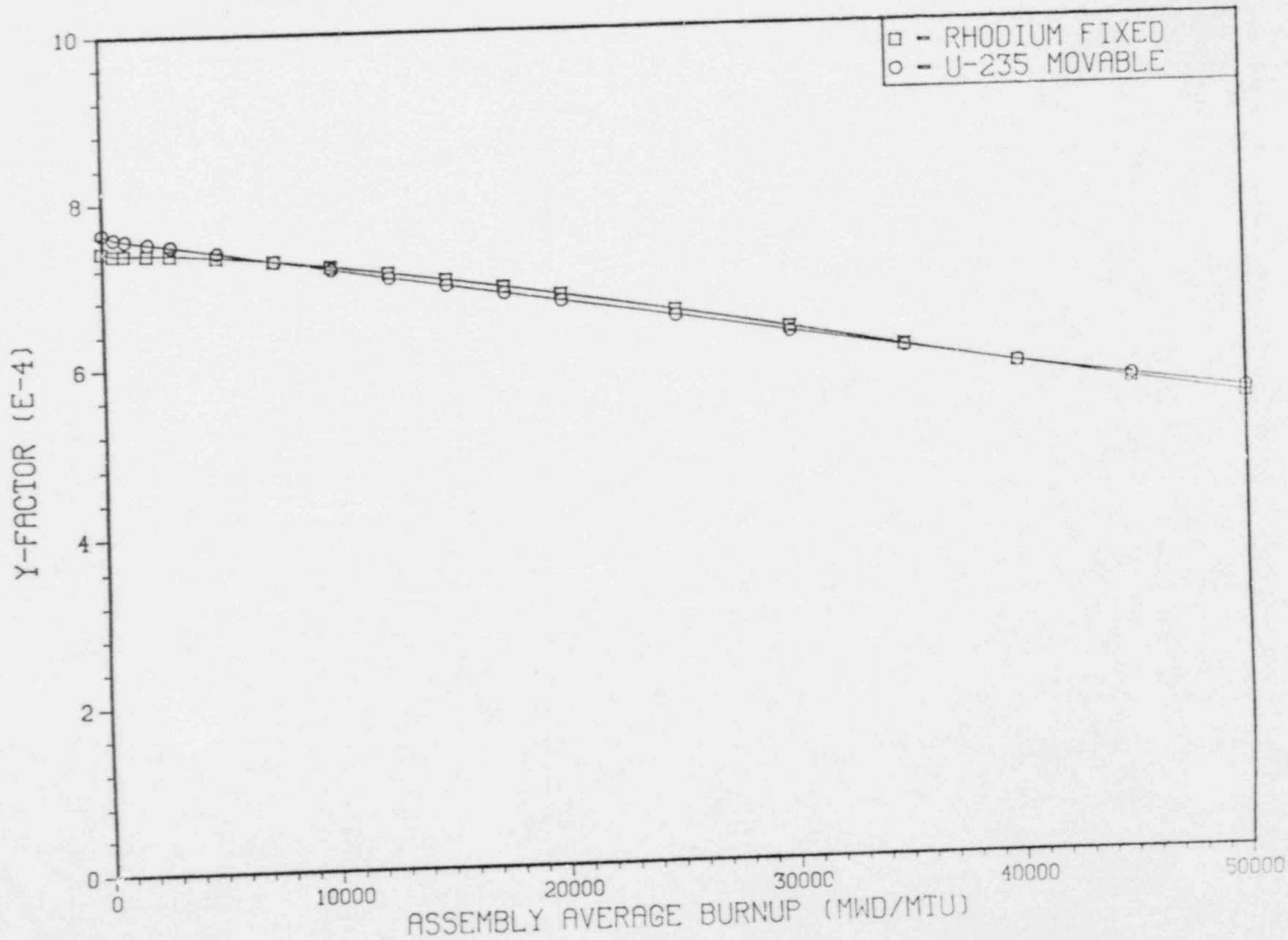


FIGURE 4-2

5.0 STEADY-STATE POWER DISTRIBUTIONS

The primary function of the Incore Detection System is to measure the three-dimensional neutron flux distribution in the reactor core during steady-state operation. Given the flux distribution, power distribution and peaking factors can be determined using the data analysis INCORE code. Once the peaking factors have been calculated, compliance to operation within established limits can be shown, and verification of the physics parameters assumed in the safety analysis can be made.

This section deals with the individual components of the measured flux distributions and provides comparisons of the measured data taken during Cycle 19, the operating cycle, for the MIDS, FIDS, and combination Incore Detection Systems. All measured data is taken during steady-state operation; a prerequisite for movable detector mapping. Detailed comparisons of measured reaction rates, axial power profiles, and nuclear peaking factors are provided for the Fixed, Movable, and combination Incore Detector Systems. Comparisons are made based on eight movable flux mappings taken from startup to approximately the middle of Cycle 19. The reactor conditions prevailing during the eight maps are provided for reference in Table 5-1.

Figures 5-1A through 5-1H show the measured and analytical relative reaction rates for the movable maps for Cycle 19. These maps all had 12 operable thimbles and represent the base cases for the purpose of discussion of the subsequent cases presented. The fixed detector only comparisons of measured and analytical reaction rates are provided in Figures 5-2A through 5-2H, while Figures 5-3A through 5-3H provide the reaction rate comparisons for the combination Incore Detection System. As can be seen from the latter figures, the differences between both the MIDS and FIDS and the analytical data has remained constant. The use of one normalization factor, as described in Section 4.0, has allowed us to maintain the relationship between both the movable and fixed detector signals and the analytical data. Based on the agreement between the combination system data and our analytical model, we feel the combination system is capable of providing better core-wide power distribution information than the Movable System alone. Given more measured

data (18 versus 12 locations), less inference of the radial power distribution values is made by the INCORE code. The INCORE code determines "measured" assembly power distribution based on measured-to-predicted reaction rate comparisons and input theoretical power distributions. Based on the results presented, we feel the radial component of the core power distribution, as determined by the combination system, has been justified.

The second component of the three-dimensional power distributions is the axial power profiles. The MIDS provides a fine detailed trace of the axial flux distribution at 2" intervals in the Yankee core. The FIDS provides five signals approximately 18" apart based on the average flux over the fixed detector's 10" length. For the purpose of comparison, the fixed detector values are represented axially at the center of the detectors. Of the six fixed detector strings, four strings have symmetric movable locations for comparisons. As previously discussed in Section 4.0, the final axial positioning of the fixed strings was accomplished through comparison of the fixed data with symmetric movable shapes during the initial flux mappings performed in Cycle 19. The two fixed strings having no symmetric movable locations were assumed to be in the positions determined by the eddy current measurements prior to installation and adjusted by the average deviations of the four symmetric traces between the eddy current positioning and the axial shape comparisons' positioning. All fixed detector axial profiles also have the same extrapolation distances, both top and bottom, for all mappings made to date.

Figures 5-4(A-H) through 5-7(A-H) show comparisons of the normalized axial shapes of Fixed Detector Numbers 3, 4, 21, and 22 versus their symmetric movable locations for all eight flux mappings performed in Cycle 19. The movable traces can be identified by the smooth curves and grid depressions, while the fixed shapes are shown by smooth spline-fitted curves and triangles which are the actual five fixed data points. Overall, the agreement is excellent, therefore, providing sufficient justification that the fixed detectors can properly determine the axial component of the power distribution in the core.

The third aspect of steady-state power distributions to address is the peaking factors which are used to demonstrate compliance to established safety limits. Yankee's Technical Specifications have established limits on the peak linear heat generation rate (kW/ft) for both the fresh and recycled fuel batches; the maximum heat flux hot channel factor, F_q ; and the maximum enthalpy rise hot channel factor, $F_{\Delta H}^N$. Comparison of the measured peaking factor values as a function of cycle burnup for the MIDS and the combination system are shown for the fresh and recycled fuel batches in Figures 5-8 through 5-13 for the respective parameters. The peaking factors as determined by the different systems agree well within expected tolerances. No one system is always conservative or nonconservative versus the other. This trend is due to the specific loading pattern where peak local powers may or may not be in the area of instrumented locations. This is shown in Table 5-2, A Summary of the Calculated Peaking Factors, where the peak values sometimes occur in different core locations for the different combinations of available measurement locations. In general, however, none of the peaking factors calculated for Cycle 19 are close to the established limits and the minor variances have no impact on actual operation.

Comparison of the average absolute error and RMS error of the MIDS and combination system versus the analytical predictions, are presented in Figures 5-14 and 5-15. Once again, both curves agree closely with the larger error seen in the combination system. However, both sets of measured data agree very well with the analytical data further supporting the use of the combination system.

TABLE 5-1

Summary of Incore Mappings for Yankee Cycle 19

<u>Map ID</u>	<u>Date</u>	<u>Cycle Burnup (MWd/Mtu)</u>	<u>Power Level (MWt)</u>
07	07/09/87	71.	382.8
08	07/12/87	161.	597.7
09	08/19/87	1373.	599.7
11	09/23/87	2573.	600.0
14	10/28/87	3683.	600.0
15	12/02/87	4843.	600.0
16	12/22/87	5524.	600.0
38	01/27/88	6735.	600.0

TABLE 5-2
SUMMARY OF PEAKING FACTOR VALUES

INCORE RUN #	F&H		FQ		KW/FT		AXIAL
	FRESH ID	BURNT ID	FRESH ID	BURNT ID	FRESH	BURNT	OFFSET
MOVABLE INCORE DETECTION SYSTEM							
YR19007	1.4595 H8	1.5337 E7	2.0180 C8	2.0670 E7	6.246	6.398	1.719
YR19008	1.4532 H8	1.5457 E7	1.9860 C8	2.0825 E7	9.598	10.064	0.892
YR19009	1.4391 H8	1.5247 D5	1.9668 C8	2.0124 D5	9.537	9.758	-2.724
YR19011	1.4302 H8	1.5052 D5	1.8879 C8	1.9276 D5	9.159	9.351	-0.547
YR19014	1.4385 H8	1.4991 D5	1.8761 C8	1.9045 D5	9.101	9.239	-2.029
YR19015	1.4212 H8	1.4809 D5	1.7955 H3	1.8417 D5	8.711	8.935	-2.475
YR19016	1.4253 H8	1.4721 D5	1.7996 H3	1.8423 E7	8.730	8.937	-4.008
YR19038	1.4038 H8	1.4646 E7	1.7161 H3	1.7548 E7	8.373	8.561	0.224
FIXED INCORE DETECTION SYSTEM							
YR19307	1.5058 B7	1.5348 D5	2.0783 B7	2.1035 D5	6.432	6.511	0.739
YR19308	1.5143 B7	1.5492 D5	2.0702 B7	2.1042 D5	10.004	10.169	-0.608
YR19309	1.4709 B7	1.5321 D5	1.9921 J7	2.0441 D5	9.660	9.912	-3.857
YR19311	1.4486 B7	1.5131 D5	1.9122 J7	1.9628 D5	9.276	9.522	-1.250
YR19314	1.4518 B7	1.5111 D5	1.8950 J7	1.9453 D5	9.193	9.437	-2.328
YR19315	1.4276 B7	1.4981 D5	1.8240 J7	1.8767 D5	8.849	9.104	-2.390
YR19316	1.4300 J7	1.4999 E7	1.8188 J7	1.8651 G6	8.823	9.048	-2.968
YR19338	1.4109 J7	1.4862 E7	1.7462 B7	1.8218 E7	8.520	8.888	0.239
COMBINATION INCORE DETECTION SYSTEM							
YR19207	1.4732 B7	1.5287 E7	2.0371 B7	2.0633 D5	6.305	6.386	1.382
YR19208	1.4735 B7	1.5429 E7	2.0177 B7	2.0787 E7	9.751	10.046	0.351
YR19209	1.4497 B7	1.5235 D5	1.9621 C8	2.0142 D5	9.514	9.766	-3.111
YR19211	1.4365 B7	1.5036 D5	1.8797 C8	1.9271 D5	9.119	9.349	-0.800
YR19214	1.4418 B7	1.4992 D5	1.8712 C8	1.9063 D5	9.078	9.248	-2.167
YR19215	1.4198 H8	1.4831 D5	1.7912 C8	1.8437 D5	8.690	8.944	-2.504
YR19216	1.4243 H8	1.4759 D5	1.7926 H8	1.8410 E7	8.696	8.931	-3.706
YR19238	1.4014 H8	1.4649 D5	1.7102 J4	1.7526 D5	8.344	8.551	0.220

NOTE:

AXIAL OFFSET REFERS TO CORE AVERAGE VALUE

MAPS ARE LABELLED YR19 SS WHERE:

OSS REFERS TO MOVABLE ONLY MAPS

3SS REFERS TO FIXED ONLY MAPS

2SS REFERS TO COMBINATION SYSTEM MAPS

FIGURE 5-1A
 COMPARISON OF MEASURED AND PREDICTED SIGNALS
 INCORE RUN YR-19-007
 382.8 MWT. GROUP C AT 85.875 INCHES 71. MWD/MTU

			0.682 0.713 -4.3						
					0.972 0.995 -2.3				
						1.000 1.010 -1.0			
		1.003 1.022 -1.8		1.150 1.111 3.5					
			1.151 1.116 3.2						
						1.147 1.113 3.1			
					1.159 1.121 3.4		1.016 1.022 -0.6		
			1.022 1.028 -0.6			0.995 1.003 -0.8			
		0.703 0.747 -5.9							

MEASURED SIGNAL
 PREDICTED SIGNAL
 PERCENT DIFFERENCE

AVERAGE ABSOLUTE DIFFERENCE BETWEEN
 MEASURED AND PREDICTED 2.540 PERCENT

RMS ERROR 2.999

597.7 MWT. GROUP C AT 86.625 INCHES 161. MWD/MTU

MEASURED SIGNAL	PREDICTED SIGNAL	PERCENT DIFFERENCE
1	1	0
2	2	0
3	3	0
4	4	0
5	5	0
6	6	0
7	7	0
8	8	0
9	9	0
10	10	0
11	11	0
12	12	0
13	13	0
14	14	0
15	15	0
16	16	0
17	17	0
18	18	0
19	19	0
20	20	0
21	21	0
22	22	0
23	23	0
24	24	0
25	25	0
26	26	0
27	27	0
28	28	0
29	29	0
30	30	0
31	31	0
32	32	0
33	33	0
34	34	0
35	35	0
36	36	0
37	37	0
38	38	0
39	39	0
40	40	0
41	41	0
42	42	0
43	43	0
44	44	0
45	45	0
46	46	0
47	47	0
48	48	0
49	49	0
50	50	0
51	51	0
52	52	0
53	53	0
54	54	0
55	55	0
56	56	0
57	57	0
58	58	0
59	59	0
60	60	0
61	61	0
62	62	0
63	63	0
64	64	0
65	65	0
66	66	0
67	67	0
68	68	0
69	69	0
70	70	0
71	71	0
72	72	0
73	73	0
74	74	0
75	75	0
76	76	0
77	77	0
78	78	0
79	79	0
80	80	0
81	81	0
82	82	0
83	83	0
84	84	0
85	85	0
86	86	0
87	87	0
88	88	0
89	89	0
90	90	0
91	91	0
92	92	0
93	93	0
94	94	0
95	95	0
96	96	0
97	97	0
98	98	0
99	99	0
100	100	0

RMS ERROR 3.467

599.7 MWT. GROUP C AT 81.000 INCHES 1373. MWD/MTU

[illegible]

AVERAGE ABSOLUTE DIFFERENCE BETWEEN
MEASURED AND PREDICTED 1.766 PERCENT

RMS ERROR 2.024

FIGURE 5-1D
 COMPARISON OF MEASURED AND PREDICTED SIGNALS
 INCORE RUN YR-19-011
 600.0 MWT. GROUP C AT 85.500 INCHES 2573. MWD/MTU

			0.689 0.709 -2.8						
					0.992 0.997 -0.5				
						1.031 1.020 1.1			
		1.018 1.024 -0.6		1.139 1.119 1.8					
			1.142 1.120 2.0						
						1.144 1.118 2.3			
					1.120 1.122 -0.1		1.007 1.023 -1.5		
			1.026 1.024 0.3			0.991 1.005 -1.4			
		0.699 0.719 -2.8							

MEASURED SIGNAL
 PREDICTED SIGNAL
 PERCENT DIFFERENCE

AVERAGE ABSOLUTE DIFFERENCE BETWEEN
 MEASURED AND PREDICTED 1.440 PERCENT

RMS ERROR 1.697

FIGURE 5-1E
 COMPARISON OF MEASURED AND PREDICTED SIGNALS
 INCORE RUN YR-19-014
 600.0 MWT. GROUP C AT 83.625 INCHES 3683. MWD/MTU

			0.693 0.711 -2.6						
					0.985 1.000 -1.5				
						1.027 1.023 0.3			
		1.022 1.025 -0.4		1.137 1.117 1.7					
			1.134 1.117 1.5						
						1.130 1.116 1.3			
					1.123 1.118 0.4		1.023 1.024 -0.1		
			1.029 1.023 0.6			1.002 1.006 -0.5			
		0.696 0.719 -3.2							

MEASURED SIGNAL
 PREDICTED SIGNAL
 PERCENT DIFFERENCE

AVERAGE ABSOLUTE DIFFERENCE BETWEEN
 MEASURED AND PREDICTED 1.176 PERCENT

RMS ERROR 1.507

FIGURE 5-1F
 COMPARISON OF MEASURED AND PREDICTED SIGNALS
 INCORE RUN YR-19-015
 600.0 MWT. GROUP C AT 84.750 INCHES 4843. MWD/MTU

			0.700 0.712 -1.6						
					0.995 1.003 -0.7				
						1.030 1.027 0.3			
		1.019 1.027 -0.8		1.127 1.118 0.8					
			1.128 1.116 1.0						
						1.126 1.116 0.9			
					1.122 1.117 0.5		1.027 1.026 0.1		
			1.027 1.023 0.4			1.011 1.009 0.3			
		0.687 0.708 -2.9							

MEASURED SIGNAL
 PREDICTED SIGNAL
 PERCENT DIFFERENCE

AVERAGE ABSOLUTE DIFFERENCE BETWEEN
 MEASURED AND PREDICTED .863 PERCENT

RMS ERROR 1.131

FIGURE 5-1G
 COMPARISON OF MEASURED AND PREDICTED SIGNALS
 INCORE RUN YR-19-016
 600.0 MWT. GROUP C AT 84.750 INCHES 5524. MWD/MTU

			0.707 0.711 -0.6						
					1.000 1.003 -0.2				
						1.034 1.028 0.6			
		1.023 1.028 -0.4		1.121 1.117 0.4					
			1.121 1.116 0.4						
						1.117 1.115 0.2			
					1.116 1.116 0.0		1.029 1.026 0.2		
			1.030 1.024 0.6			1.013 1.010 0.2			
		0.688 0.705 -2.4							

MEASURED SIGNAL
 PREDICTED SIGNAL
 PERCENT DIFFERENCE

AVERAGE ABSOLUTE DIFFERENCE BETWEEN
 MEASURED AND PREDICTED .539 PERCENT

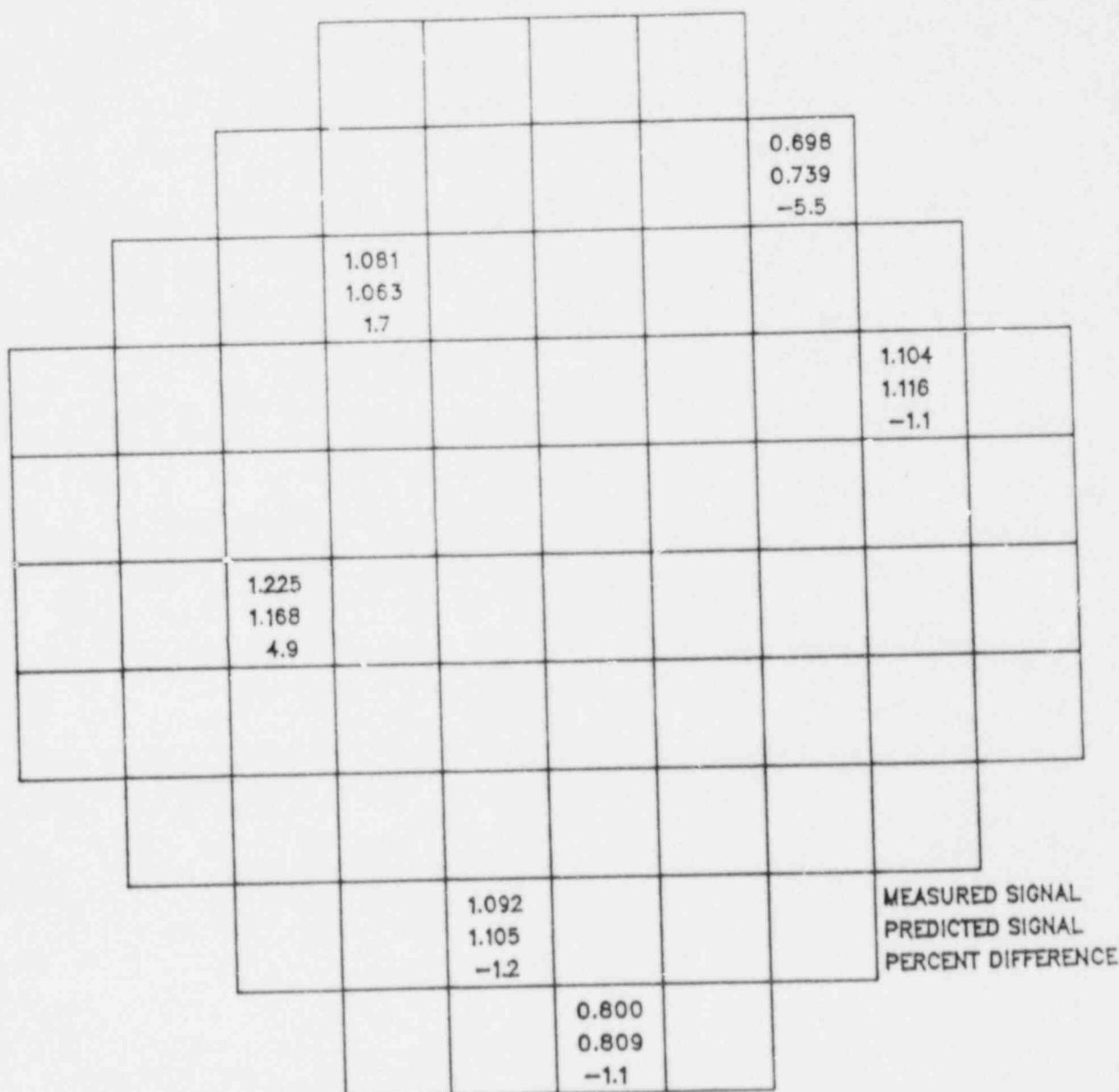
RMS ERROR .804

			0.704 0.711 -1.0						
					1.002 1.004 -0.2				
						1.035 1.030 0.5			
		1.022 1.029 -0.7		1.123 1.115 0.7					
			1.121 1.114 0.6						
						1.123 1.114 0.8			
					1.120 1.115 0.5		1.031 1.028 0.2		
			1.029 1.025 0.4			1.012 1.013 -0.1			
		0.678 0.700 -3.1							

MEASURED SIGNAL
PREDICTED SIGNAL
PERCENT DIFFERENCE

RMS ERROR 1.067

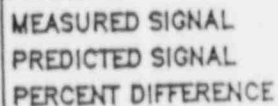
FIGURE 5-2A
 COMPARISON OF MEASURED AND PREDICTED SIGNALS
 INCORE RUN YR-19-307
 382.8 MWT. GROUP C AT 85.875 INCHES 71. MWD/MTU



AVERAGE ABSOLUTE DIFFERENCE BETWEEN
 MEASURED AND PREDICTED 2.587 PERCENT

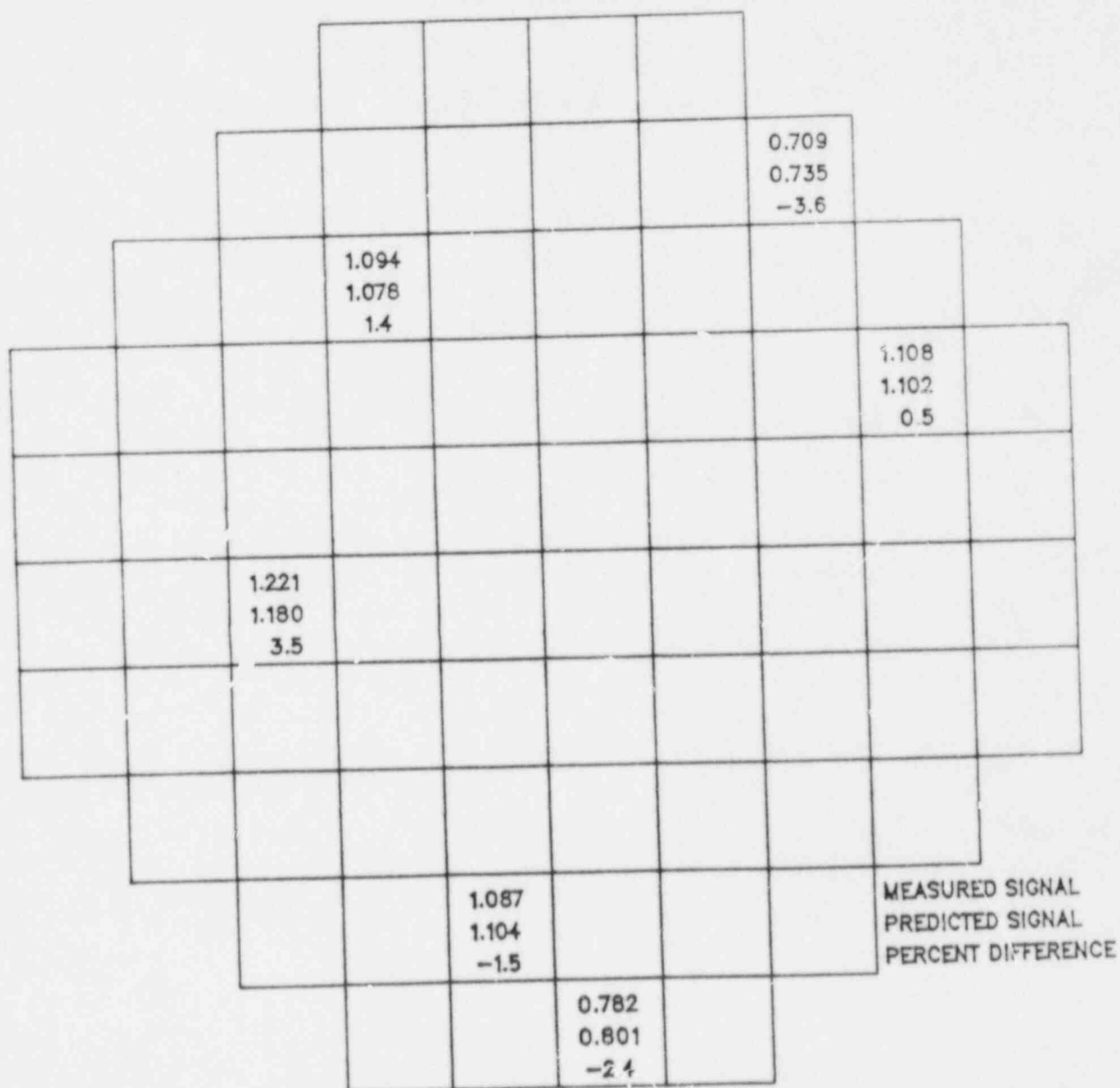
RMS ERROR 3.198

597.7 MWT. GROUP C AT 86.625 INCHES 161. MWD/MTU



RMS ERROR 3.707

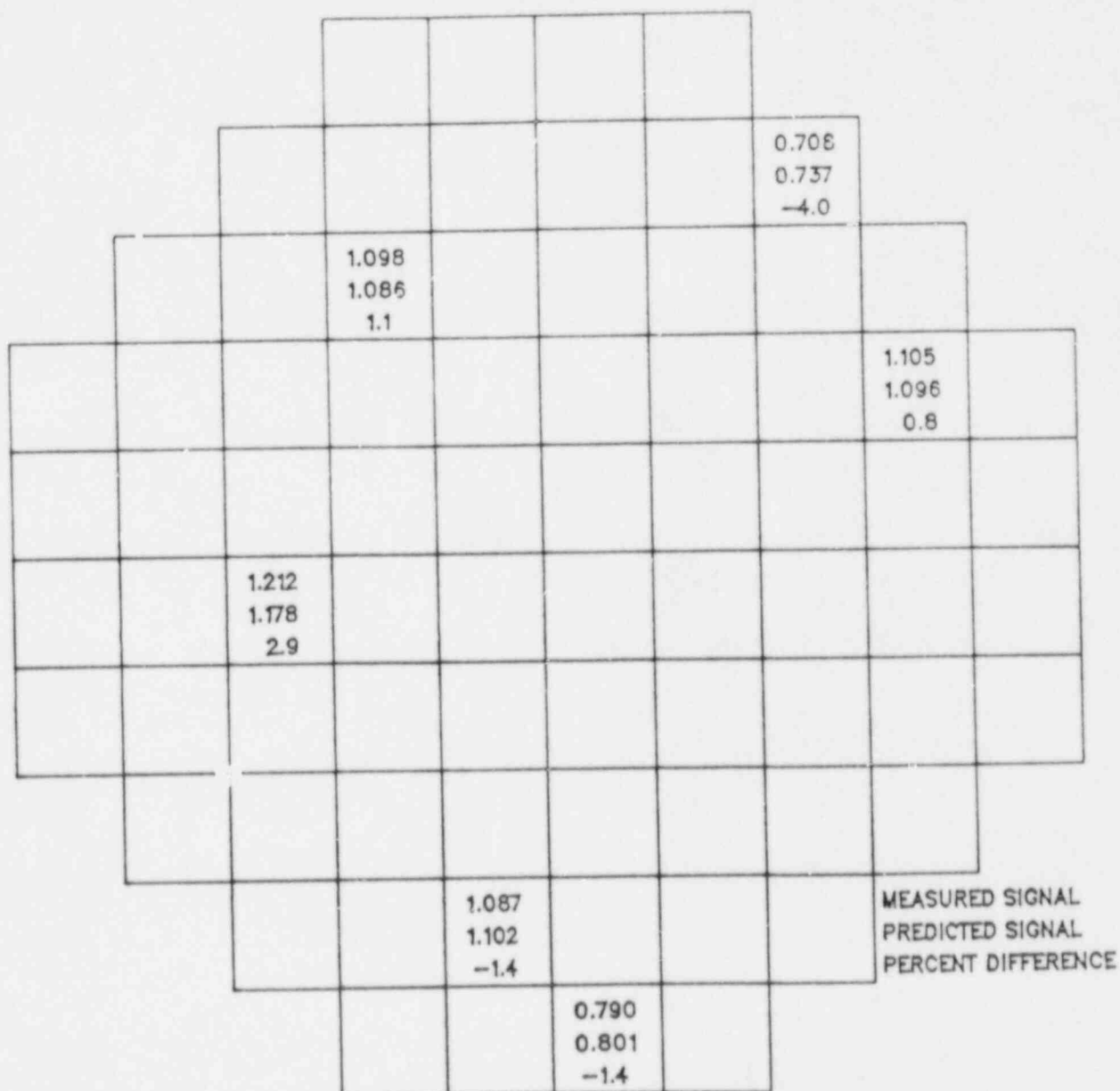
FIGURE 5-2C
 COMPARISON OF MEASURED AND PREDICTED SIGNALS
 INCORE RUN YR-19-309
 599.7 MWT. GROUP C AT 81.000 INCHES 1373. MWD/MTU



AVERAGE ABSOLUTE DIFFERENCE BETWEEN
 MEASURED AND PREDICTED 2.158 PERCENT

RMS ERROR 2.434

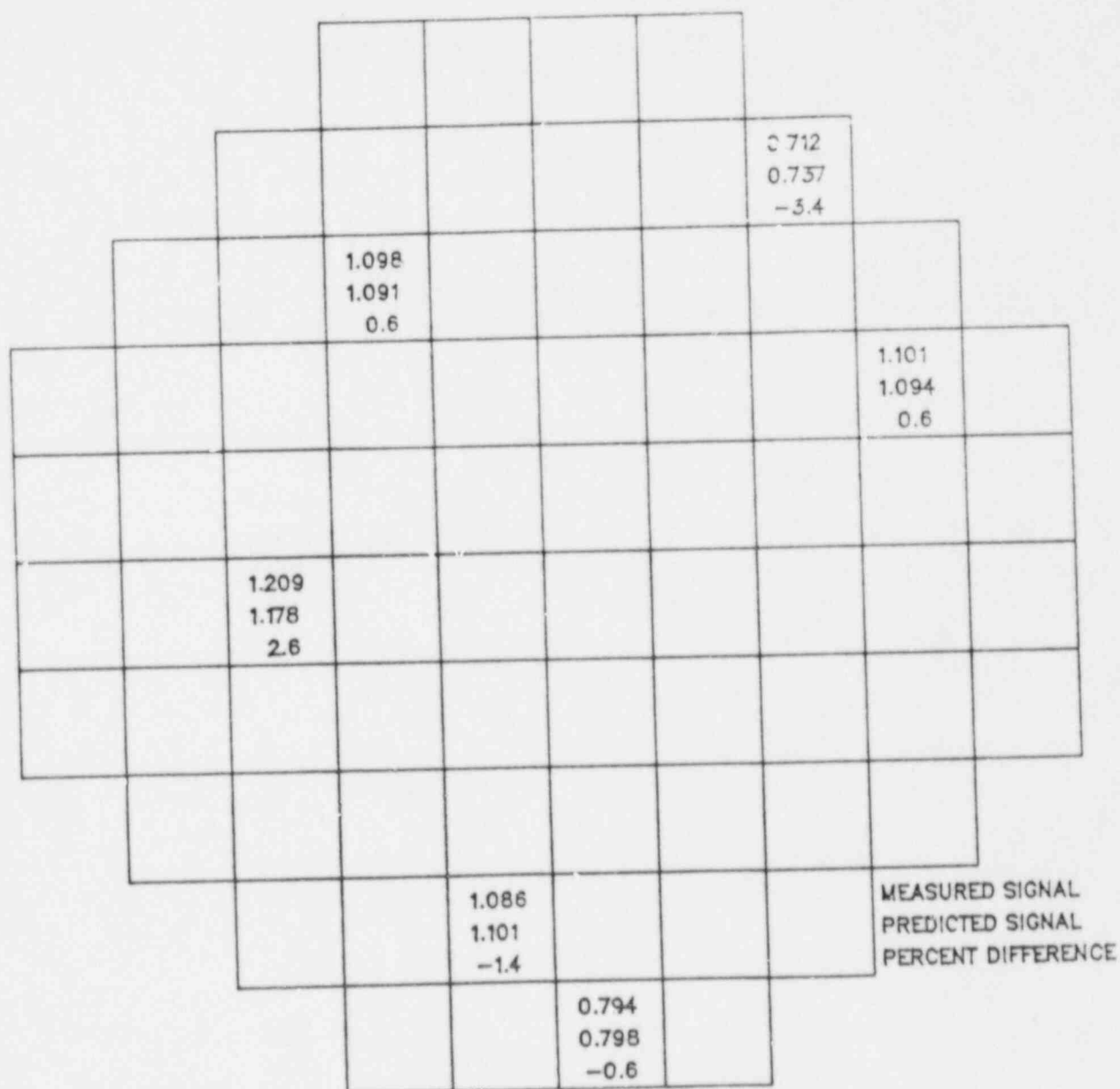
FIGURE 5-2D
 COMPARISON OF MEASURED AND PREDICTED SIGNALS
 INCORE RUN YR-19-311
 600.0 MWT. GROUP C AT 85.500 INCHES 2573. MWD/MTU



AVERAGE ABSOLUTE DIFFERENCE BETWEEN
 MEASURED AND PREDICTED 1.934 PERCENT

RMS ERROR 2.244

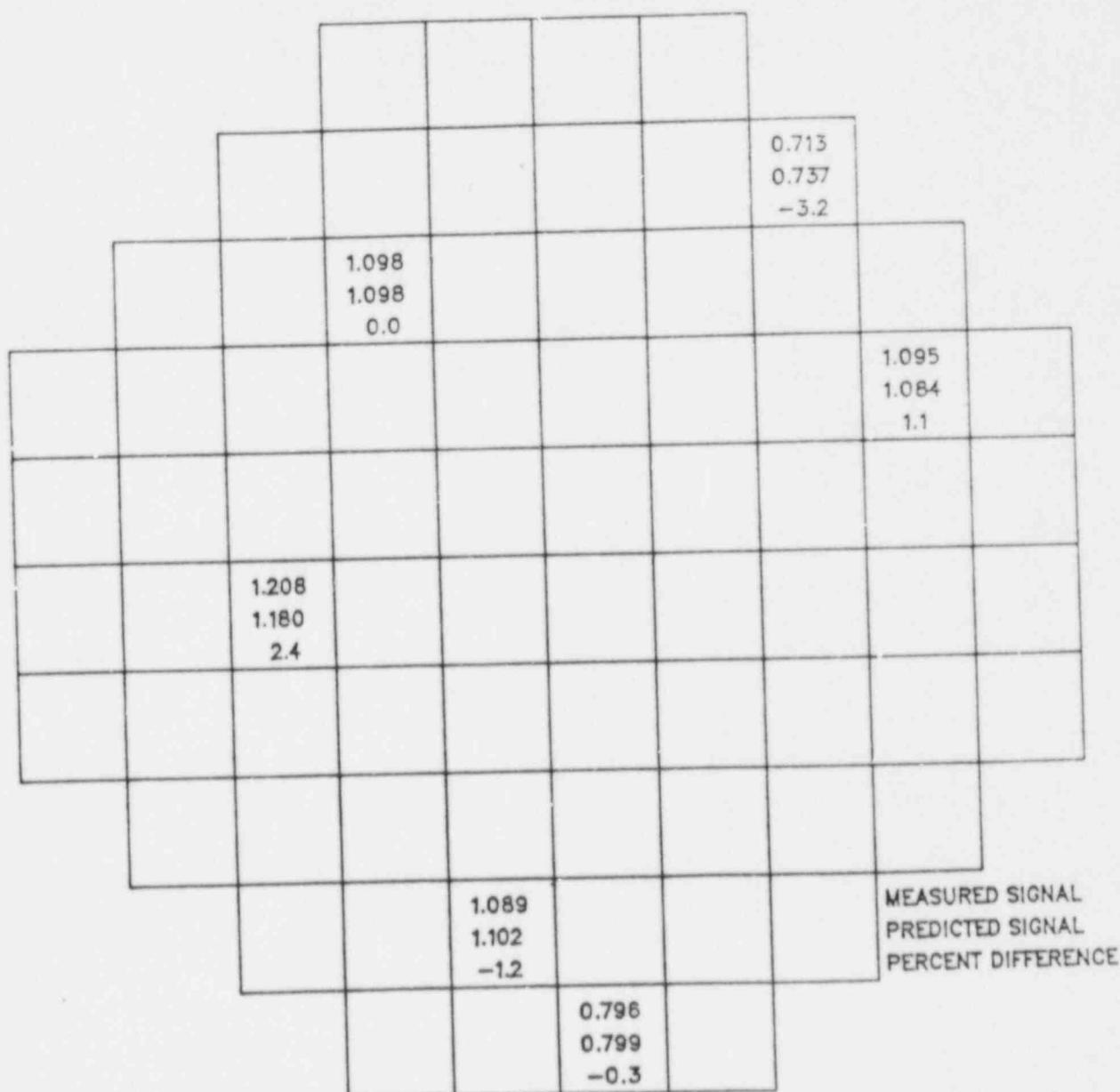
FIGURE 5-2E
 COMPARISON OF MEASURED AND PREDICTED SIGNALS
 INCORE RUN YR--19-314
 600.0 MWT. GROUP C AT 83.625 INCHES 3683. MWD/MTU



AVERAGE ABSOLUTE DIFFERENCE BETWEEN
 MEASURED AND PREDICTED 1.533 PERCENT

RMS ERROR 1.887

FIGURE 5-2F
 COMPARISON OF MEASURED AND PREDICTED SIGNALS
 INCORE RUN YR-19-315
 600.0 MWT. GROUP C AT 84.750 INCHES 4843. MWD/MTU



AVERAGE ABSOLUTE DIFFERENCE BETWEEN
 MEASURED AND PREDICTED 1.376 PERCENT

RMS ERROR 1.777

MEASURED SIGNAL	PREDICTED SIGNAL	PERCENT DIFFERENCE
1.100	1.101	-0.1
1.206	1.181	2.1
1.092	1.082	1.0
1.090	1.103	-1.2
0.713	0.735	-3.0
0.799	0.798	0.1

RMS ERROR 1.635

MEASURED SIGNAL
PREDICTED SIGNAL
PERCENT DIFFERENCE

RMS ERROR 1.699

FIGURE 5-3A
COMPARISON OF MEASURED AND PREDICTED SIGNALS
INCORE RUN YR--19--207
382.8 MWT. GROUP C AT 85.875 INCHES 71. MWD/MTU

			0.698 0.729 -4.3							
					0.995 1.017 -2.2		0.666 0.706 -5.7			
			1.030 1.014 1.5				1.023 1.033 -1.0			
		1.027 1.045 -1.7		1.177 1.136 3.6				1.052 1.065 -1.3		
			1.179 1.141 2.3							
		1.168 1.115 4.7				1.174 1.138 3.2				
					1.186 1.146 3.4		1.040 1.045 -0.5			
			1.046 1.052 -0.5			1.018 1.026 -0.8				
		0.719 0.764 -5.9		1.041 1.055 -1.4						
					0.763 0.772 -1.2					

MEASURED SIGNAL
PREDICTED SIGNAL
PERCENT DIFFERENCE

AVERAGE ABSOLUTE DIFFERENCE BETWEEN
MEASURED AND PREDICTED 2.557 PERCENT

RMS ERROR 3.070

FIGURE 5-3B
 COMPARISON OF MEASURED AND PREDICTED SIGNALS
 INCORE RUN YR-19-208
 597.7 MWT. GROUP C AT 86.625 INCHES 161. MWD/MTU

			0.690 0.730 -5.5						
					1.000 1.013 -1.2		0.668 0.707 -5.6		
			1.033 1.012 2.0			1.036 1.031 0.5			
		1.027 1.042 -1.5		1.181 1.141 3.6				1.045 1.067 -2.1	
			1.193 1.145 4.2						
		1.172 1.115 5.1				1.185 1.142 3.8			
					1.197 1.150 4.0		1.038 1.042 -0.4		
			1.040 1.048 -0.8			1.004 1.023 -1.9			
		0.716 0.767 -6.6		1.036 1.051 -1.4					
					0.740 0.774 -4.4				

MEASURED SIGNAL
 PREDICTED SIGNAL
 PERCENT DIFFERENCE

AVERAGE ABSOLUTE DIFFERENCE BETWEEN
 MEASURED AND PREDICTED 3.034 PERCENT

RMS ERROR 3.575

FIGURE 5-3C
 COMPARISON OF MEASURED AND PREDICTED SIGNALS
 INCORE RUN YR-19-209
 599.7 MWT. GROUP C AT 81.000 INCHES 1375. MWD/MTU

			0.702 0.722 -2.9						
					0.996 1.017 -2.0		0.673 0.697 -3.4		
			1.039 1.022 1.6			1.054 1.040 1.4			
		1.038 1.048 -1.0		1.174 1.150 2.1				1.052 1.045 0.7	
			1.182 1.153 2.5						
		1.160 1.118 3.7				1.173 1.150 2.0			
					1.165 1.156 0.8		1.042 1.047 -0.5		
			1.046 1.051 -0.5			1.011 1.029 -1.8			
		0.717 0.747 -3.9		1.032 1.046 -1.4					
					0.743 0.759 -2.2				

MEASURED SIGNAL
 PREDICTED SIGNAL
 PERCENT DIFFERENCE

AVERAGE ABSOLUTE DIFFERENCE BETWEEN
 MEASURED AND PREDICTED 1.907 PERCENT

RMS ERROR 2.170

FIGURE 5-3D
 COMPARISON OF MEASURED AND PREDICTED SIGNALS
 INCORE RUN YR-19-211
 600.0 MWT. GROUP C AT 85.500 INCHES 2573. MWD/MTU

			0.706 0.728 -3.0						
					1.016 1.023 -0.7		0.674 0.698 -3.5		
			1.045 1.029 1.6				1.056 1.047 0.8		
		1.043 1.051 -0.8		1.167 1.149 1.6				1.052 1.038 1.3	
			1.170 1.149 1.8						
		1.154 1.116 3.4				1.172 1.148 2.1			
					1.147 1.151 -0.4		1.032 1.050 -1.8		
			1.051 1.051 0.1			1.015 1.032 -1.7			
		0.716 0.738 -3.0		1.035 1.044 -0.9					
					0.752 0.759 -0.9				

MEASURED SIGNAL
 PREDICTED SIGNAL
 PERCENT DIFFERENCE

AVERAGE ABSOLUTE DIFFERENCE BETWEEN
 MEASURED AND PREDICTED 1.631 PERCENT

RMS ERROR 1.918

FIGURE 5-3E
 COMPARISON OF MEASURED AND PREDICTED SIGNALS
 INCORE RUN YR-19-214
 600.0 MWT. GROUP C AT 83.625 INCHES 3683. MWD/MTU

			0.710 0.730 -2.7						
					1.010 1.027 -1.6		0.676 0.697 -3.1		
			1.042 1.032 1.0				1.053 1.051 0.2		
		1.047 1.053 -0.5		1.166 1.148 1.6				1.045 1.035 0.9	
			1.163 1.147 1.3						
		1.147 1.114 3.0					1.159 1.146 1.1		
					1.132 1.148 0.3		1.049 1.051 -0.2		
			1.055 1.050 0.5			1.027 1.033 -0.6			
		0.713 0.738 -3.4		1.031 1.042 -1.0					
					0.753 0.755 -0.2				

MEASURED SIGNAL
 PREDICTED SIGNAL
 PERCENT DIFFERENCE

AVERAGE ABSOLUTE DIFFERENCE BETWEEN
 MEASURED AND PREDICTED 1.296 PERCENT

RMS ERROR 1.655

FIGURE 5-3F
 COMPARISON OF MEASURED AND PREDICTED SIGNALS
 INCORE RUN YR-19-215
 600.0 MWT. GROUP C AT 84.750 INCHES 4843. MWD/MTU

			0.720 0.732 -1.6						
				1.024 1.030 -0.7		0.673 0.696 -3.3			
		1.036 1.037 -0.1			1.059 1.035 0.3				
	1.048 1.055 -0.7		1.159 1.149 0.9				1.034 1.024 1.0		
		1.159 1.147 1.1							
	1.140 1.115 2.3				1.158 1.147 1.0				
				1.154 1.148 0.6		1.056 1.054 0.2			
		1.056 1.051 0.4			1.040 1.037 0.3				
	0.707 0.728 -2.9		1.028 1.041 -1.3						
				0.751 0.754 -0.4					

MEASURED SIGNAL
 PREDICTED SIGNAL
 PERCENT DIFFERENCE

AVERAGE ABSOLUTE DIFFERENCE BETWEEN
 MEASURED AND PREDICTED 1.054 PERCENT

RMS ERROR 1.384

FIGURE 5-3G
 COMPARISON OF MEASURED AND PREDICTED SIGNALS
 INCORE RUN YR-19-216
 600.0 MWT. GROUP C AT 84.750 INCHES 5524. MWD/MTU

			0.727 0.731 -0.6						
				1.029 1.031 -0.2		0.673 0.694 -3.1			
		1.038 1.039 -0.1			1.063 1.056 0.6				
	1.052 1.057 -0.4		1.153 1.148 0.4				1.031 1.021 1.0		
		1.152 1.147 0.4							
	1.138 1.115 2.1				1.149 1.147 0.2				
				1.147 1.148 0.0		1.058 1.053 0.2			
		1.059 1.052 0.6			1.041 1.039 0.2				
	0.708 0.725 -2.4		1.029 1.041 -1.2						
				0.754 0.753 0.1					

MEASURED SIGNAL
 PREDICTED SIGNAL
 PERCENT DIFFERENCE

AVERAGE ABSOLUTE DIFFERENCE BETWEEN
 MEASURED AND PREDICTED .780 PERCENT

RMS ERROR 1.150

FIGURE 5-3H
COMPARISON OF MEASURED AND PREDICTED SIGNALS
INCORE RUN YR-19-238
600.0 MWT. GROUP C AT 85.500 INCHES 6735. MWD/MTU

			0.724 0.732 -1.0						
					1.031 1.033 -0.2		0.671 0.692 -3.0		
			1.044 1.043 0.1			1.064 1.059 0.5			
		1.051 1.059 -0.8		1.155 1.147 0.6				1.023 1.011 1.2	
			1.153 1.146 0.6						
		1.140 1.115 2.3				1.155 1.146 0.8			
					1.152 1.147 0.5		1.060 1.058 0.2		
			1.059 1.055 0.4			1.041 1.042 -0.2			
		0.69/ 0.720 -3.2		1.028 1.041 -1.3					
					0.753 0.752 0.0				

MEASURED SIGNAL
PREDICTED SIGNAL
PERCENT DIFFERENCE

AVERAGE ABSOLUTE DIFFERENCE BETWEEN
MEASURED AND PREDICTED .928 PERCENT

RMS ERROR 1.312

YANKEE CORE 19

FIXED DETECTOR #3 VERSUS SYMMETRIC MOVEABLE #20
NORMALIZED RELATIVE AXIAL SHAPES 71. MWD/MTU

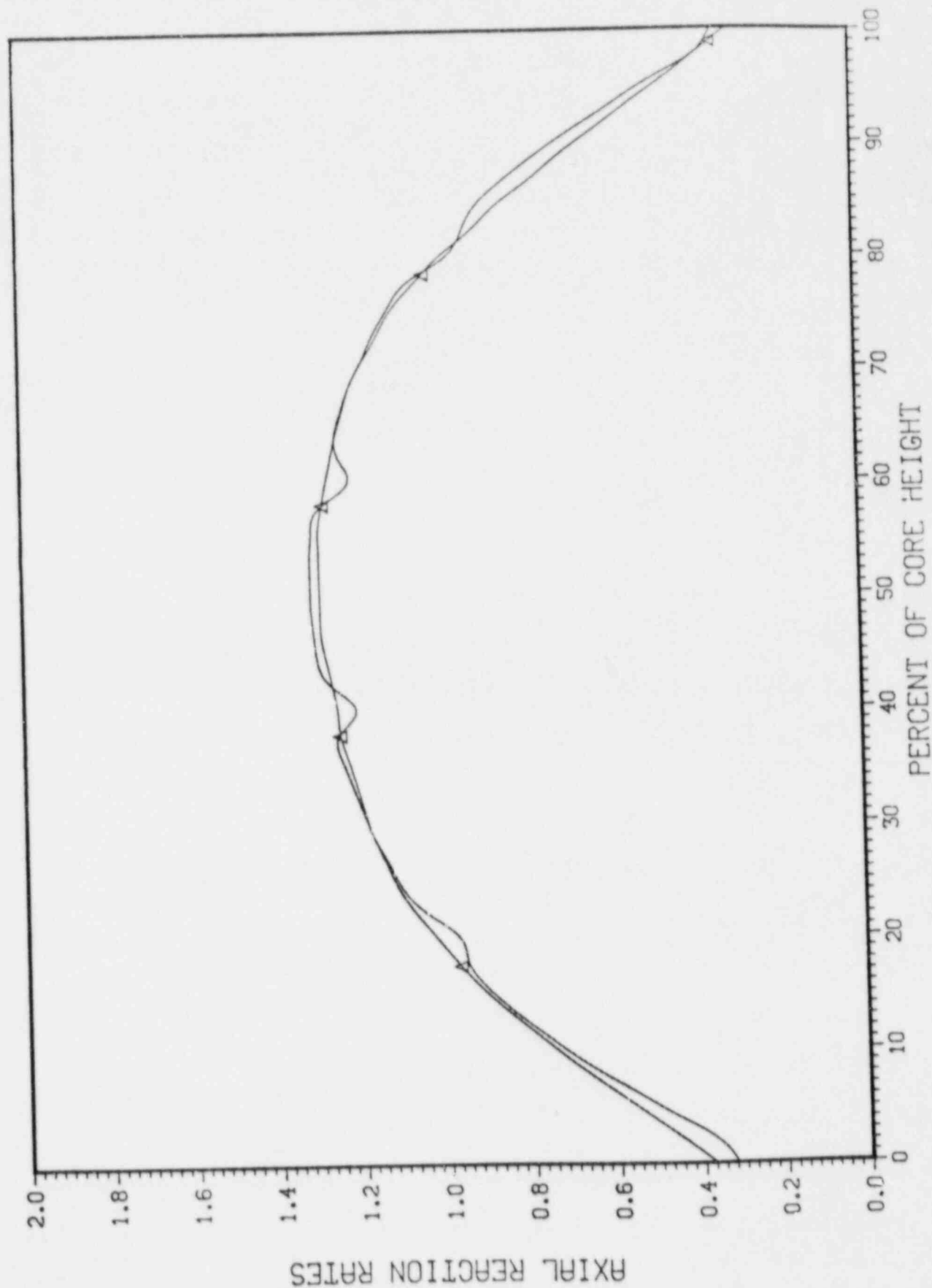


FIGURE 5-4A

YANKEE CORE 19

FIXED DETECTOR #3 VERSUS SYMMETRIC MOVEABLE #20
NORMALIZED RELATIVE AXIAL SHAPES 161. MWD/MTU

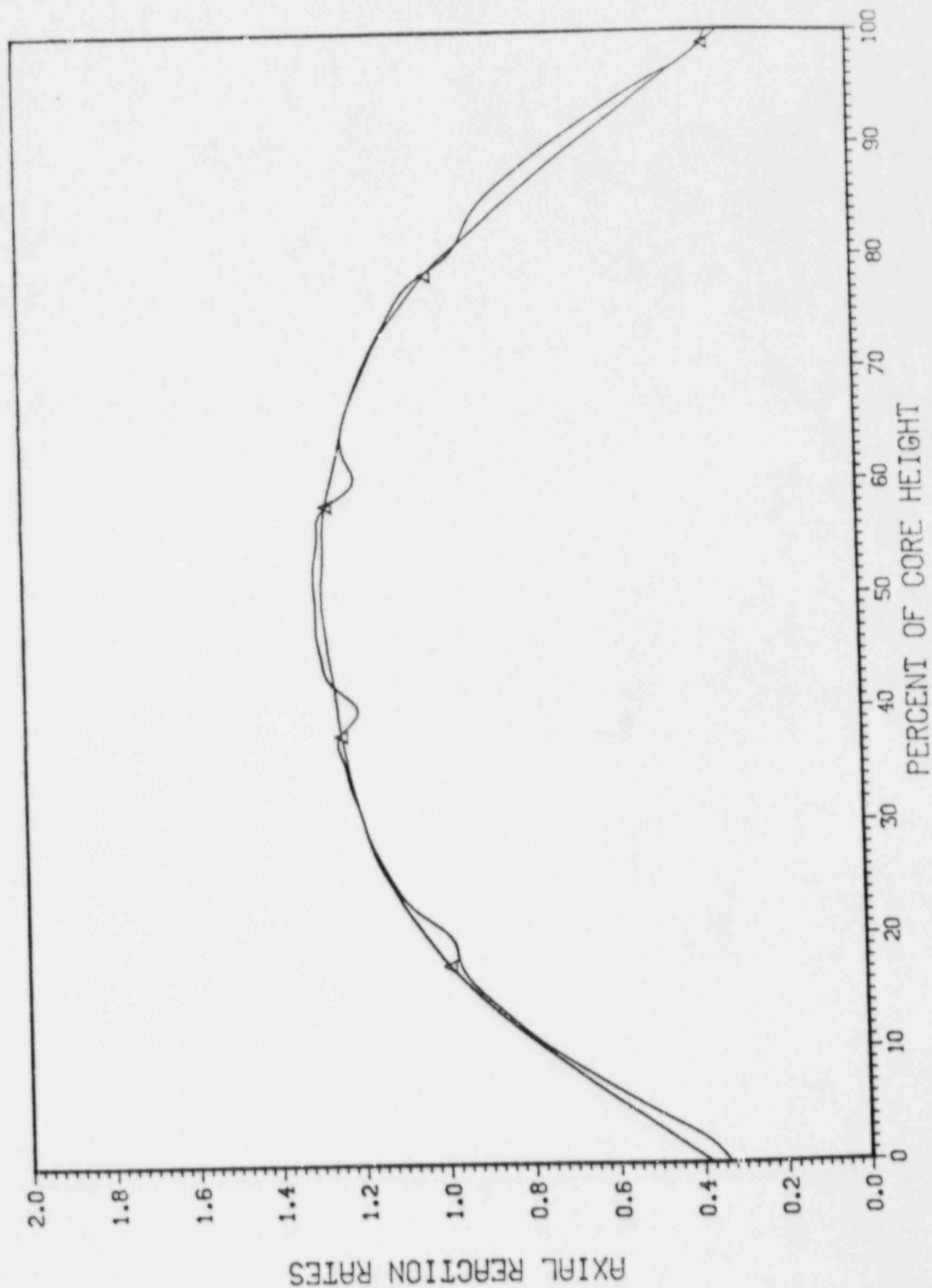


FIGURE 5-4B

YANKEE CORE 19
FIXED DETECTOR #3 VERSUS SYMMETRIC MOVEABLE #20
NORMALIZED RELATIVE AXIAL SHAPES 1373. MWD/MTU

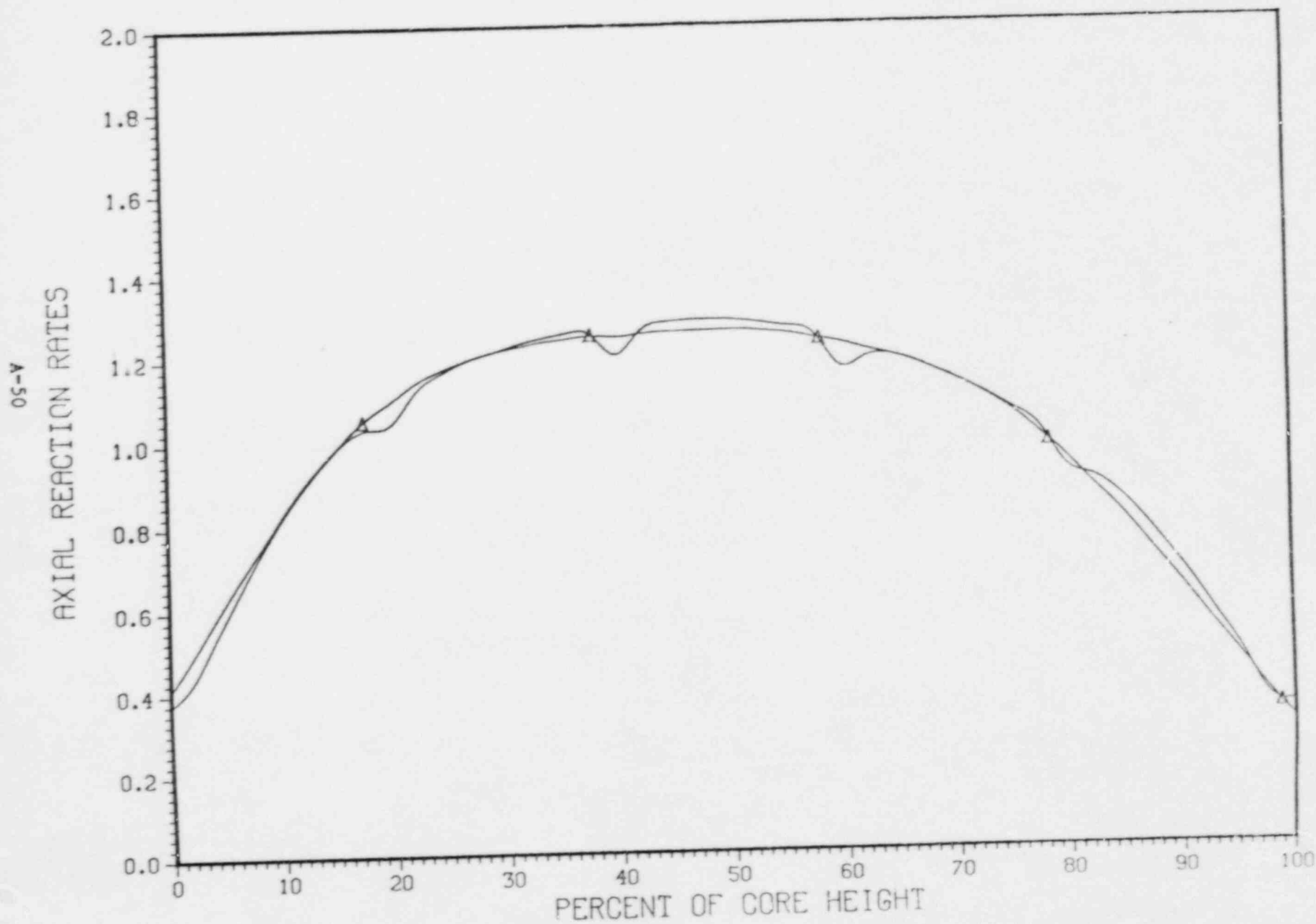


FIGURE 5-4C

YANKEE CORE 19
FIXED DETECTOR #3 VERSUS SYMMETRIC MOVEABLE #20
NORMALIZED RELATIVE AXIAL SHAPES 2573. MWD/MTU

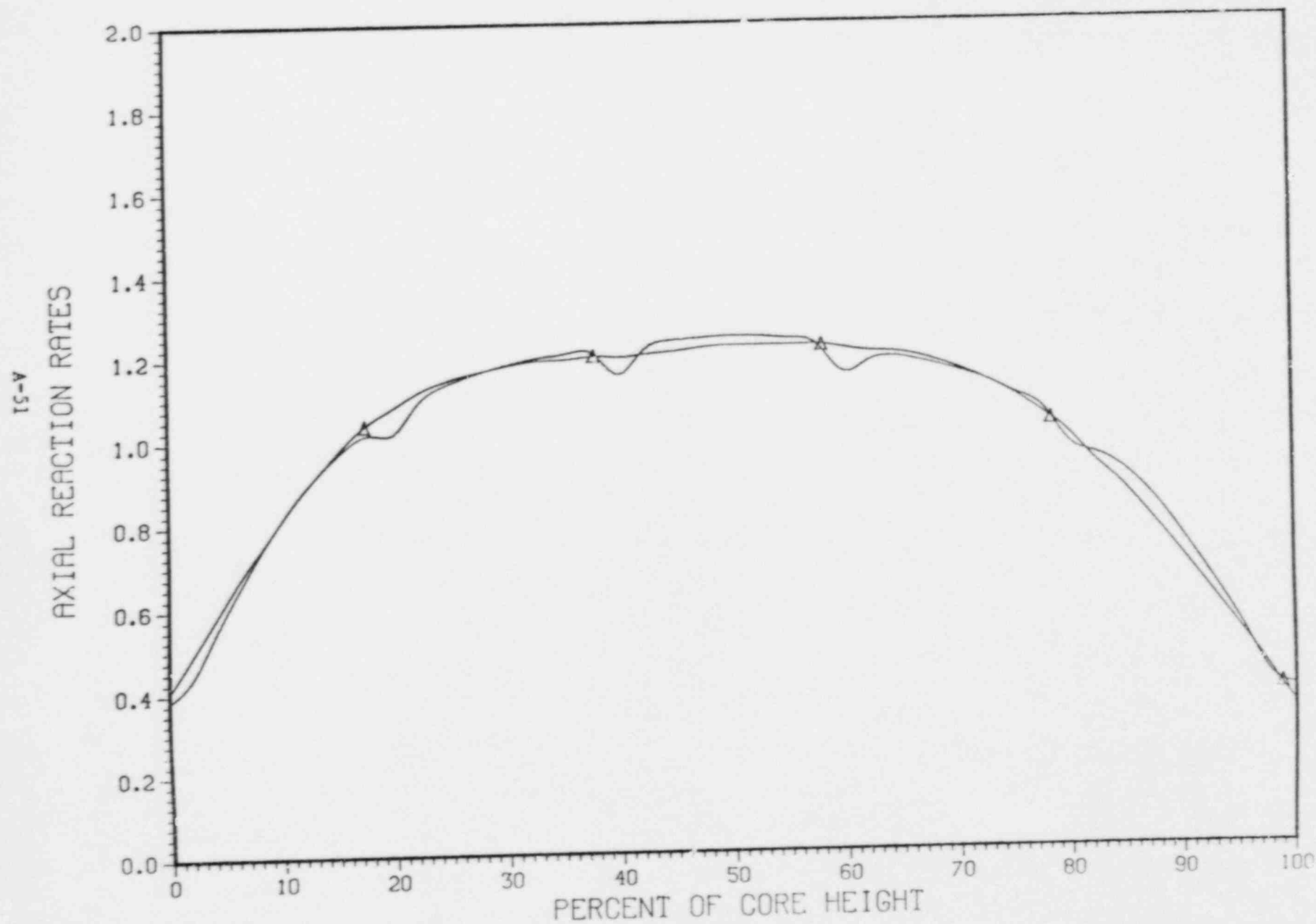


FIGURE 5-4D

YANKEE CORE 19
FIXED DETECTOR #3 VERSUS SYMMETRIC MOVEABLE #20
NORMALIZED RELATIVE AXIAL SHAPES 3683. MWD/MTU

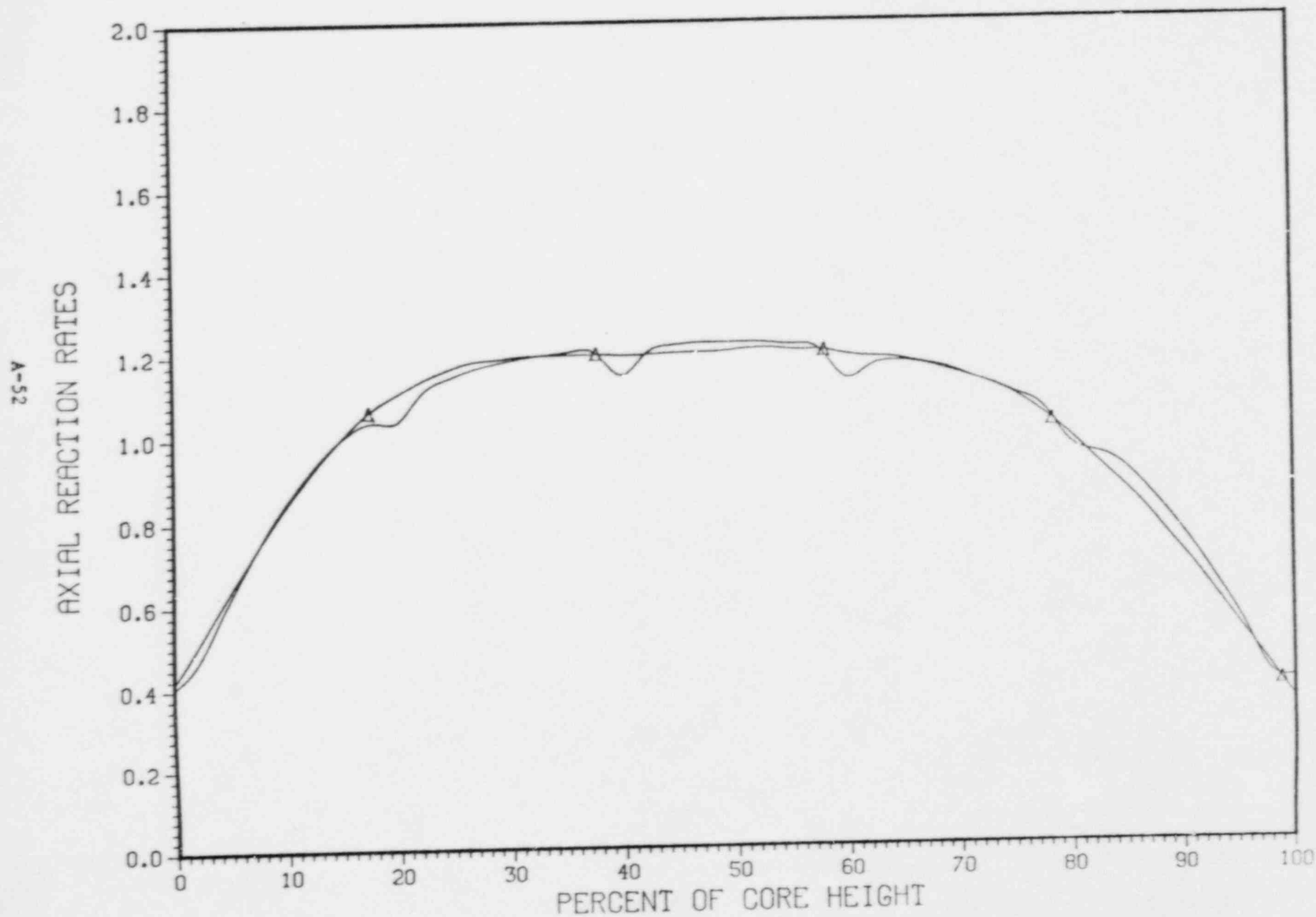


FIGURE 5-4E

YANKEE CORE 19
FIXED DETECTOR #3 VERSUS SYMMETRIC MOVEABLE #20
NORMALIZED RELATIVE AXIAL SHAPES 4843. MWD/MTU

A-53
AXIAL REACTION RATES

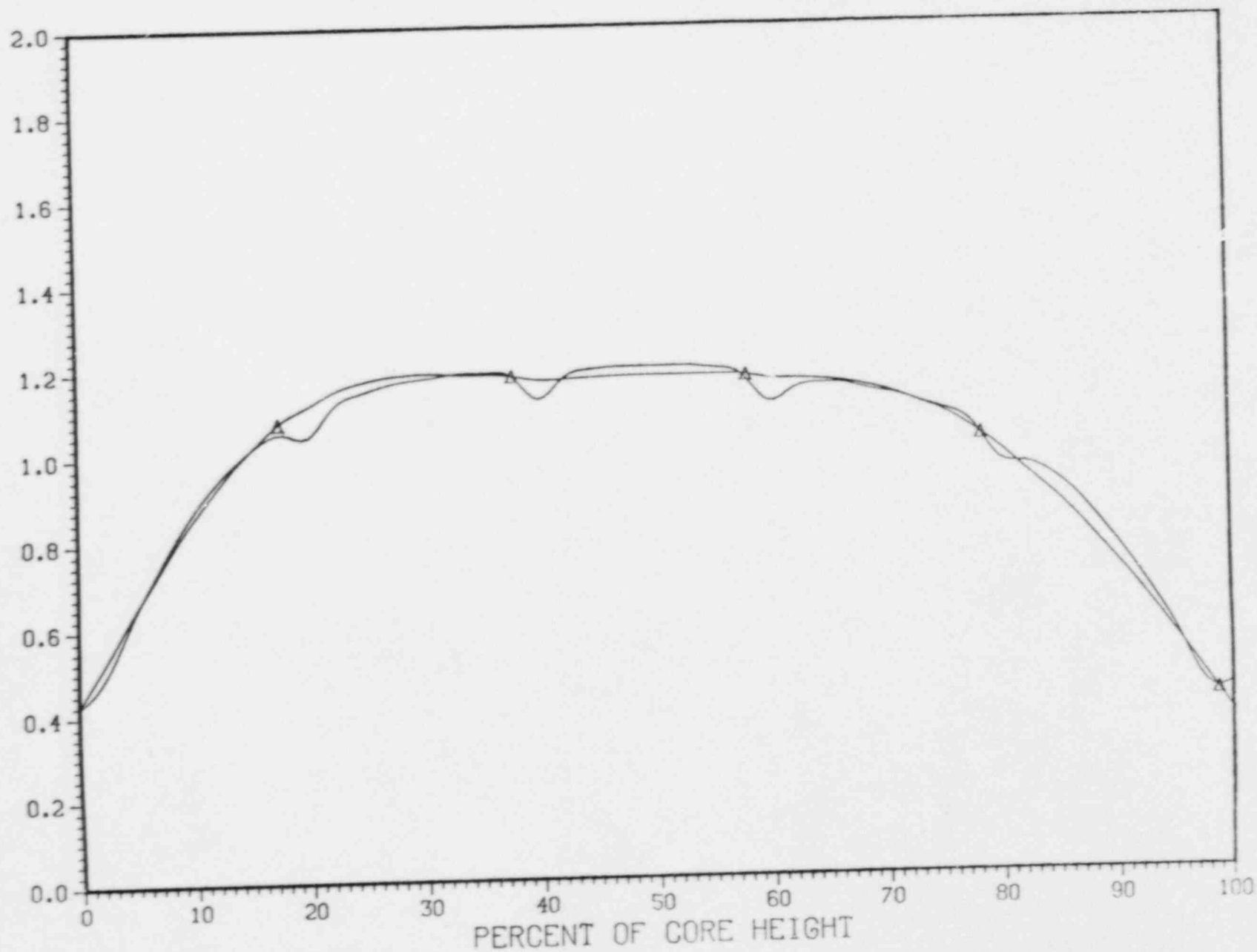


FIGURE 5-4F

YANKEE CORE 19
FIXED DETECTOR #3 VERSUS SYMMETRIC MOVEABLE #20
NORMALIZED RELATIVE AXIAL SHAPES 5524. MWD/MTU

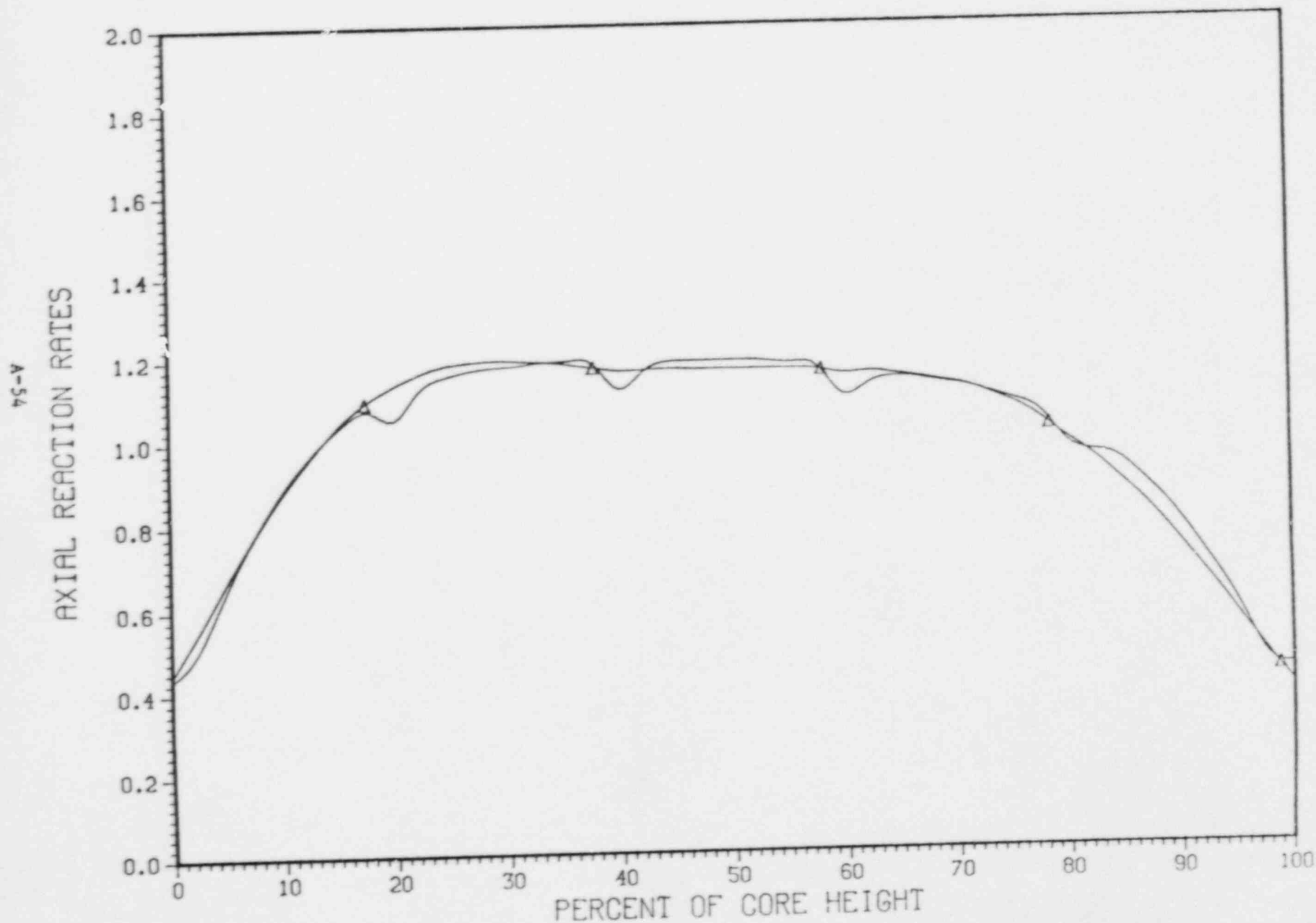


FIGURE 5-46

YANKEE CORE 19

FIXED DETECTOR #3 VERSUS SYMMETRIC MOVEABLE #20

NORMALIZED RELATIVE AXIAL SHAPES 6735. MWD/MTU

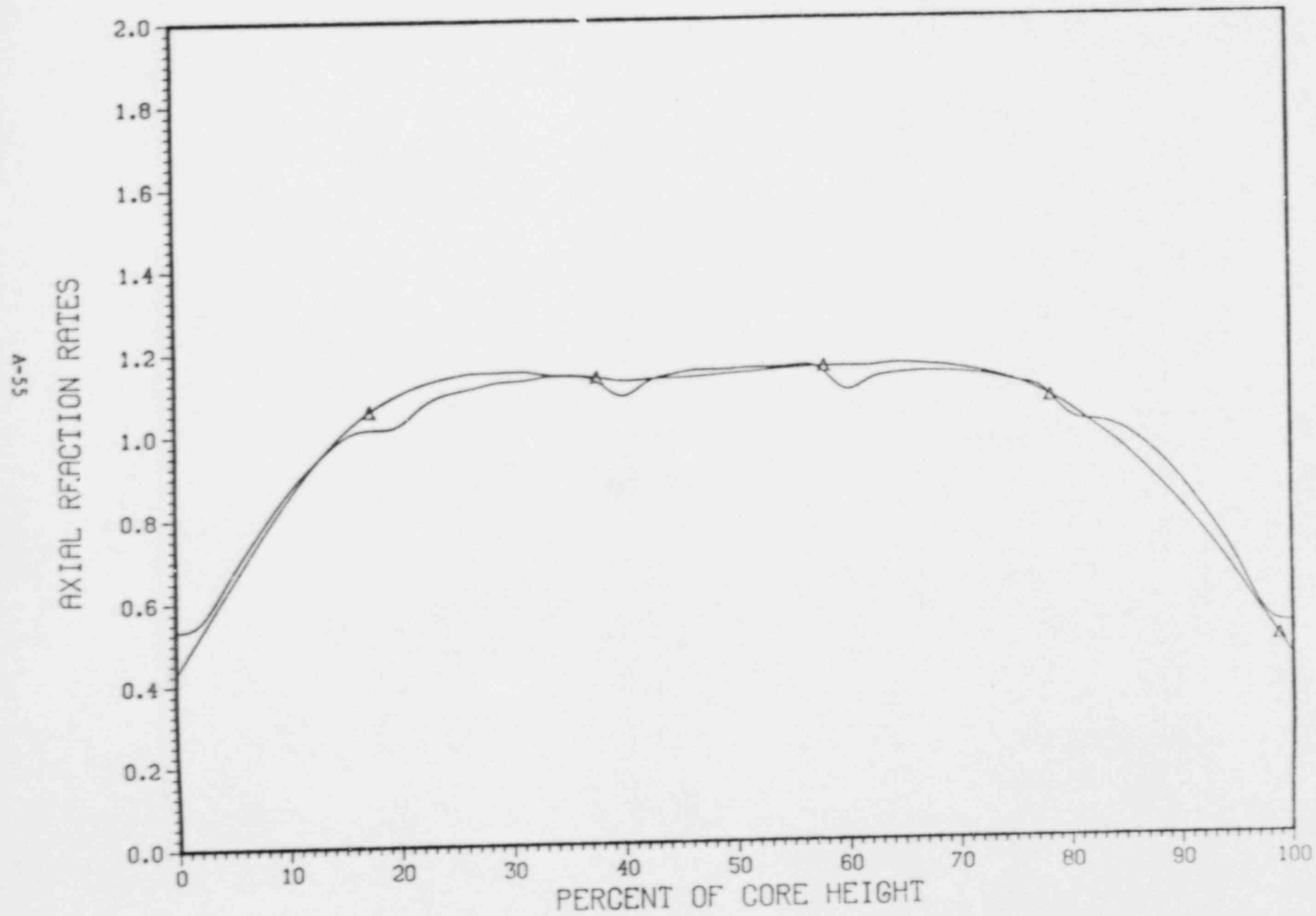
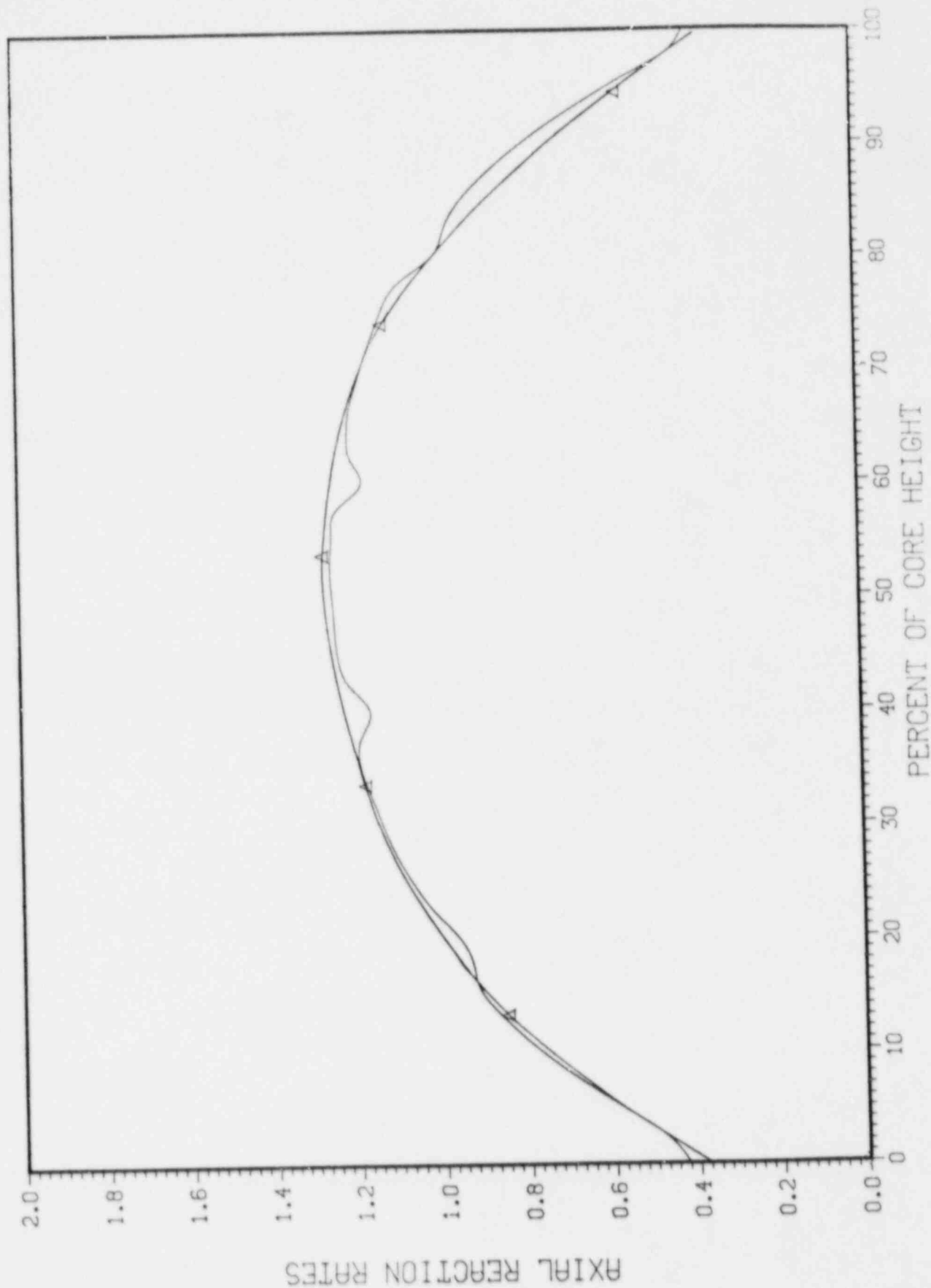


FIGURE S-4H

FIGURE 5-5A

YANKEE CORE 19
FIXED DETECTOR #4 VERSUS SYMMETRIC MOVEABLE #19
NORMALIZED RELATIVE AXIAL SHAPES 71. MWD/MTU



YANKEE CORE 19

FIXED DETECTOR #4 VERSUS SYMMETRIC MOVEABLE #19

NORMALIZED RELATIVE AXIAL SHAPES 161. MWD/MTU

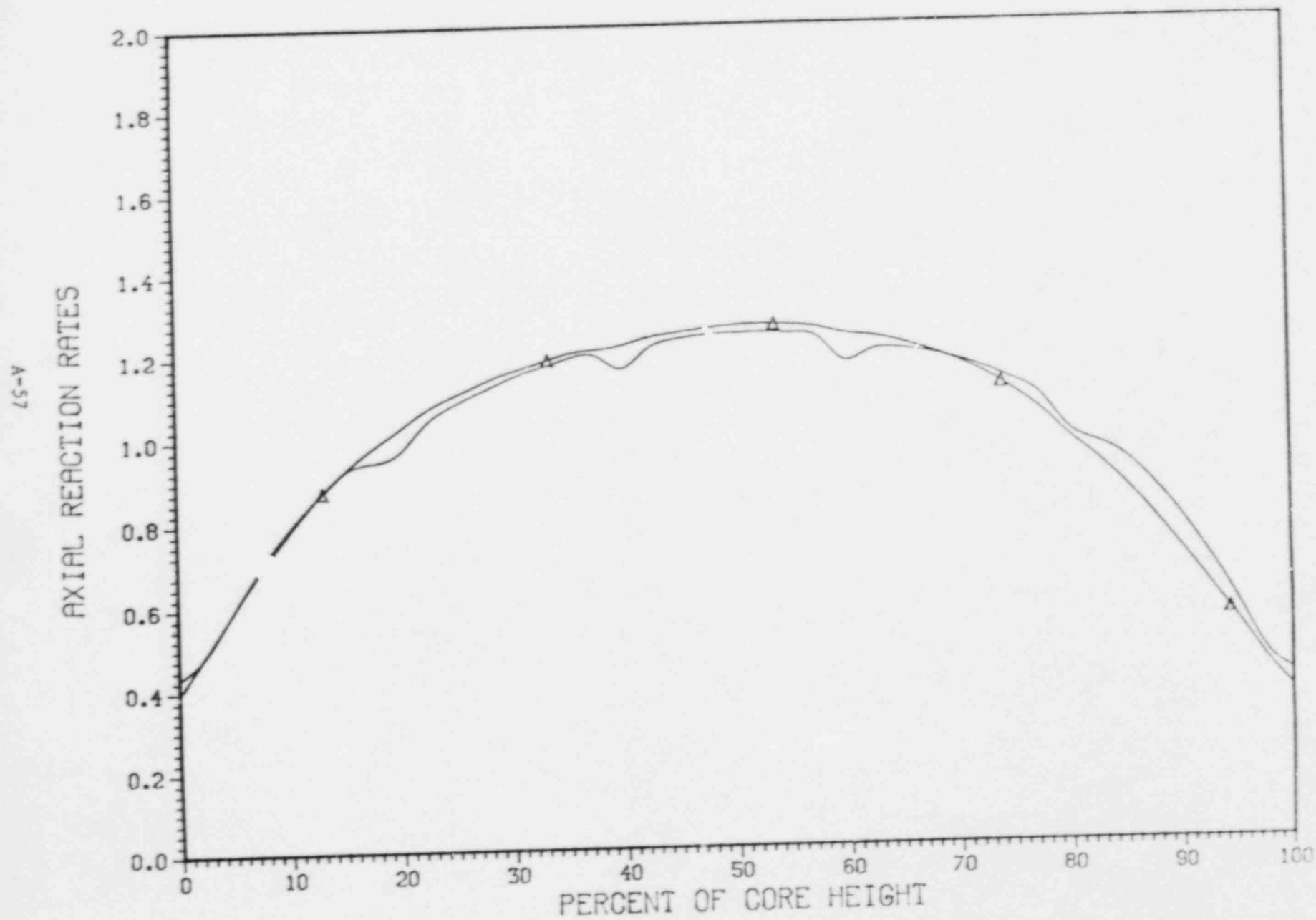


FIGURE 5-5B

YANKEE CORE 19

FIXED DETECTOR #4 VERSUS SYMMETRIC MOVEABLE #19

NORMALIZED RELATIVE AXIAL SHAPES 1373. MWD/MTU

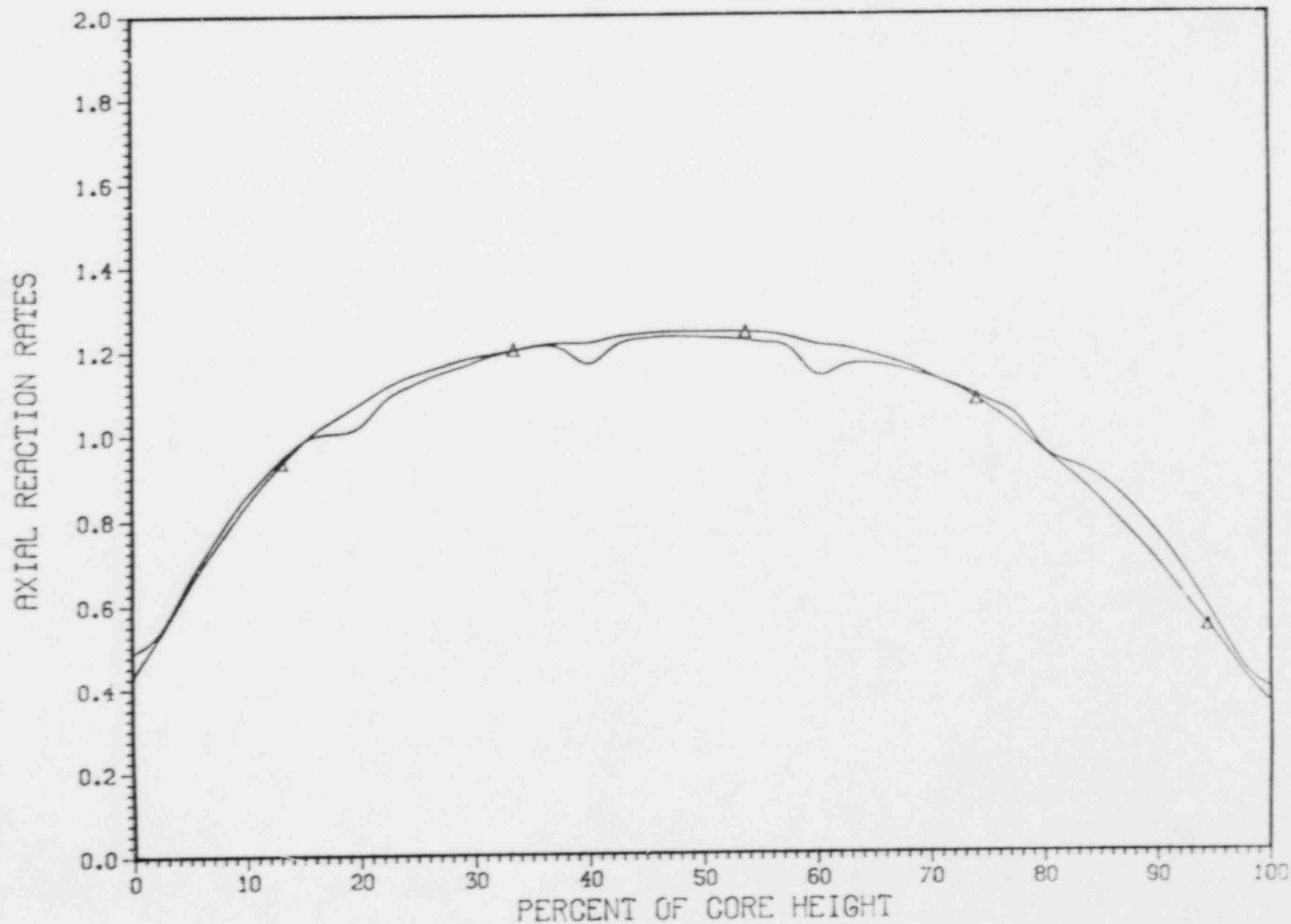


FIGURE 5-5C

YANKEE CORE 19

FIXED DETECTOR #4 VERSUS SYMMETRIC MOVEABLE #19

NORMALIZED RELATIVE AXIAL SHAPES 2573. MWD/MTU

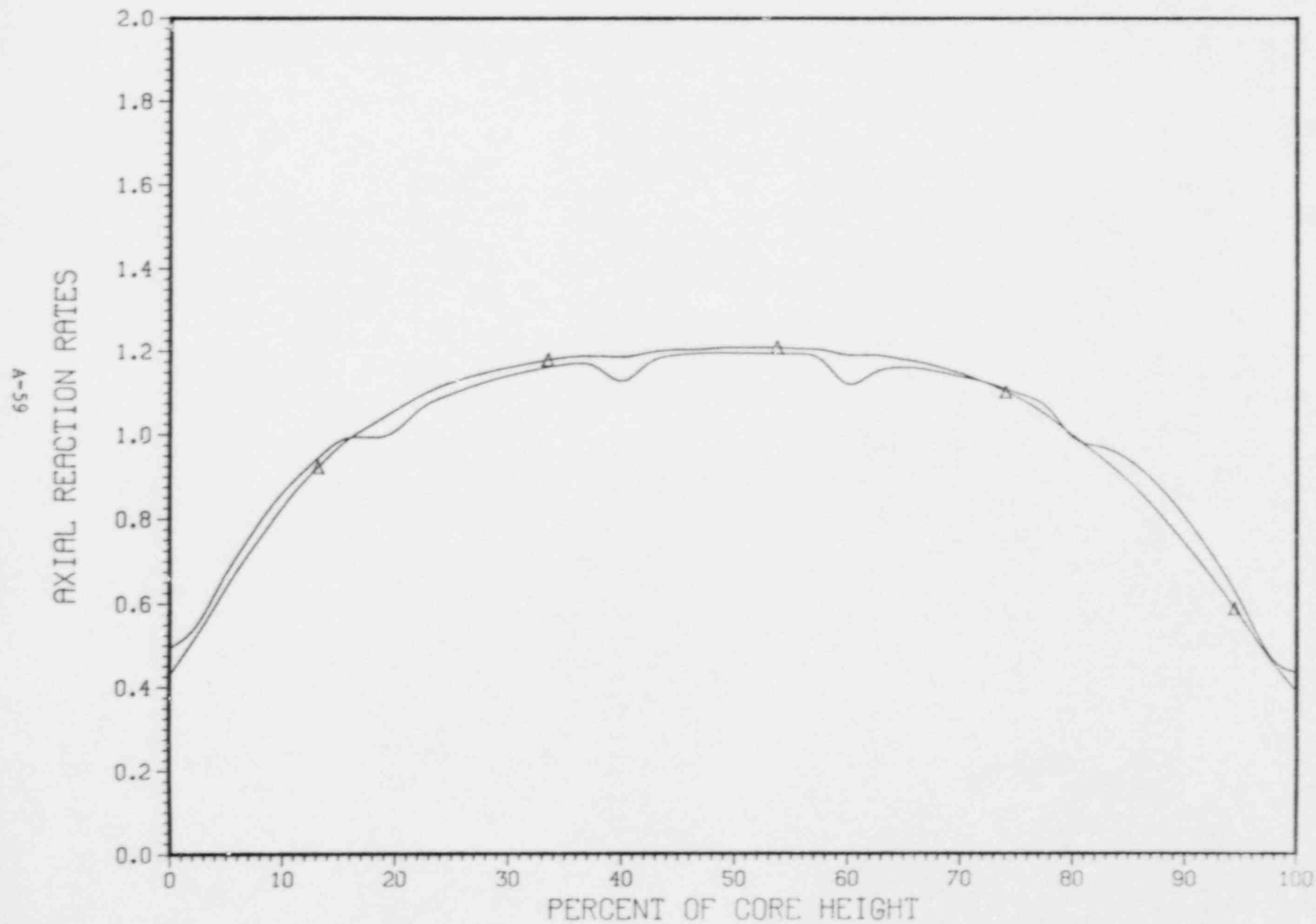


FIGURE 5-5D

YANKEE CORE 19
FIXED DETECTOR #4 VERSUS SYMMETRIC MOVEABLE #19
NORMALIZED RELATIVE AXIAL SHAPES 3683. MWD/MTU

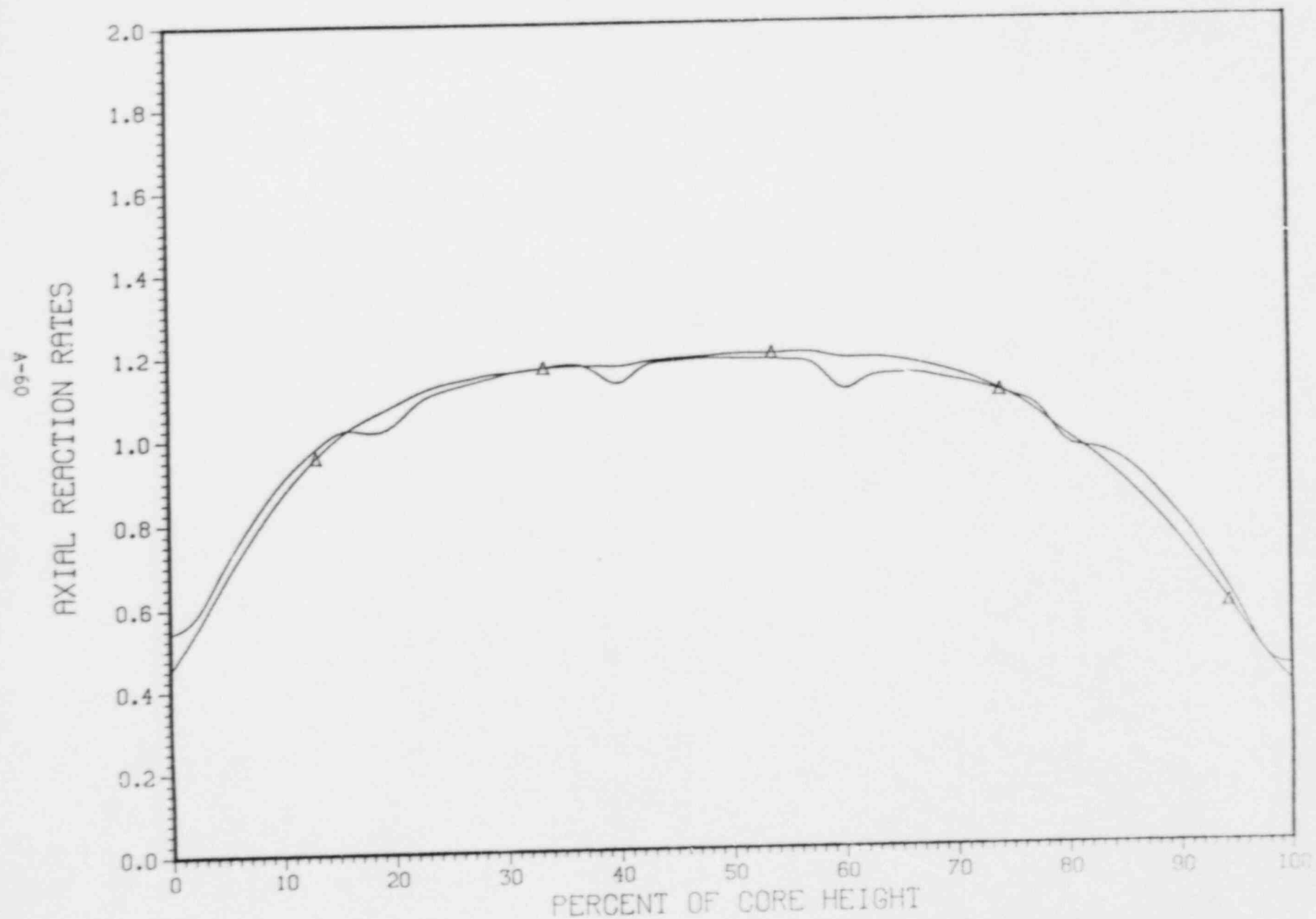


FIGURE 5-5E

YANKEE CORE 19

FIXED DETECTOR #4 VERSUS SYMMETRIC MOVEABLE #19

NORMALIZED RELATIVE AXIAL SHAPES 4843. MWD/MTU

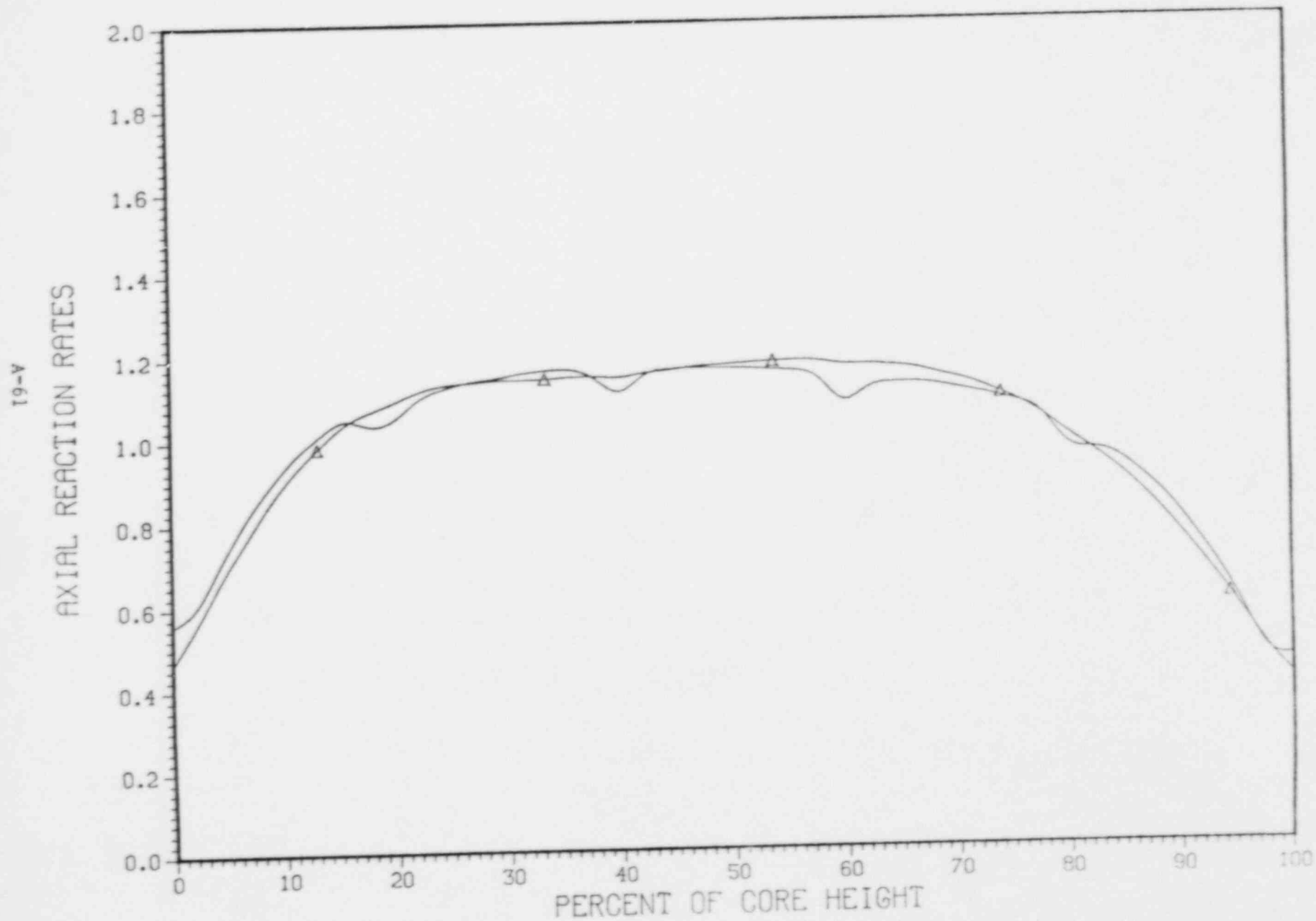


FIGURE 5-5F

YANKEE CORE 19
FIXED DETECTOR #4 VERSUS SYMMETRIC MOVEABLE #19
NORMALIZED RELATIVE AXIAL SHAPES 5524. MWD/MTU

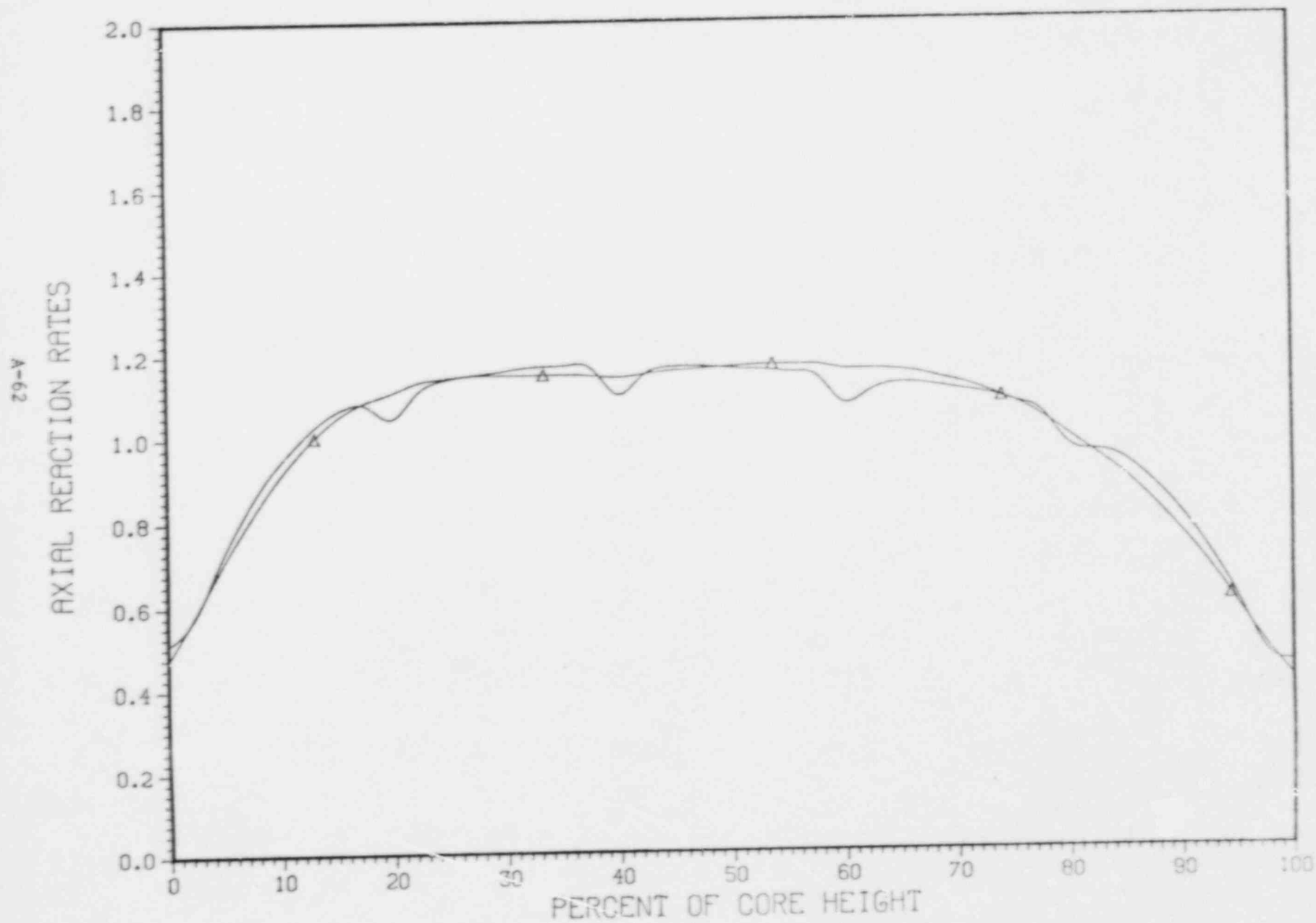


FIGURE 5-56

YANKEE CORE 19

FIXED DETECTOR #4 VERSUS SYMMETRIC MOVEABLE #19

NORMALIZED RELATIVE AXIAL SHAPES 6735. MWD/MTU

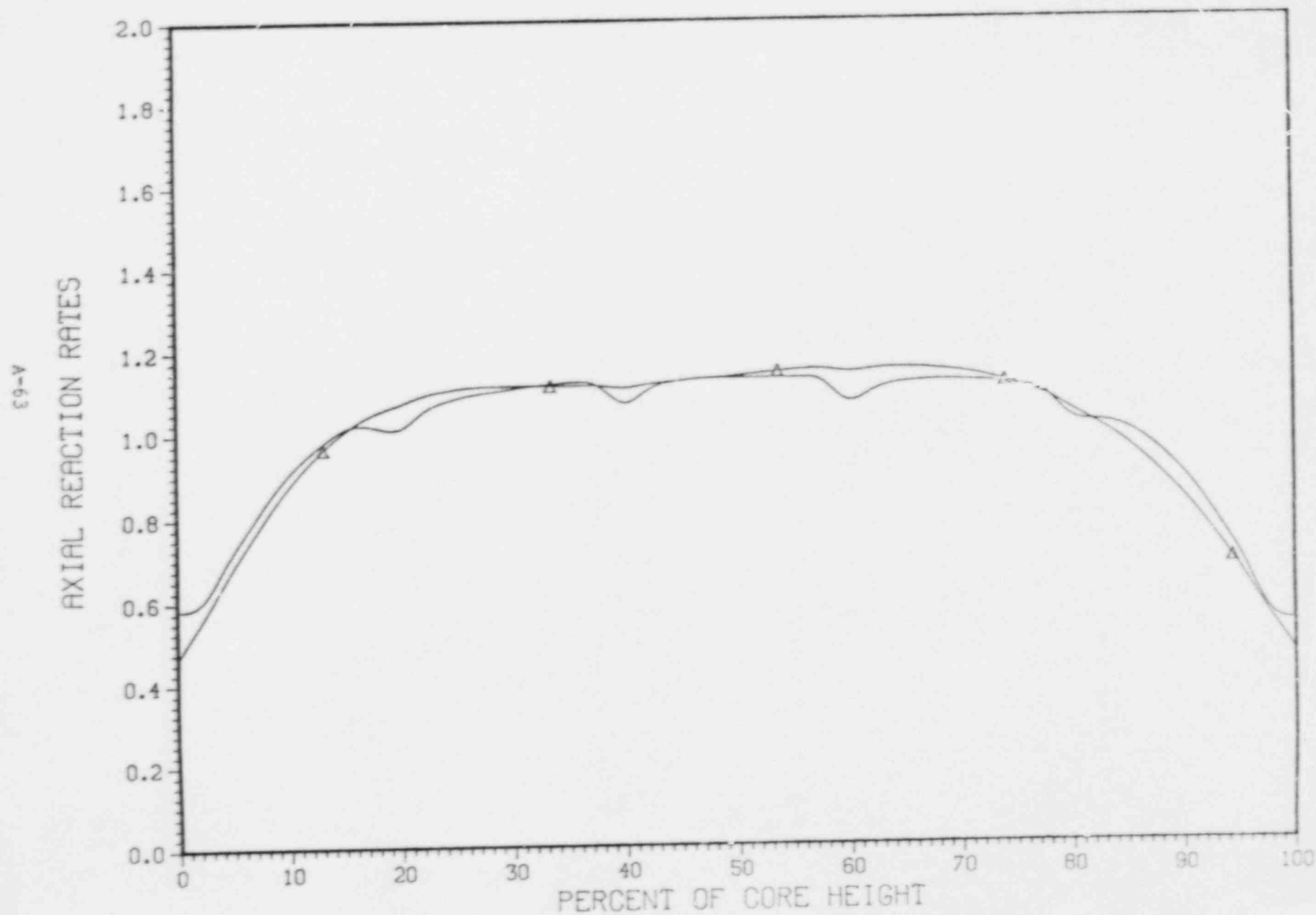


FIGURE 5-5H

YANKEE CORE 19
FIXED DETECTOR #21 VERSUS SYMMETRIC MOVEABLE #2
NORMALIZED RELATIVE AXIAL SHAPES 71. MWD/MTU

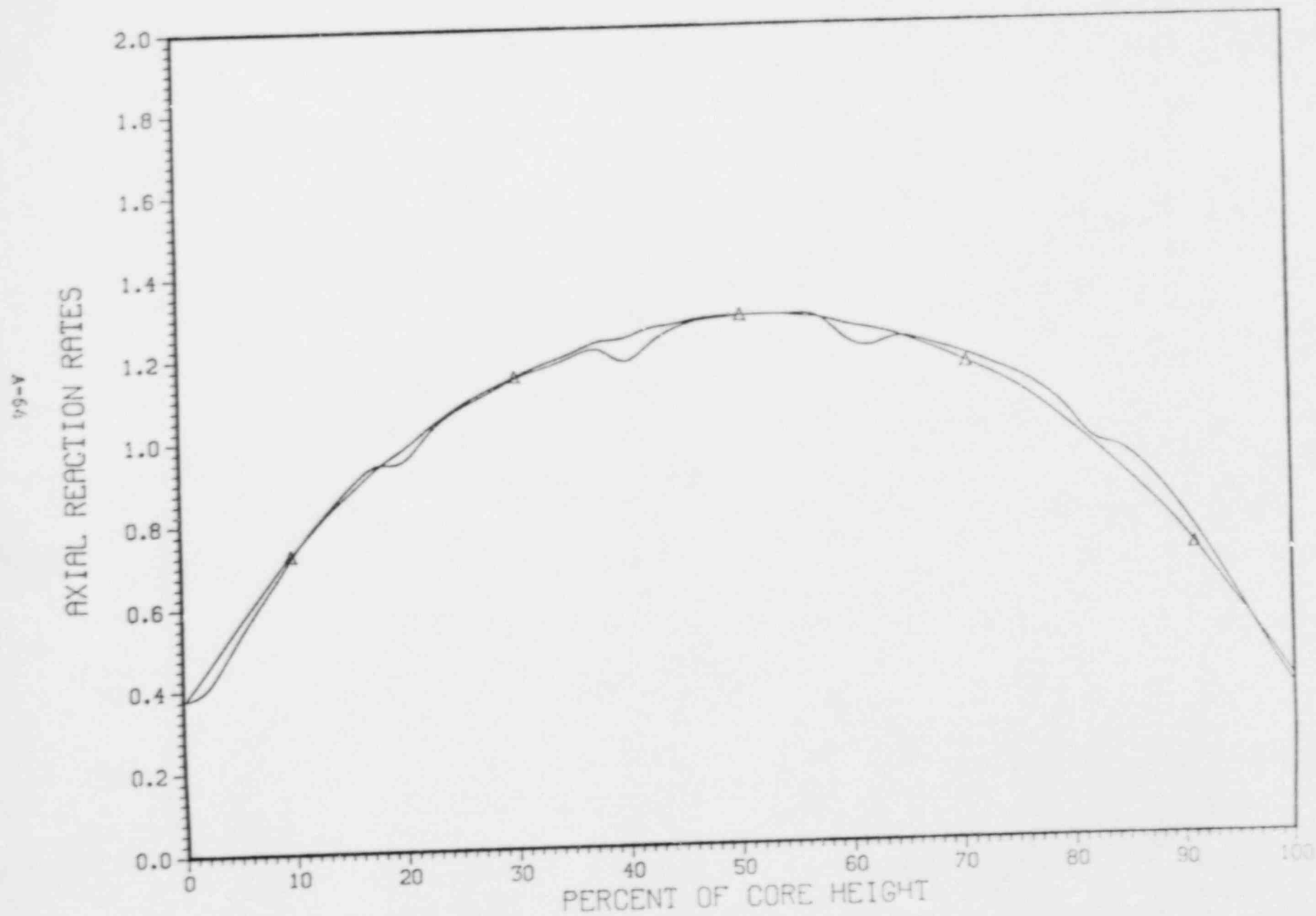


FIGURE 5-6A

YANKEE CORE 19

FIXED DETECTOR #21 VERSUS SYMMETRIC MOVEABLE #2
NORMALIZED RELATIVE AXIAL SHAPES 161. MWD/MTU

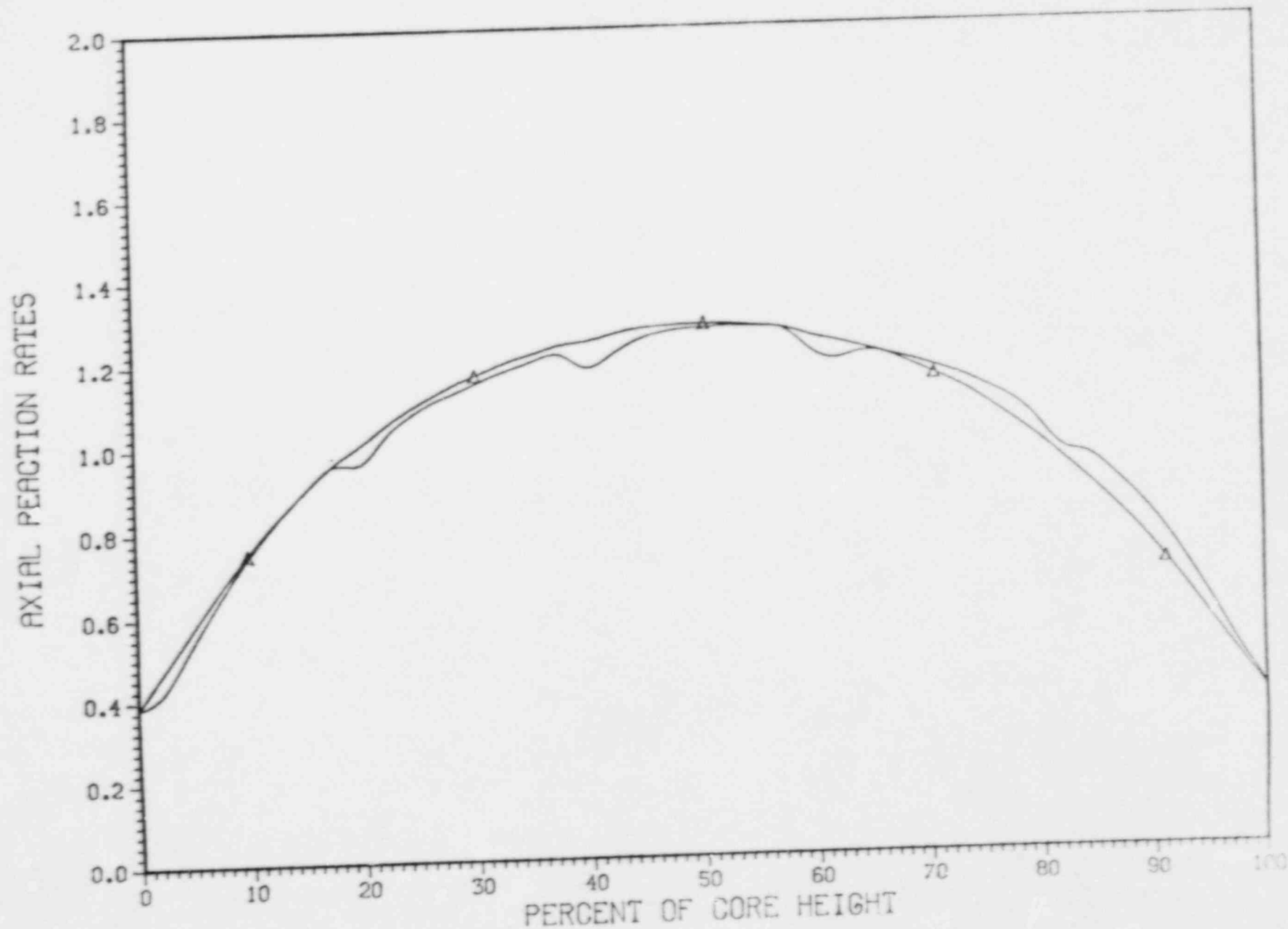


FIGURE 5-68

YANKEE CORE 19

FIXED DETECTOR #21 VERSUS SYMMETRIC MEASUREMENT #2
NORMALIZED RELATIVE AXIAL SHAPES 1373. MWD/MTU

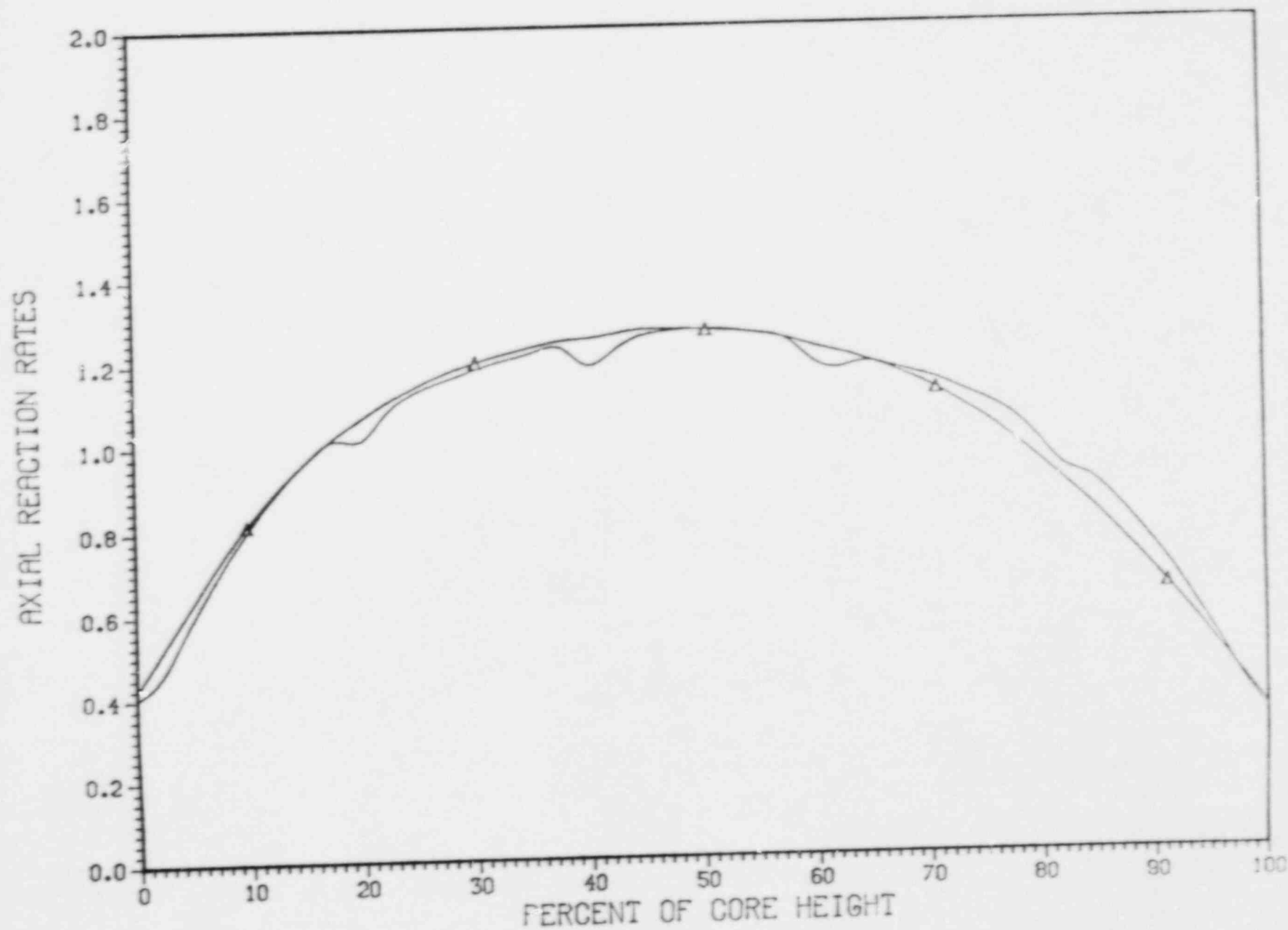


FIGURE 5-6C

YANKEE CORE 19

FIXED DETECTOR #21 VERSUS SYMMETRIC MOVEABLE #2

NORMALIZED RELATIVE AXIAL SHAPES 2573. MWD/MTU

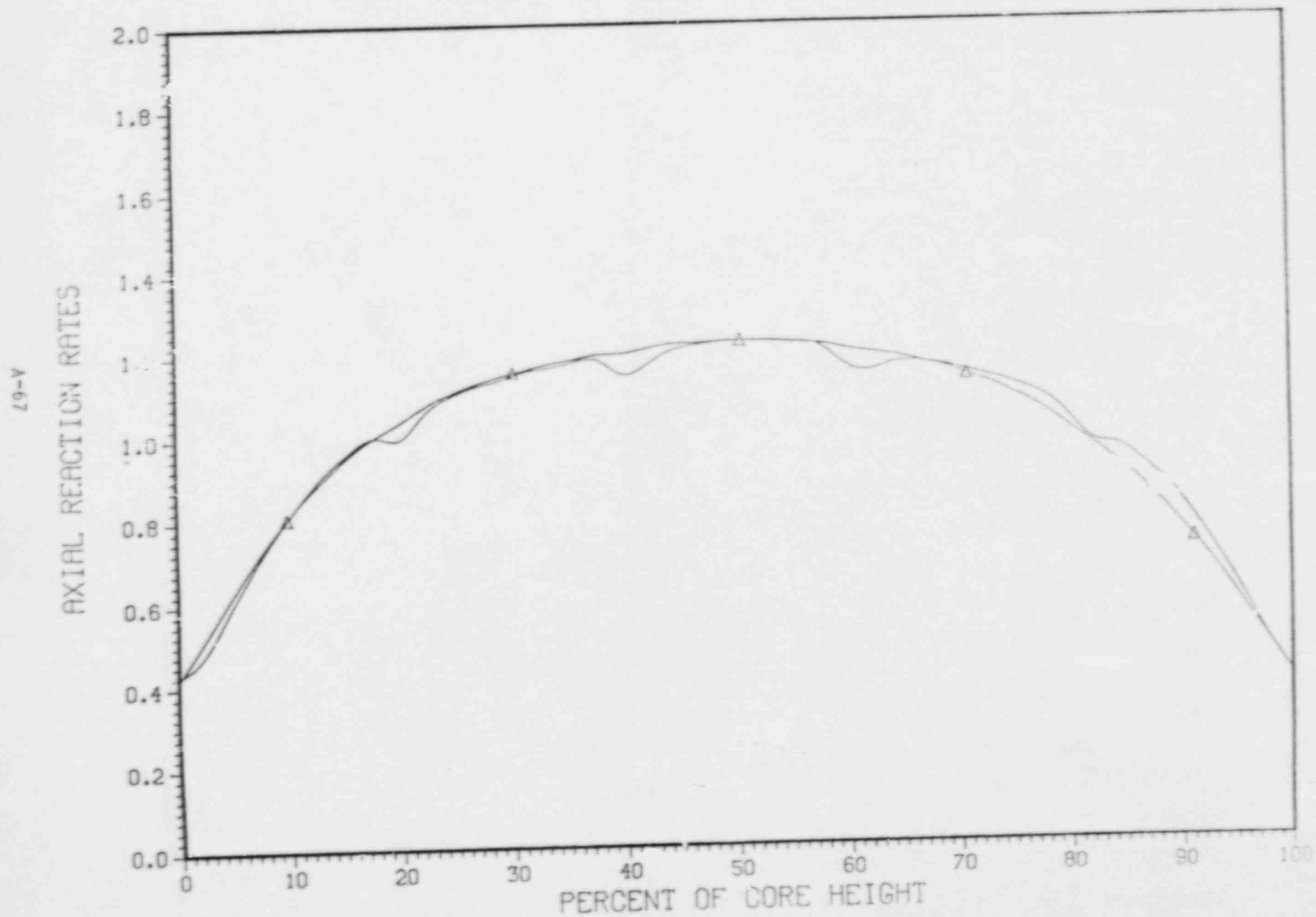


FIGURE 5-60

YANKEE CORE 19
FIXED DETECTOR #21 VERSUS SYMMETRIC MOVEABLE #2
NORMALIZED RELATIVE AXIAL SHAPES 3683. MWD/MTU

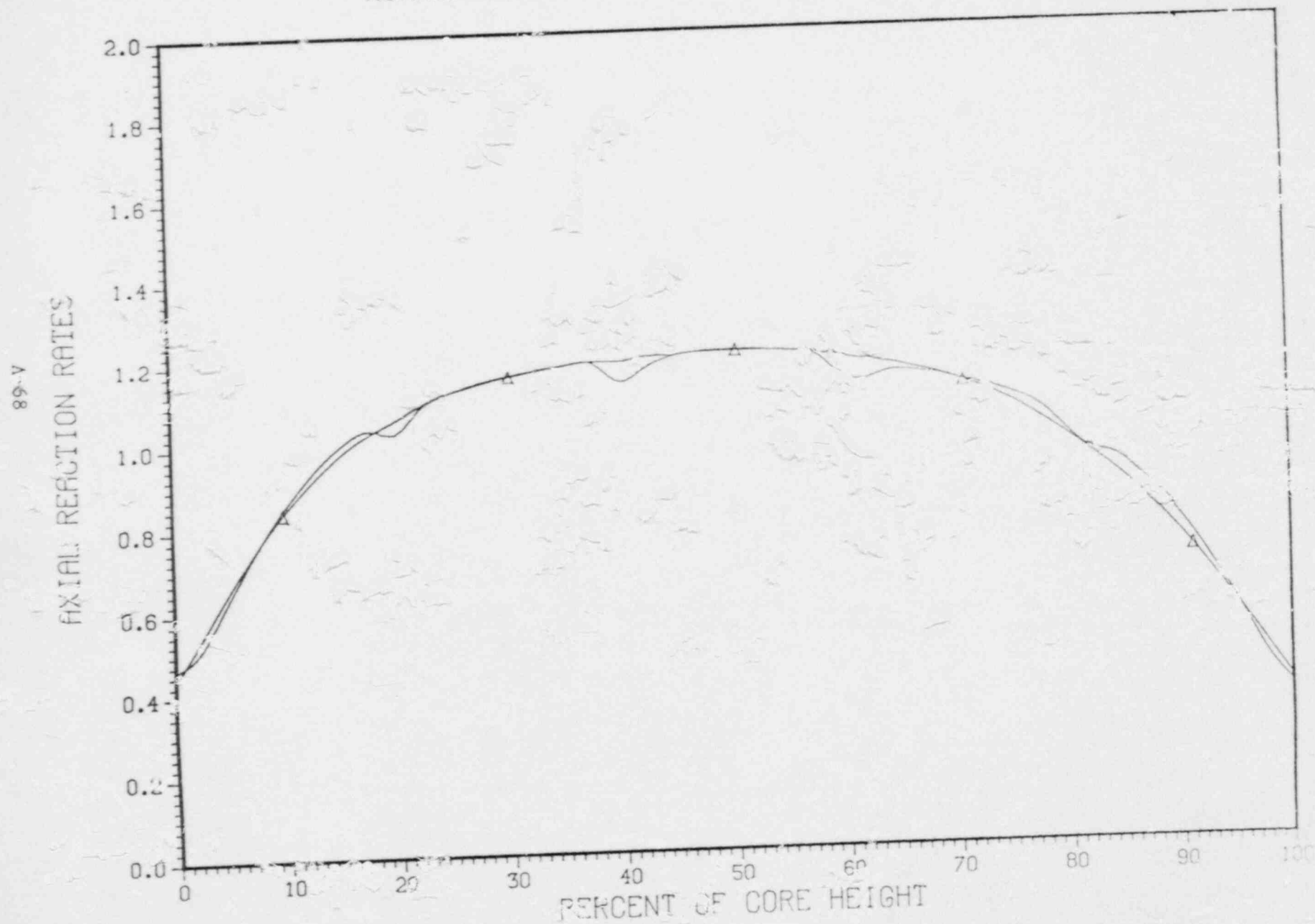


FIGURE 5-6E

YANKEE CORE 19

FIXED DETECTOR #21 VERSUS SYMMETRIC MOVEABLE #2

NORMALIZED RELATIVE AXIAL SHAPES 4843. MWD/MTU

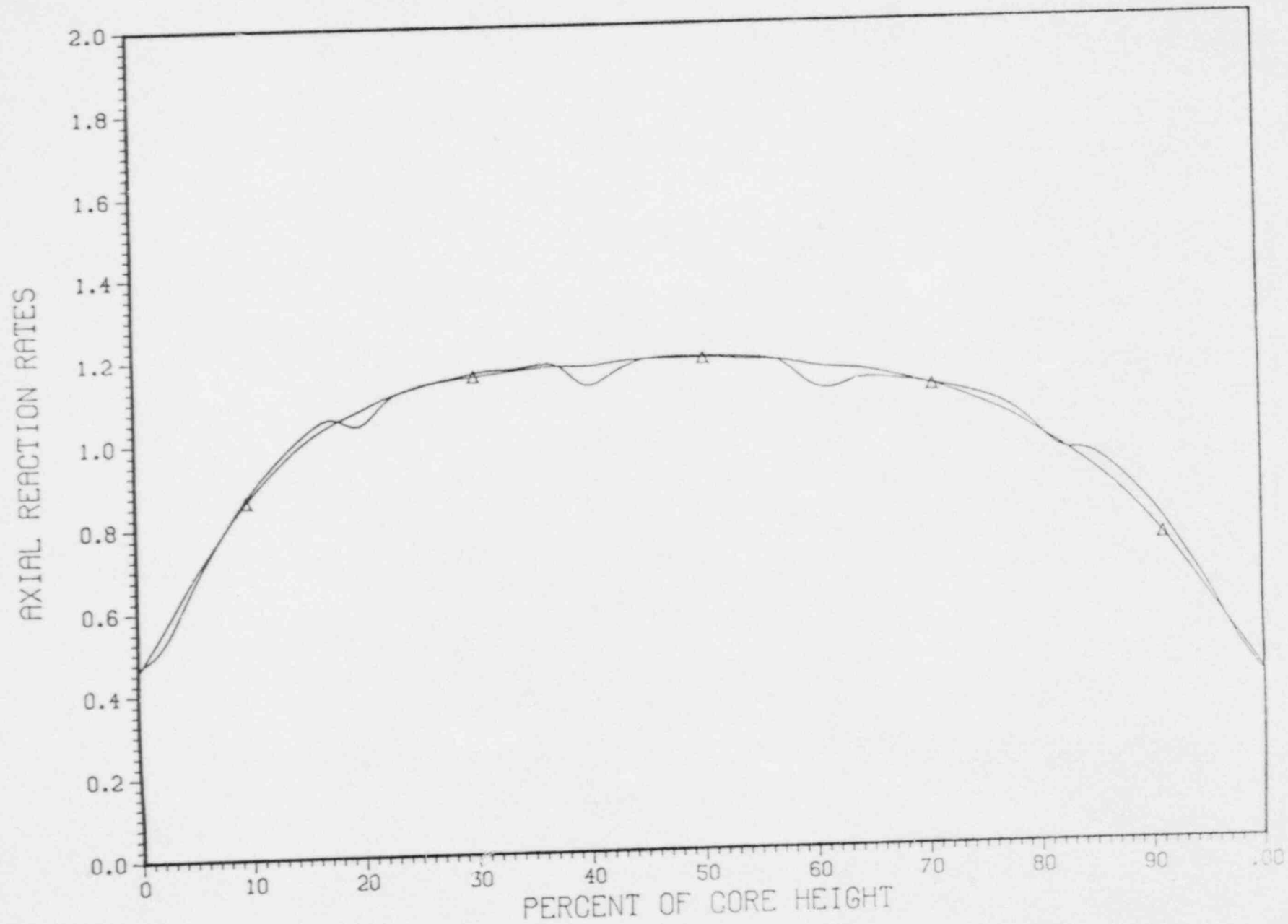


FIGURE 5-6F

YANKEE CORE 19
FIXED DETECTOR #21 VERSUS SYMMETRIC MOVEABLE #2
NORMALIZED RELATIVE AXIAL SHAPES 5524. MWD/MTU

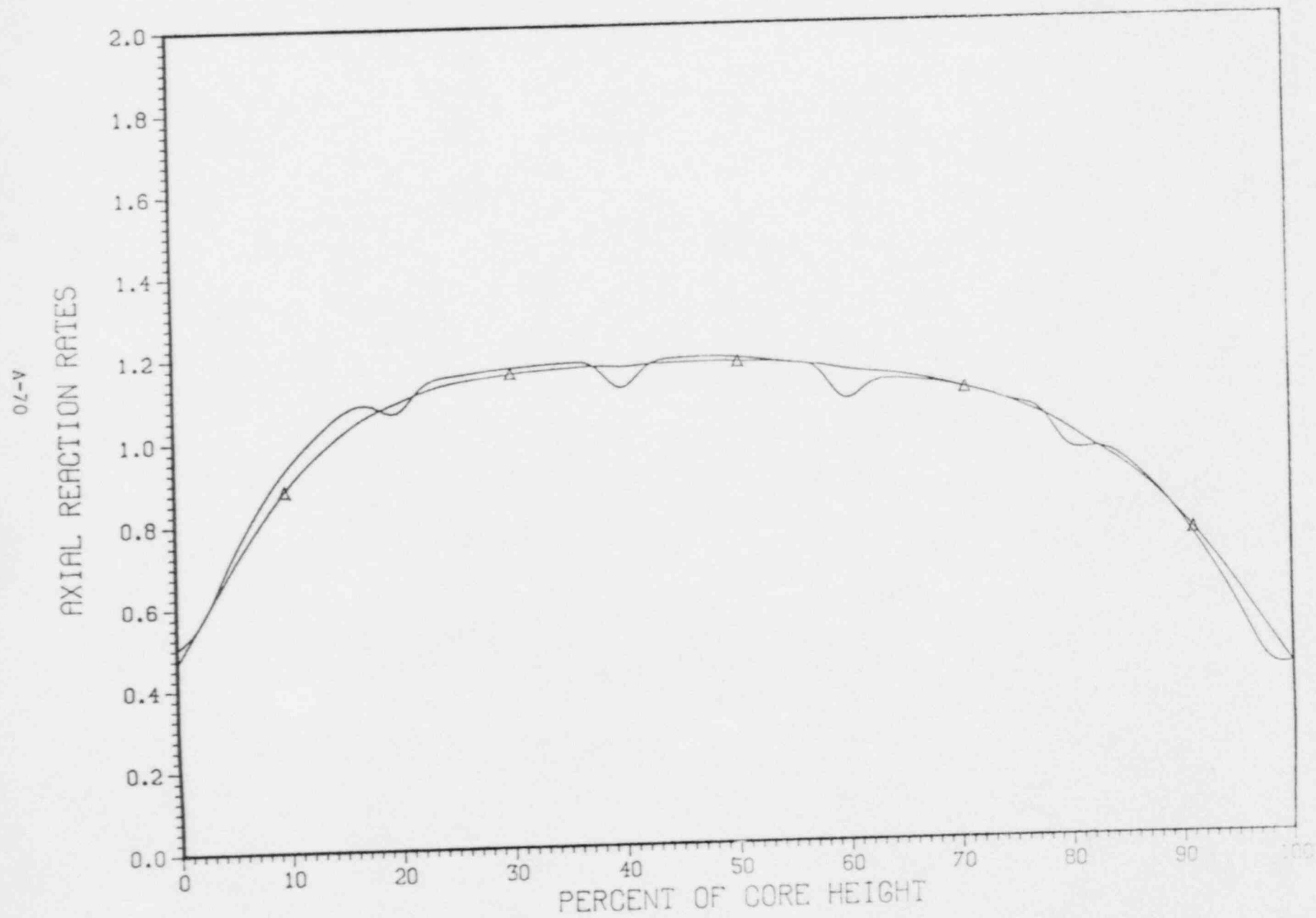


FIGURE 5-66

YANKEE CORE 19

FIXED DETECTOR #21 VERSUS SYMMETRIC MOVEABLE #2
NORMALIZED RELATIVE AXIAL SHAPES 6735. MWD/MTU

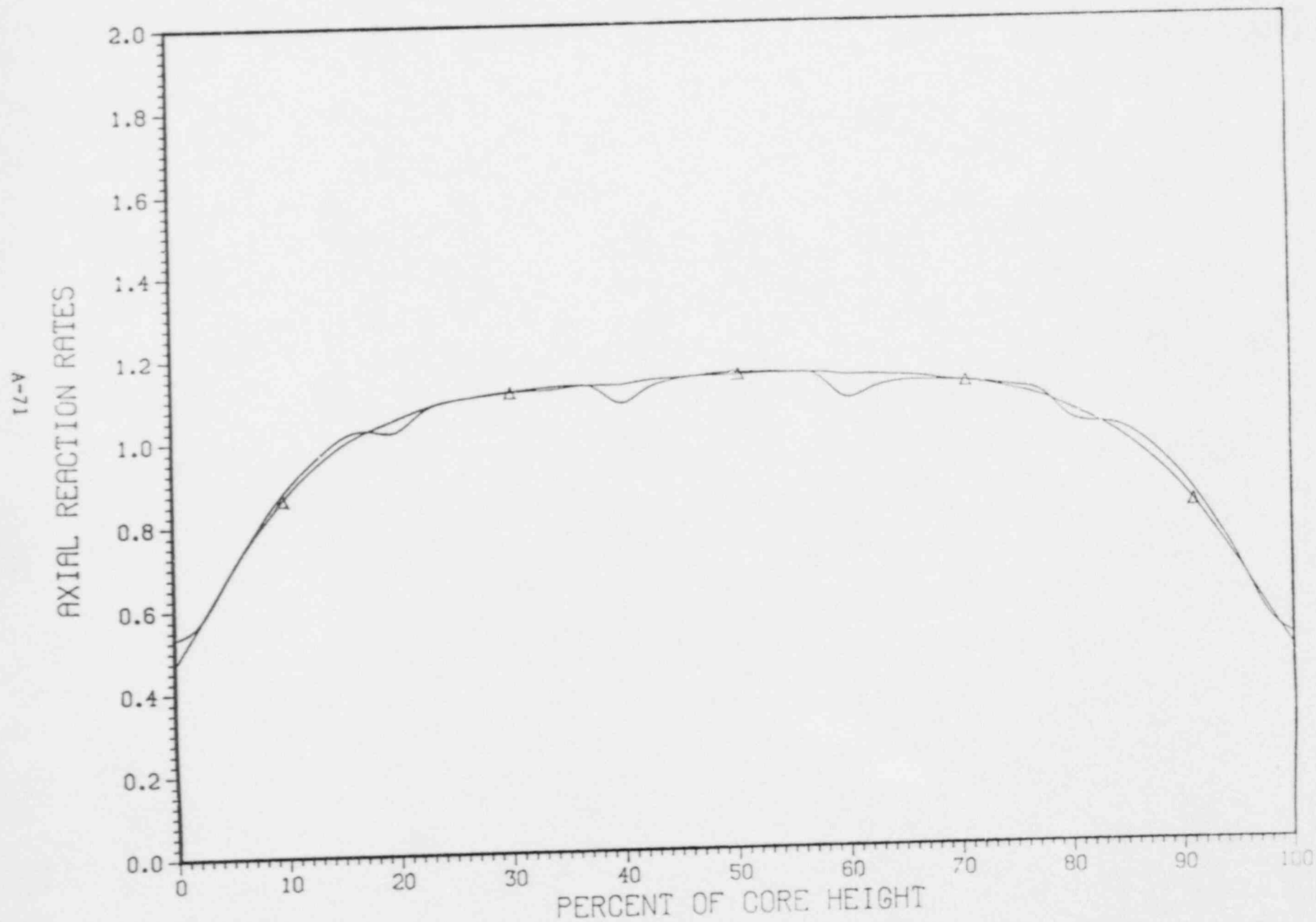


FIGURE 5-6H

YANKEE CORE 19

FIXED DETECTOR #22 VERSUS SYMMETRIC MOVEABLE #1
NORMALIZED RELATIVE AXIAL SHAPES 71. MWD/MTU

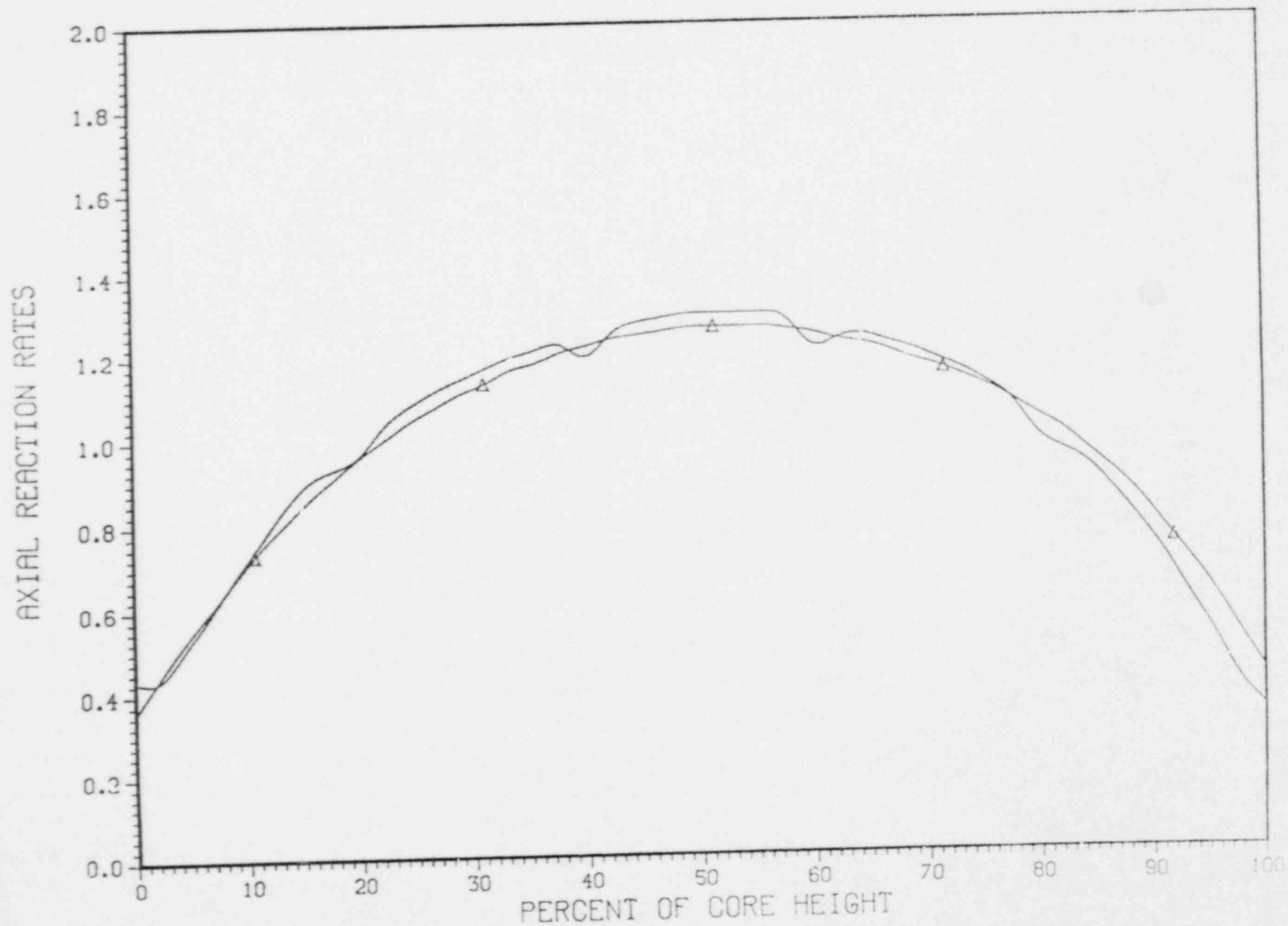


FIGURE 5-7A

YANKEE CORE 19
FIXED DETECTOR #22 VERSUS SYMMETRIC MOVEABLE #1
NORMALIZED RELATIVE AXIAL SHAPES 161. MWD/MTU

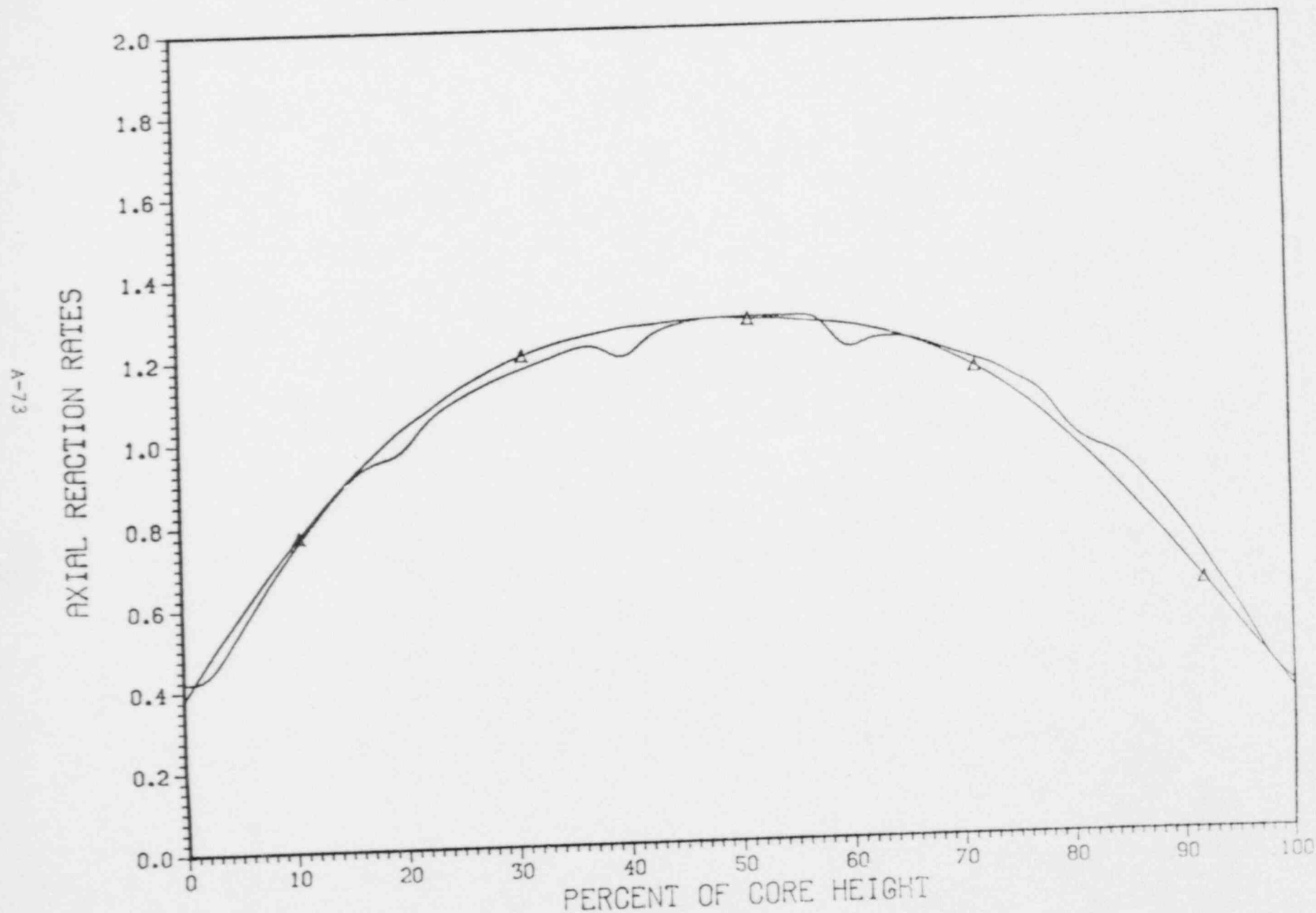


FIGURE 5-7B

YANKEE CORE 19
FIXED DETECTOR #22 VERSUS SYMMETRIC MOVEABLE #1
NORMALIZED RELATIVE AXIAL SHAPES 1373. MWD/MTU

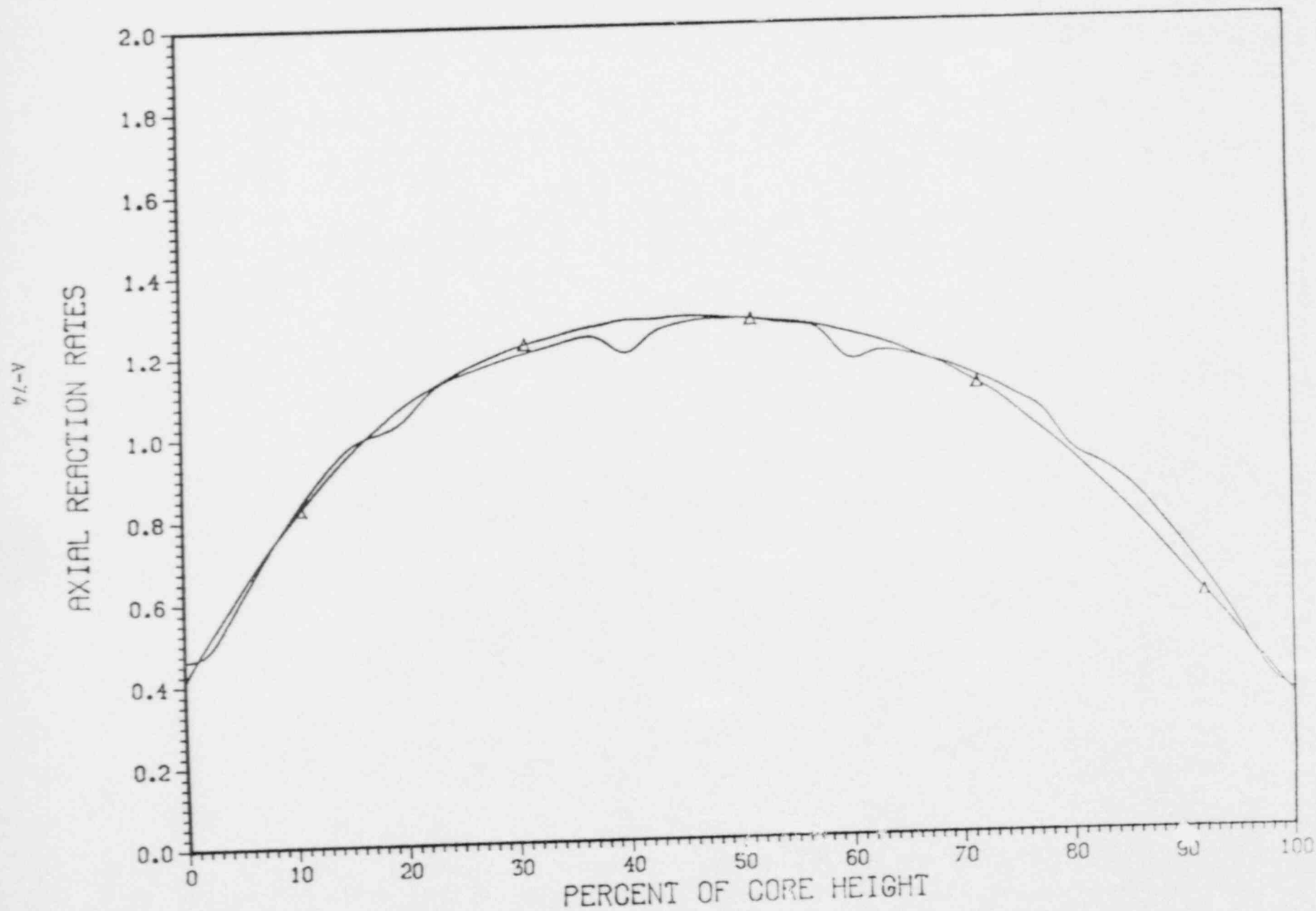


FIGURE 5-7C

YANKEE CORE 19
FIXED DETECTOR #22 VERSUS SYMMETRIC MOVEABLE #1
NORMALIZED RELATIVE AXIAL SHAPES 2573. MWD/MTU

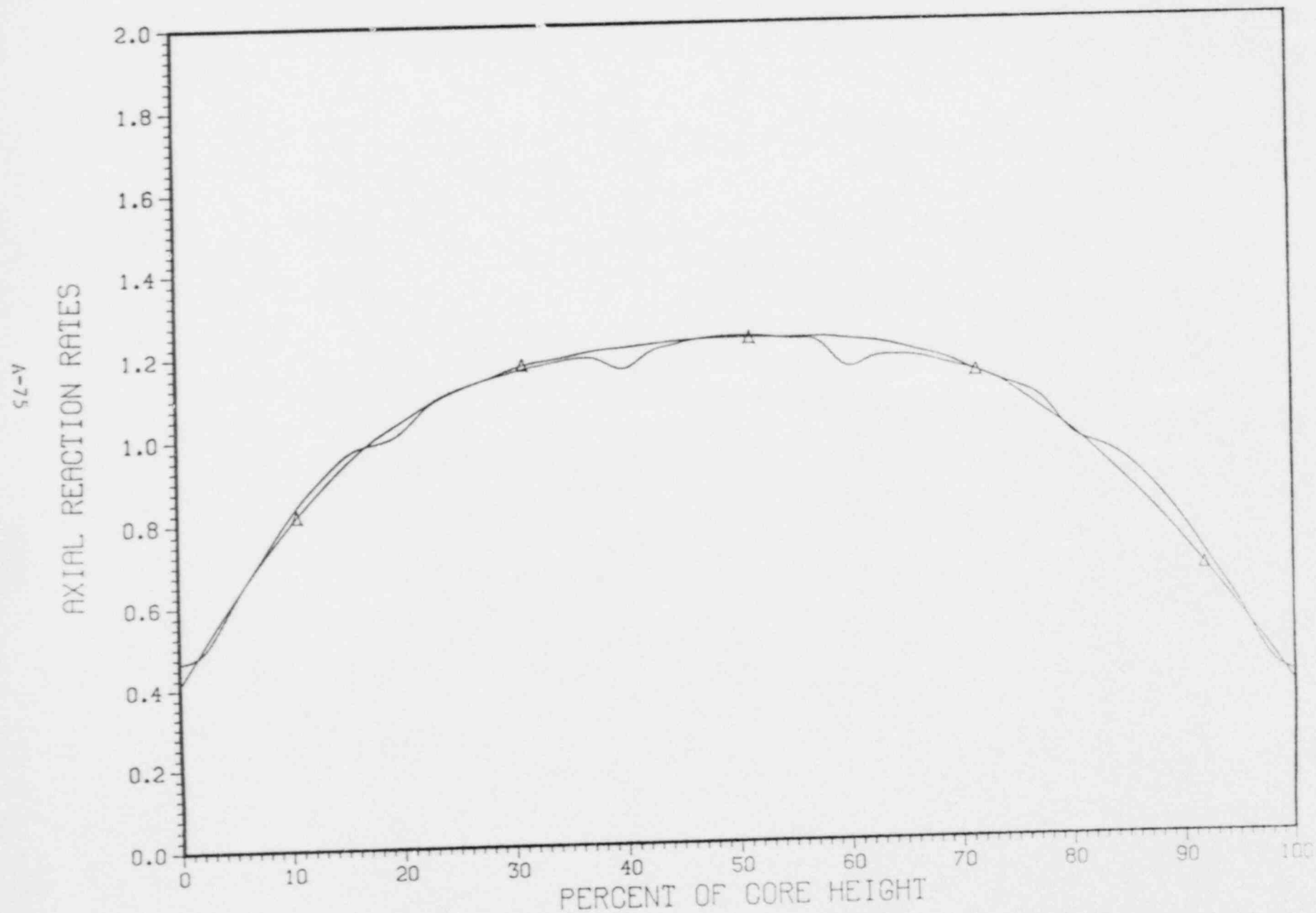


FIGURE 5-7D

YANKEE CORE 19
FIXED DETECTOR #22 VERSUS SYMMETRIC MOVEABLE #1
NORMALIZED RELATIVE AXIAL SHAPES 3683. MWD/MTU

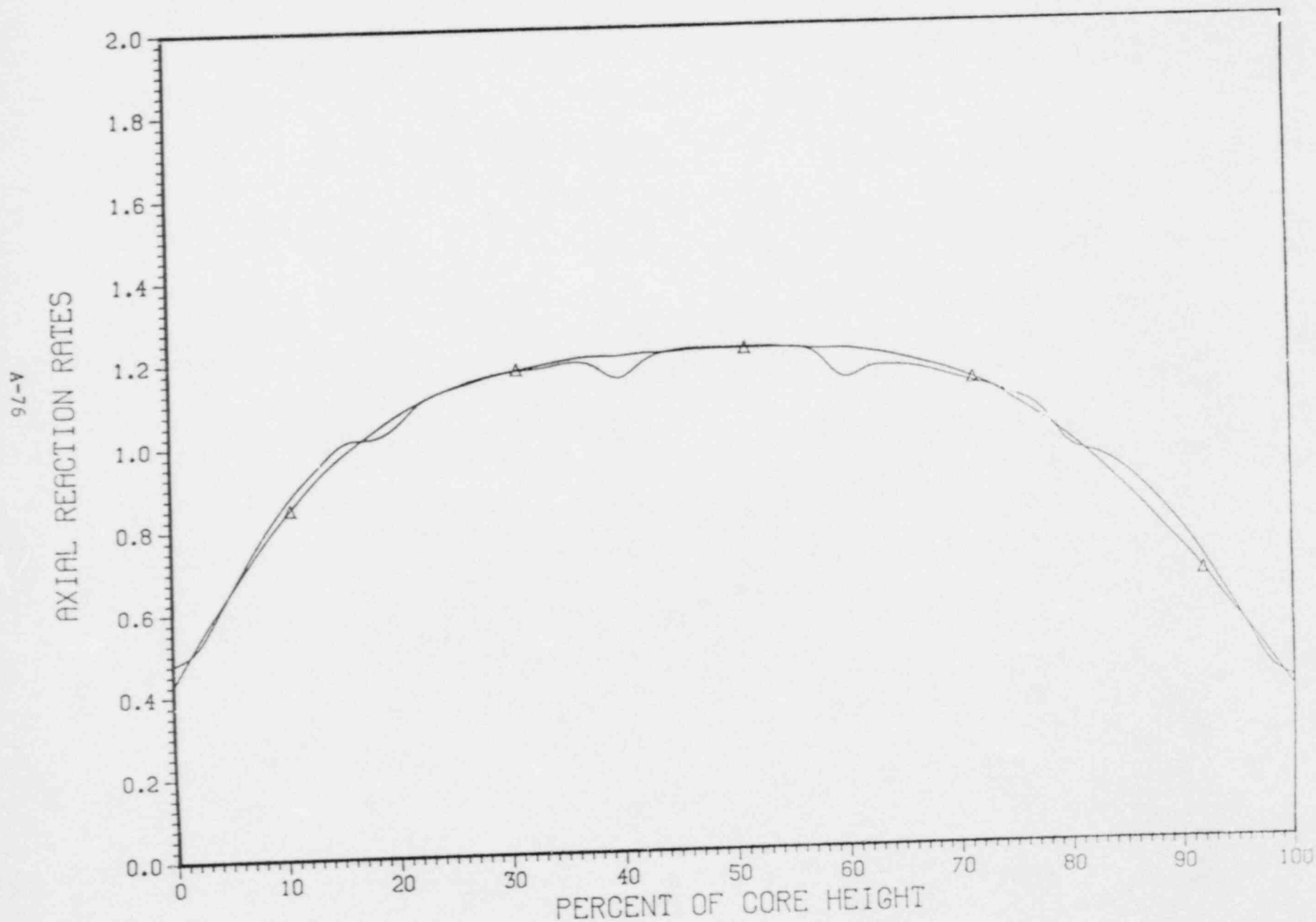


FIGURE 5-7E

YANKEE CORE 19
FIXED DETECTOR #22 VERSUS SYMMETRIC MOVEABLE #1
NORMALIZED RELATIVE AXIAL SHAPES 4843. MWD/MTU

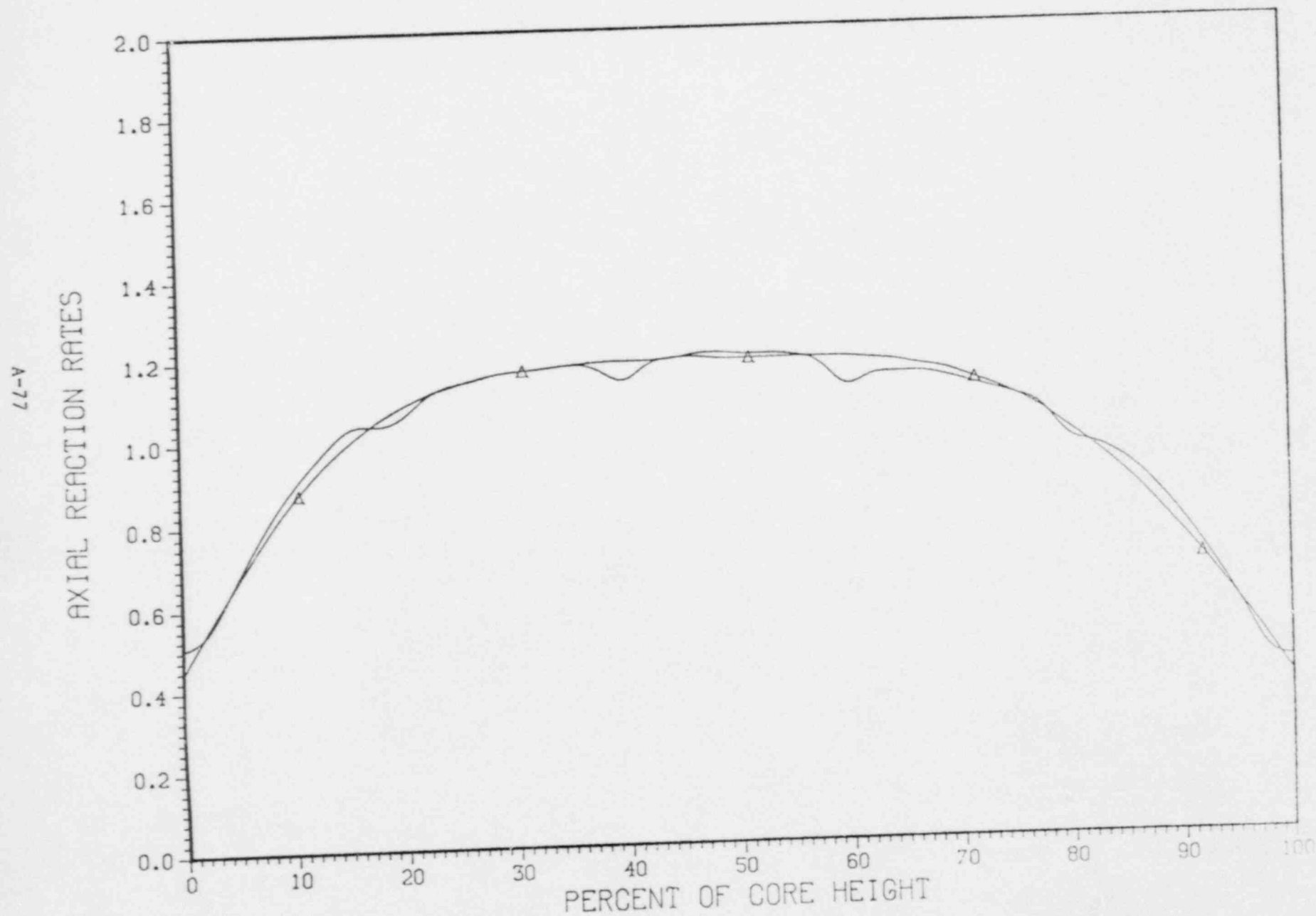


FIGURE 5-7F

YANKEE CORE 19

FIXED DETECTOR #22 VERSUS SYMMETRIC MOVEABLE #1
NORMALIZED RELATIVE AXIAL SHAPES 5524. MWD/MTU

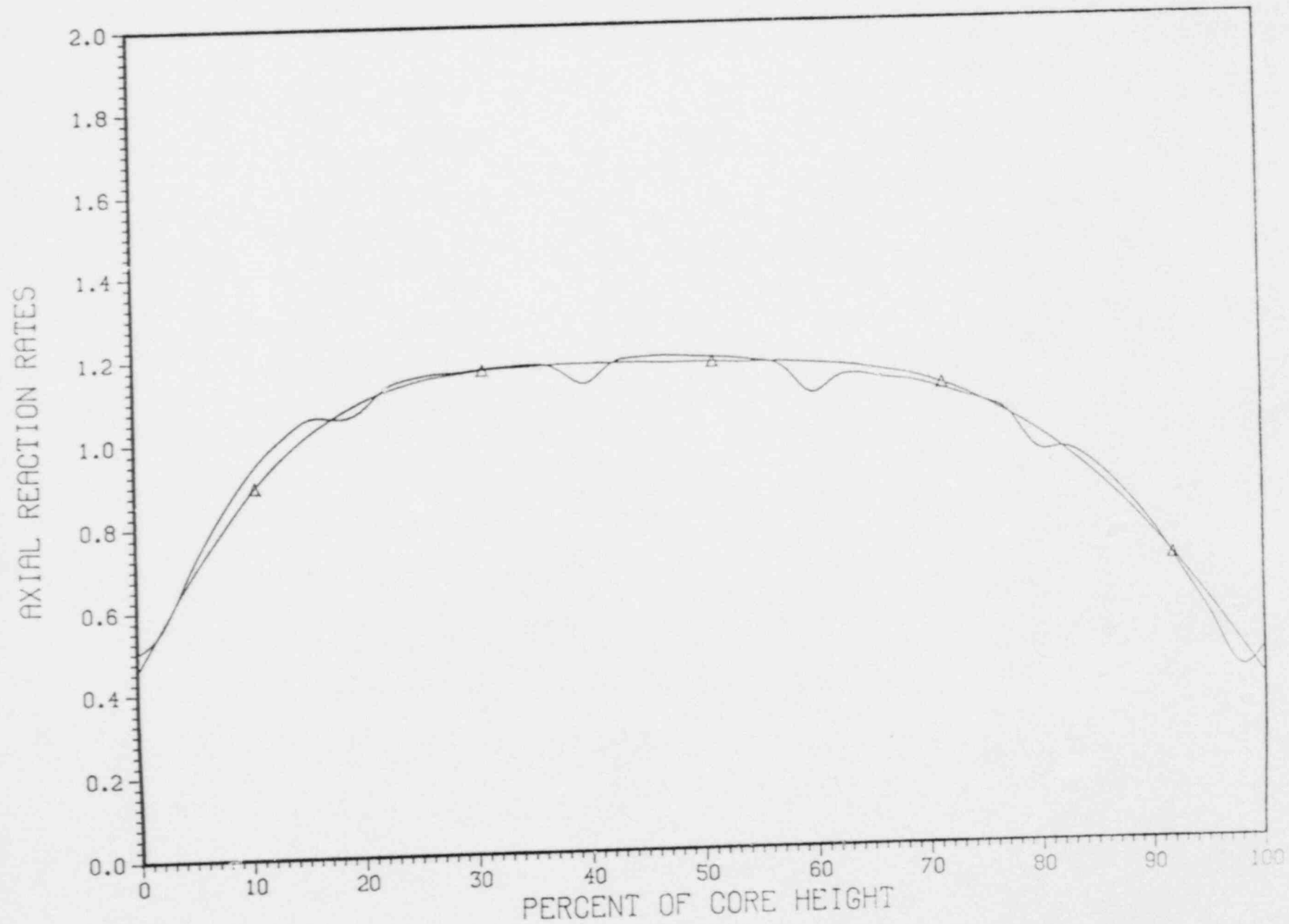


FIGURE 5-76

YANKEE CORE 19
FIXED DETECTOR #22 VERSUS SYMMETRIC MOVEABLE #1
NORMALIZED RELATIVE AXIAL SHAPES 6735. MWD/MTU

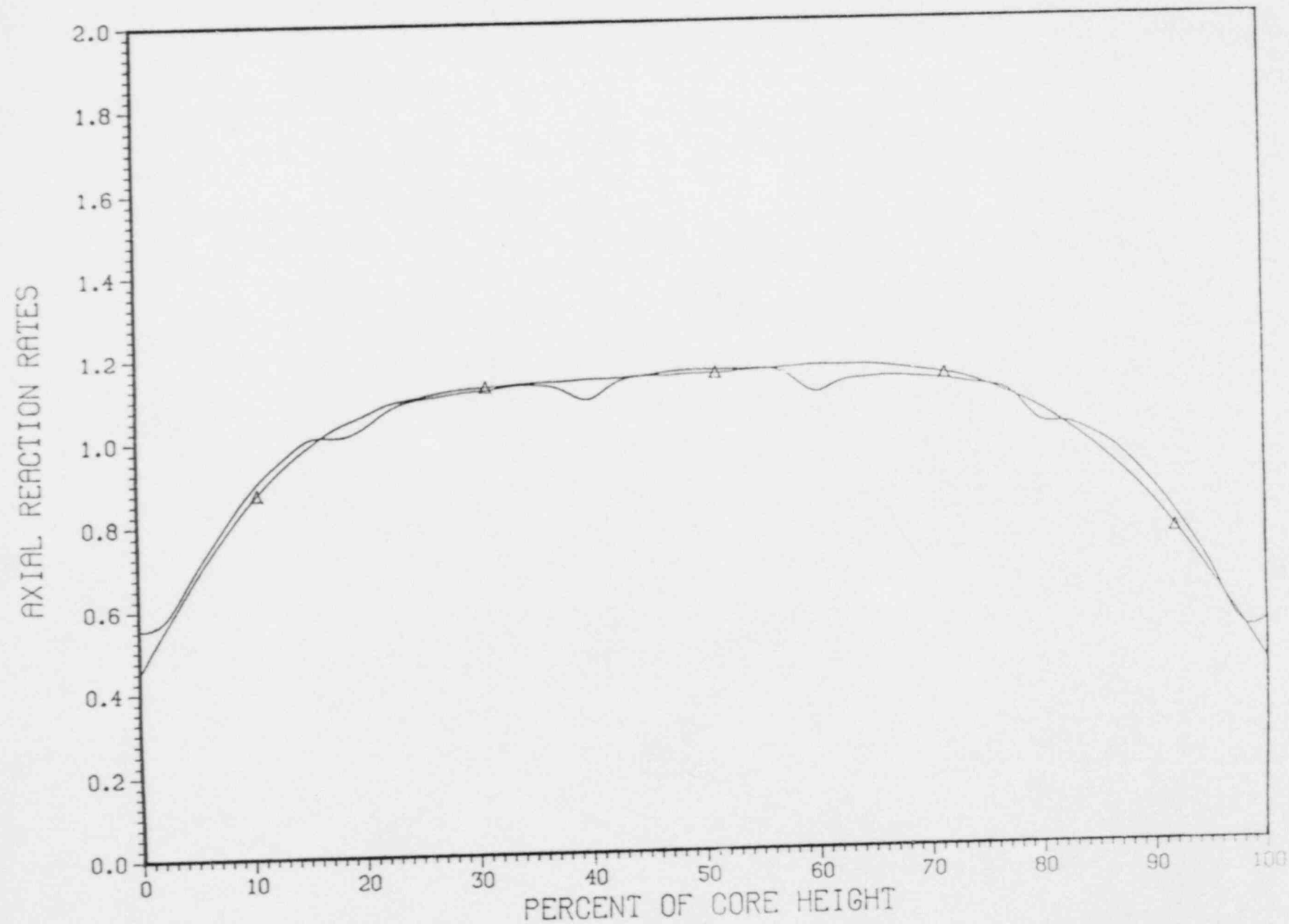


FIGURE 5-7H

YANKEE CORE 19

KW/FT VS EXPOSURE USING INCORE DETECTION SYSTEMS

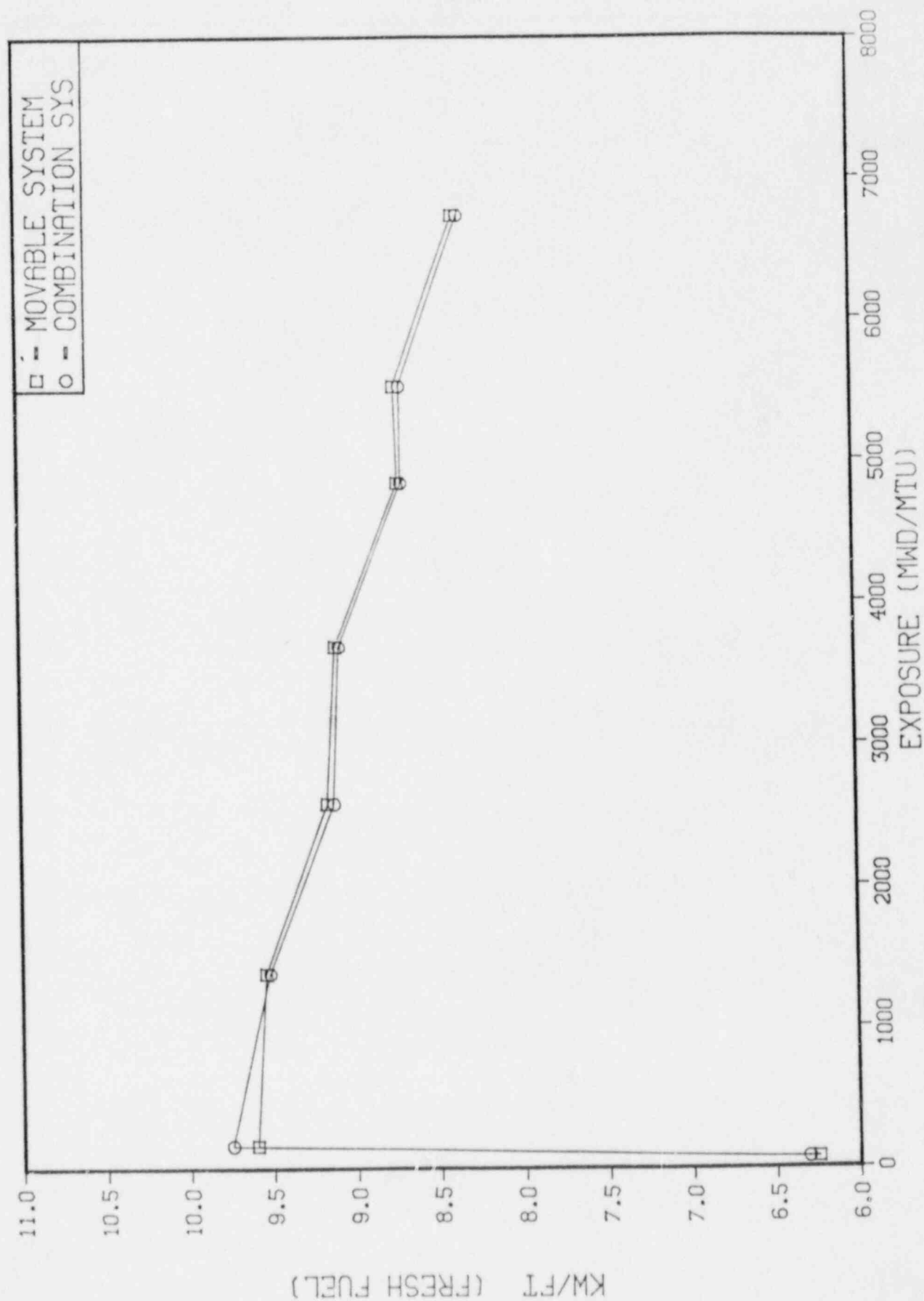
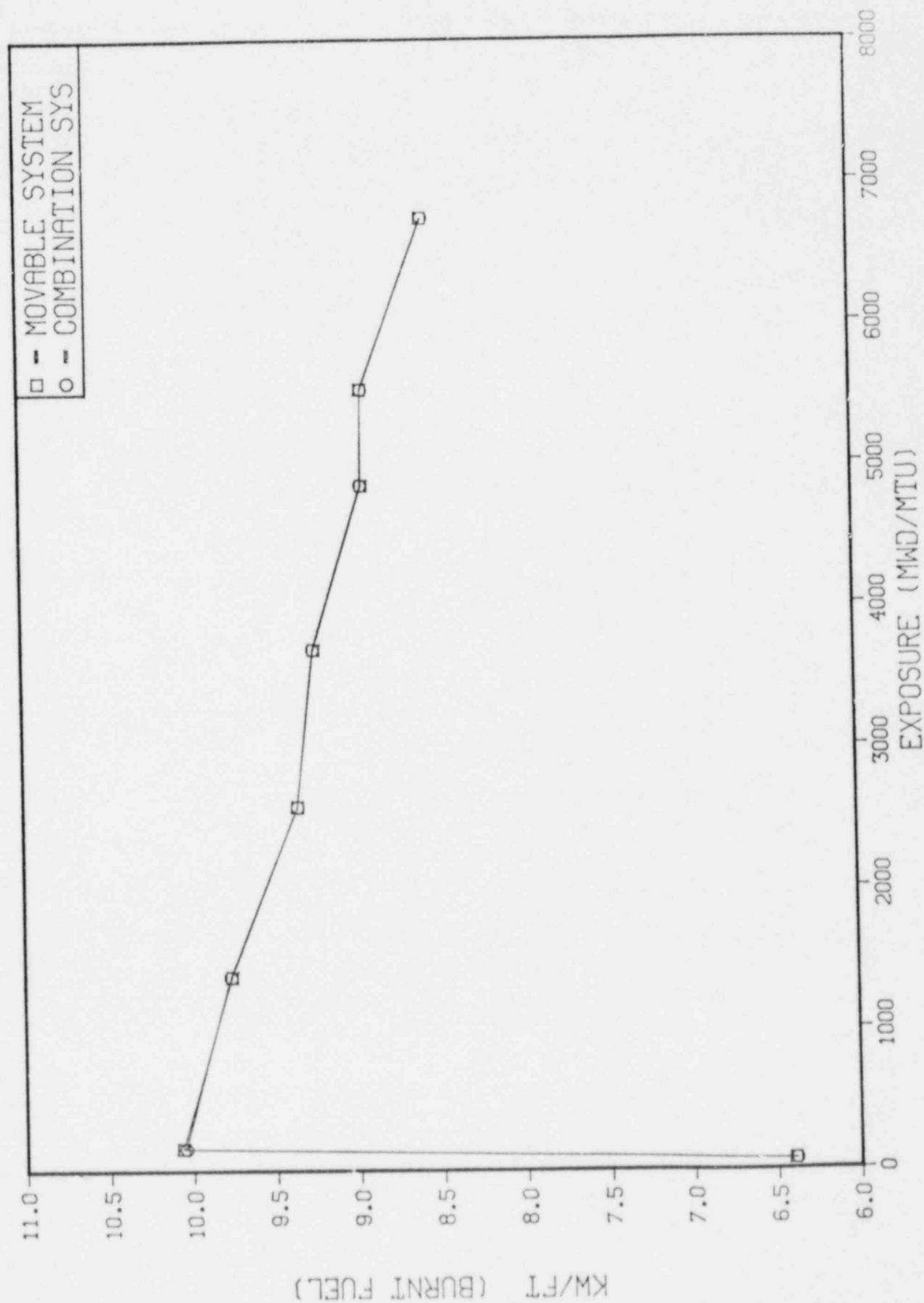


FIGURE 5-8

YANKEE CORE 19
KW/FT VS EXPOSURE USING INCORE DETECTION SYSTEMS



YANKEE CORE 19

FQ VS EXPOSURE USING COMBINATION INCORE DETECTION SYSTEMS

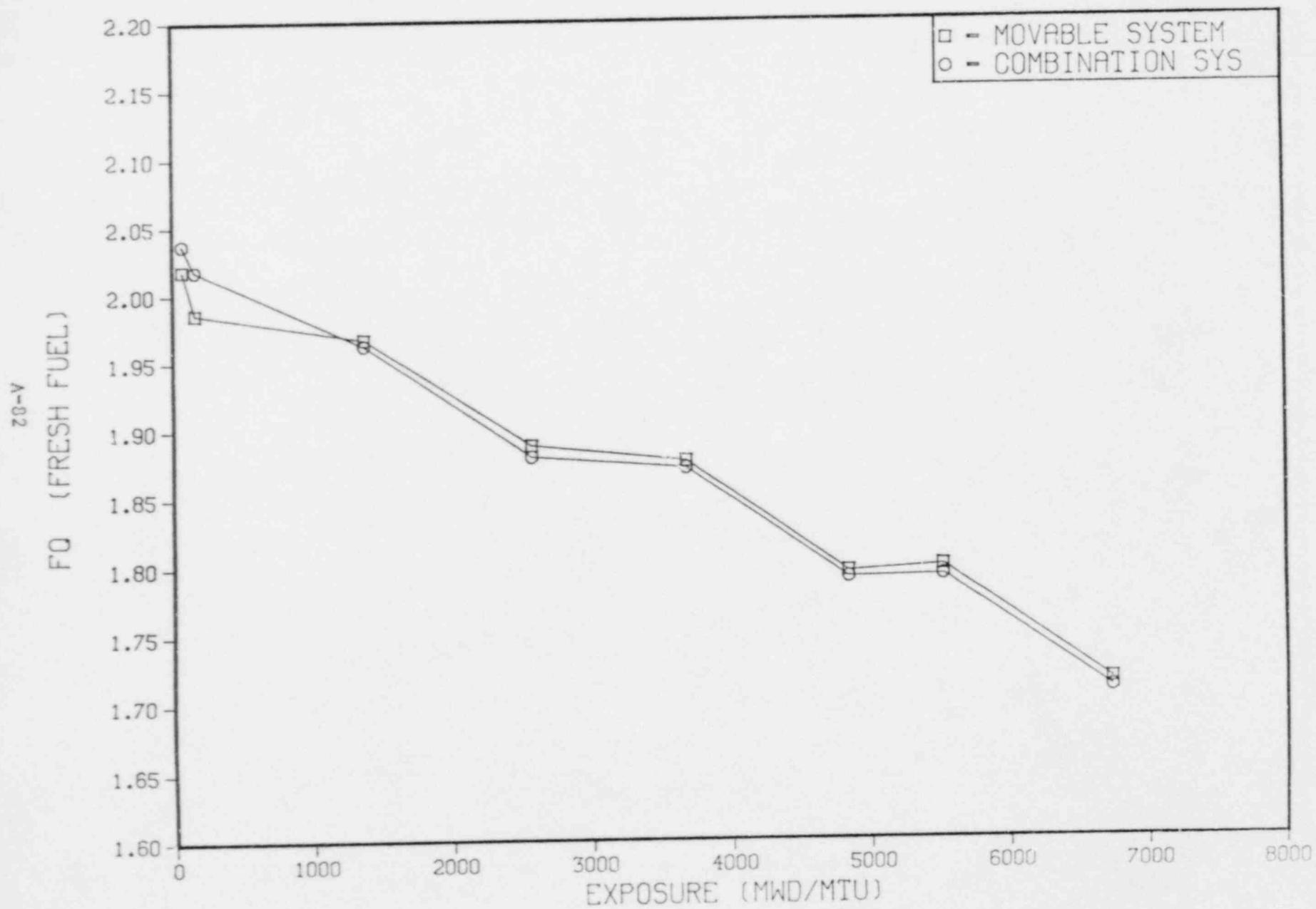


FIGURE 5-10

YANKEE CORE 19

F0 VS EXPOSURE USING COMBINATION INCORE DETECTION SYSTEMS

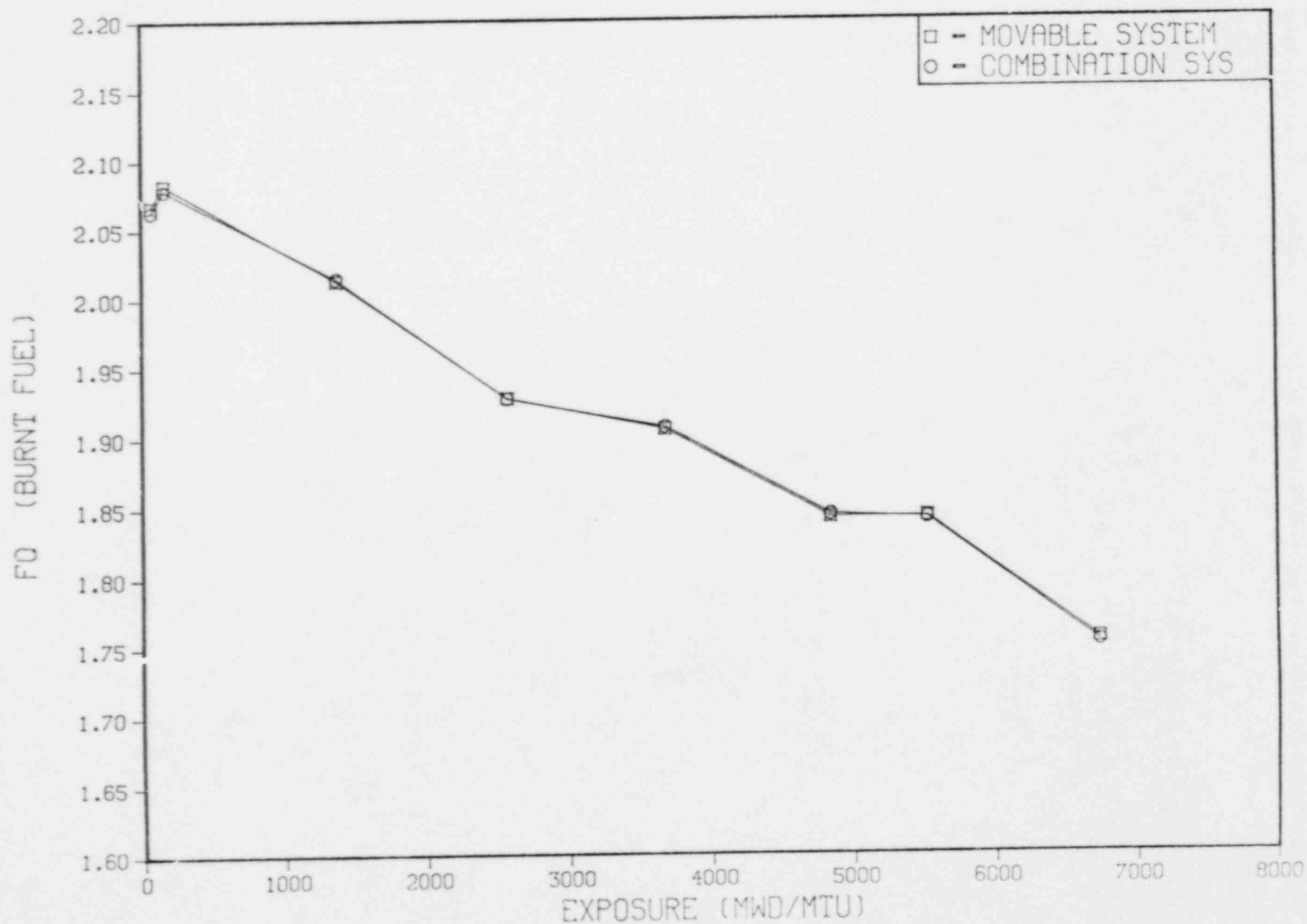


FIGURE 5-11

YANKEE CORE 19

F Δ H VS EXPOSURE USING COMBINATION INCORE DETECTION SYSTEMS

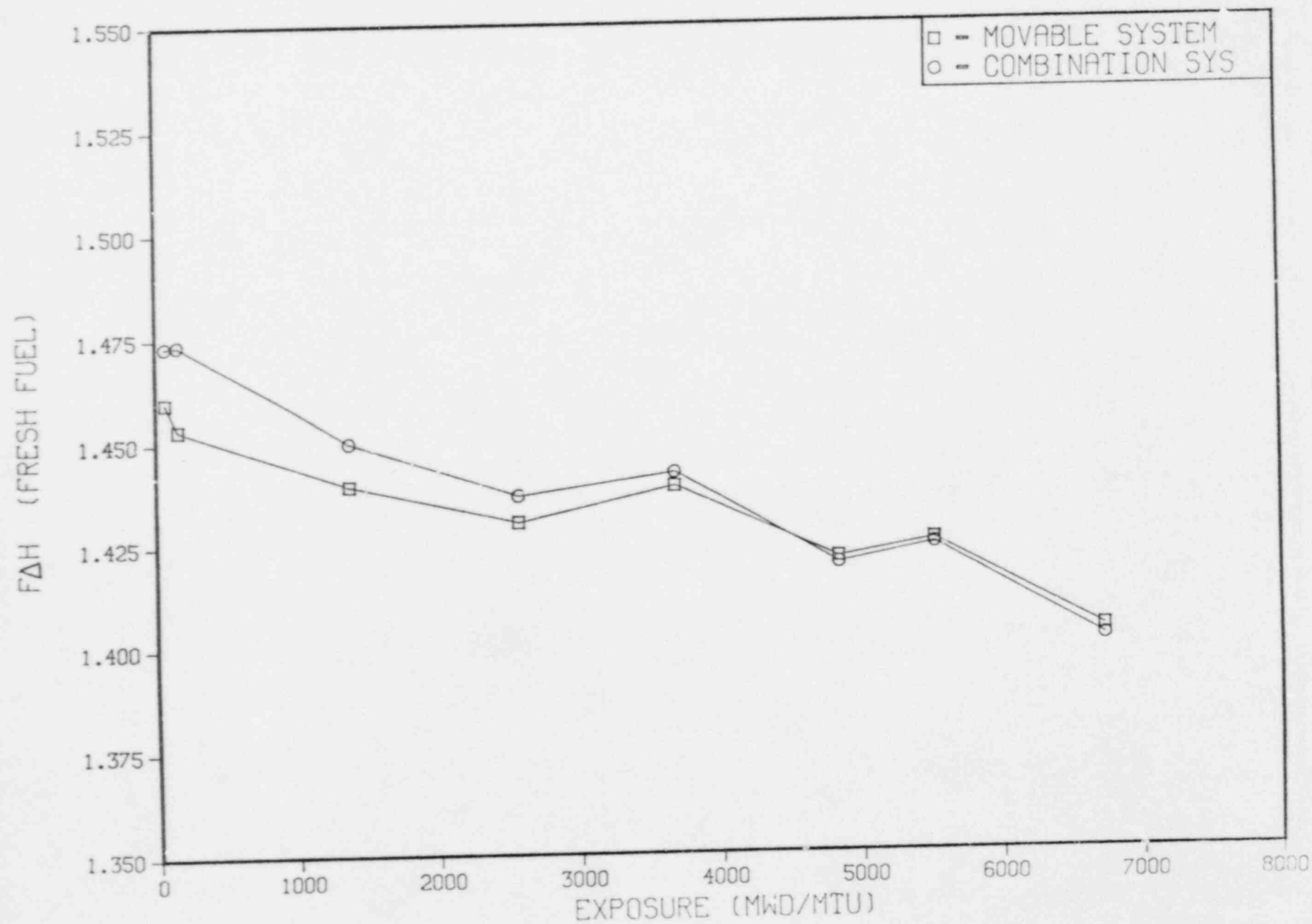


FIGURE 5-12

YANKEE CORE 19

FΔH VS EXPOSURE USING COMBINATION INCORE DETECTION SYSTEMS

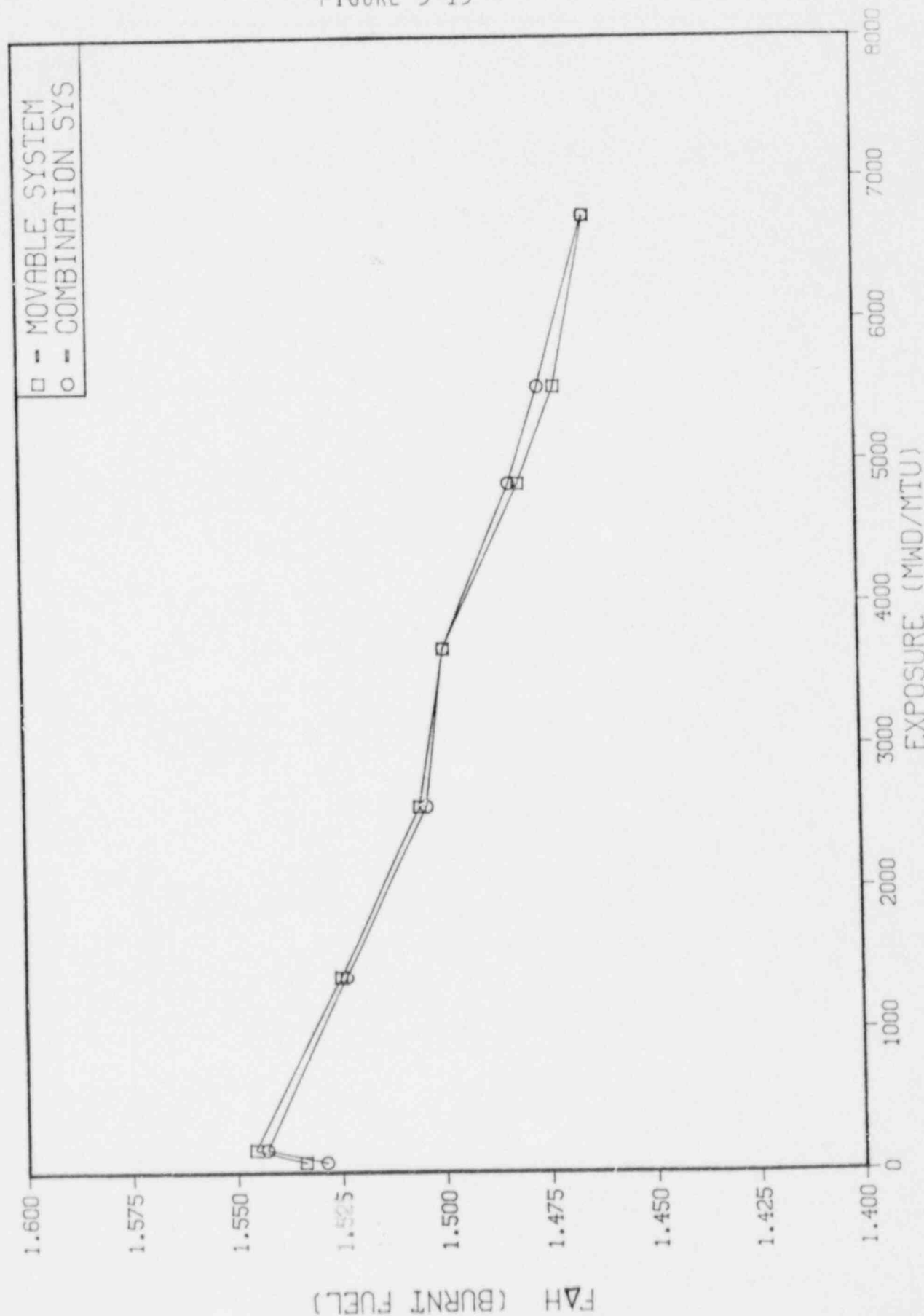
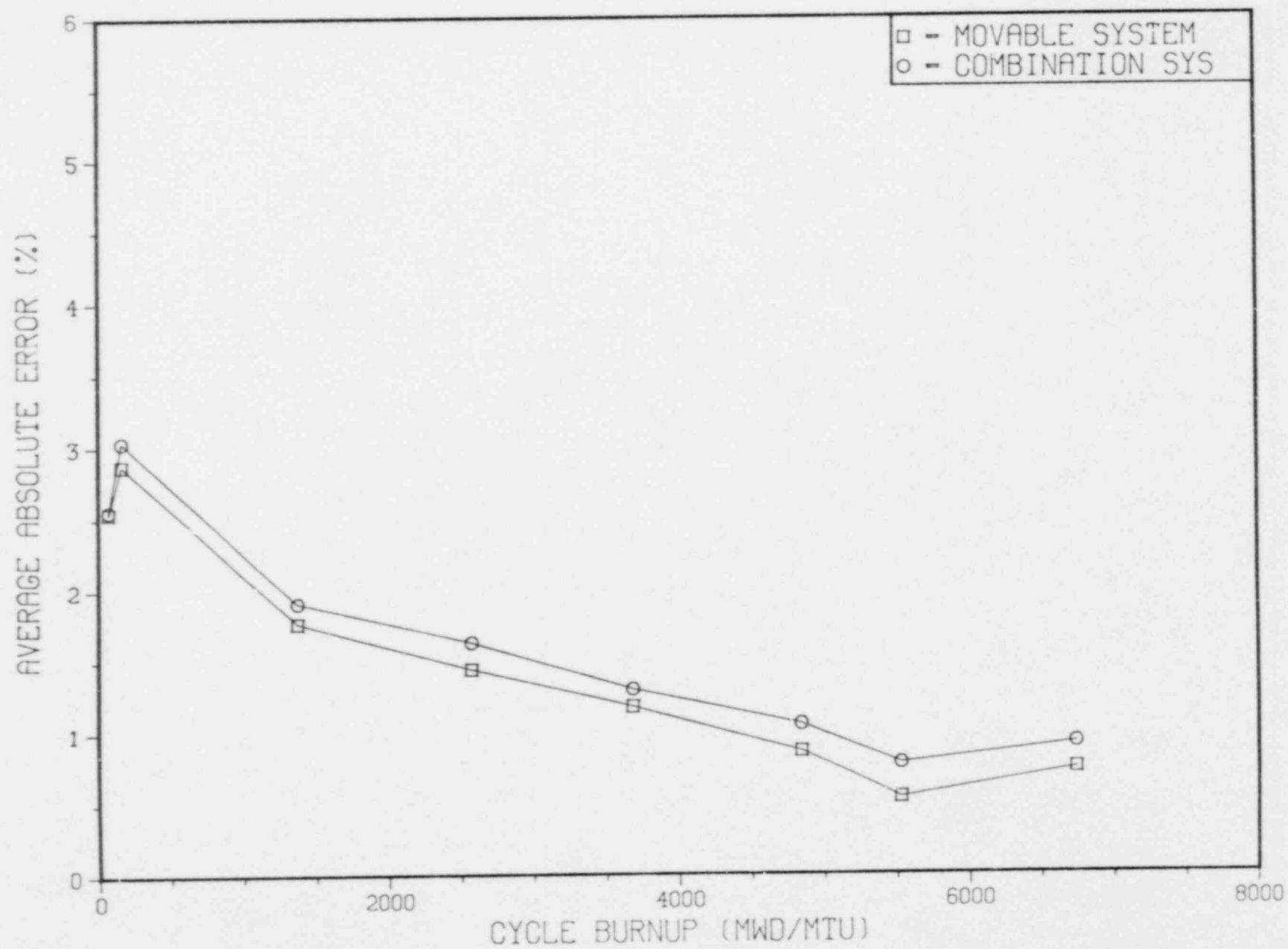


FIGURE 5-13

COMPARISON OF AVERAGE ABSOLUTE ERROR BETWEEN MEASURED
AND ANALYTICAL DATA FOR MOVABLE AND COMBINATION SYSTEMS

COMPARISON OF RMS ERROR BETWEEN MEASURED AND ANALYTICAL
DATA FOR MOVABLE AND COMBINATION SYSTEMS

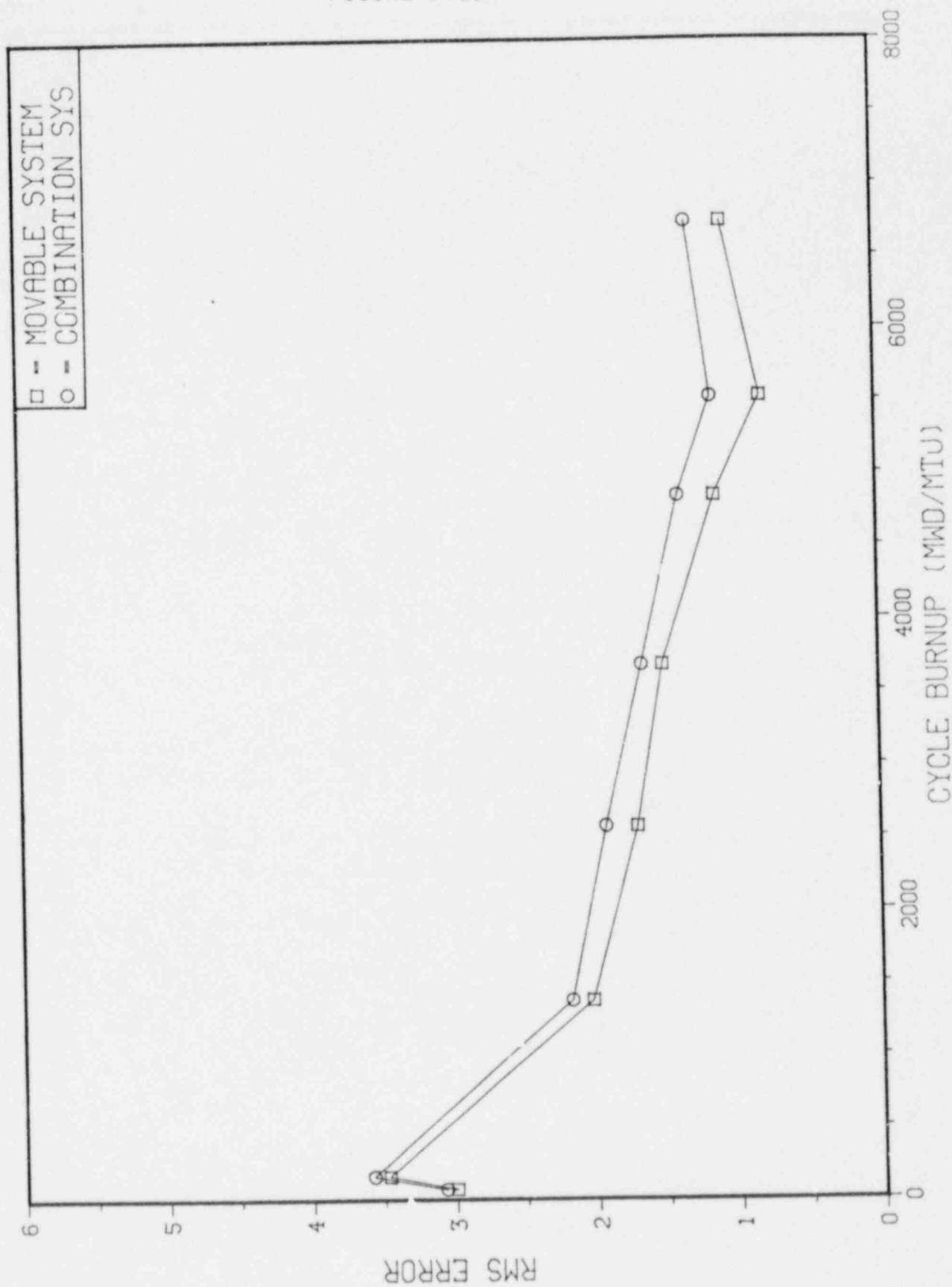


FIGURE 5-15

6.0 DETECTION OF POWER DISTRIBUTION ANOMALIES

As previously described, one function of the Incore Detection System is to aid in the detection of anomalous power distribution. The combination system proposed here enhances our ability to detect anomalous power distribution due to increased observability and greater core coverage. In a study performed by Brookhaven National Laboratory (Reference 8), it is suggested that for most perturbations, it is sufficient to consider changes in power and signals at the instrumented core location and its eight primary and secondary neighbors. For the purpose of argument here, we will consider core coverage with instrumented locations and their four primary neighbors (within one assembly pitch) only. Table 6-1 shows a comparison of the core coverage of the current MIDS, combination fixed and movable system, and the MIDS as originally designed. The combination system provides an increased detection capability versus the movable system alone. Therefore, our ability to detect core power distribution anomalies is better than previous cycles of operation where generally only 12 to 15 movable locations have been available for mapping.

In addition to the Incore Detection System, Yankee's ability to detect power distribution anomalies is supplemented by sufficient alternative means. As has been discussed in a previous submittal (Reference 4), core videotaping after refueling, start-up physics testing, an excellent analytical full core model of the Yankee core, the uniqueness of the Yankee assembly design, incore thermocouple data, excore detector signals, and loop temperature indications provide further protection from operation with any core anomalies.

TABLE 6-1

Yankee Incore Detection System
Core Coverage Summary

<u>Description (No.)</u>	<u>Total Core</u>		<u>High-Powered Assemblies</u>	
	<u>Assys/Total</u>	<u>Percent</u>	<u>Assys/Total</u>	<u>Percent</u>
Movables (12)	40/76	52.6	36/52	69.2
Combination (18)	54/76	71.1	44/52	84.6
As Designed (22)	68/76	89.5	50/52	96.2

Notes:

1. Core coverage based on instrumented location and primary neighbors.
2. High-powered assemblies defined as ≥ 1.0 relative power.

7.0 DETERMINATION OF CONTROL ROD POSITIONING

Current Yankee Technical Specification 3.1.3.2 requires that with a maximum of one primary rod position indicator channel per group inoperable; determine the position of the nonindicating rod(s) indirectly by the movable incore detectors at least once per 24 hours, and immediately after any motion of the nonindicating rod which exceeds 8" in one direction since the last determination of the rod's position. Yankee proposes that indirect determination of control rod position can be better addressed by utilizing the combination Incore Detection System versus the MIDS alone. Depending on the location of a particular control rod, we propose to use the available operable thimbles, either fixed, movable, or both, which best determines the position of a nonindicating control rod. Based on geometry alone, the closest operable thimble to a given control rod provides the best indication of that rod's position.

To qualify the ability of the FIDS to determine control rod position, a study was performed using measured data taken from routine plant operation. A monthly surveillance is performed which requires that each control rod not fully inserted shall be determined operable by moving the rod at least 4" in any one direction. During this surveillance, fixed detector data was analyzed for each of the six fixed detector strings. Figure 7-1 depicts the results of this study, and Figure 7-2 provides reference of control rod and fixed detector core locations. As can be seen, the six fixed detector strings alone are capable of detecting movement of all 24 control rods in the core. Being able to detect 4" rod movements at the top of the core, where the differential control rod worth is at a minimum, shows that the fixed detectors can determine rod movement within a specified 8" band.

The intent of determining control rod position indirectly is not based on determining the exact position of a control rod, but rather its position within a given range. Neither the Fixed or Movable System can tell you exactly where a control rod is positioned, but they can be used to determine if the control rod has moved within a given range during a specified time

interval. The movable trace represents the neutron flux at 2" intervals and provides a more detailed axial picture than the fixed detectors which represent the average over a 10" axial interval. However, the fixed detectors can provide nearly continuous flux monitoring versus the movable traces which have to be physically positioned in and out of the core at less frequent time intervals. Yankee intends to use either fixed or movable detectors, or possibly both, when making indirect determination of control rod position depending on the rod's location in the core. Generally, determination of position with the MIDS is based on some reference point where control rod position had been established. With the FIDS, since data is taken every five seconds, the establishment of a reference control rod position may be established from the history files presently kept by the DAS.

YANKEE ROWE

SIGNALS TAKEN FROM THE TOP DETECTOR ON EACH FIXED STRING
PLANT ROD MOVEMENTS OF ≥ 4 INCHES ON FEBRUARY 03, 1988

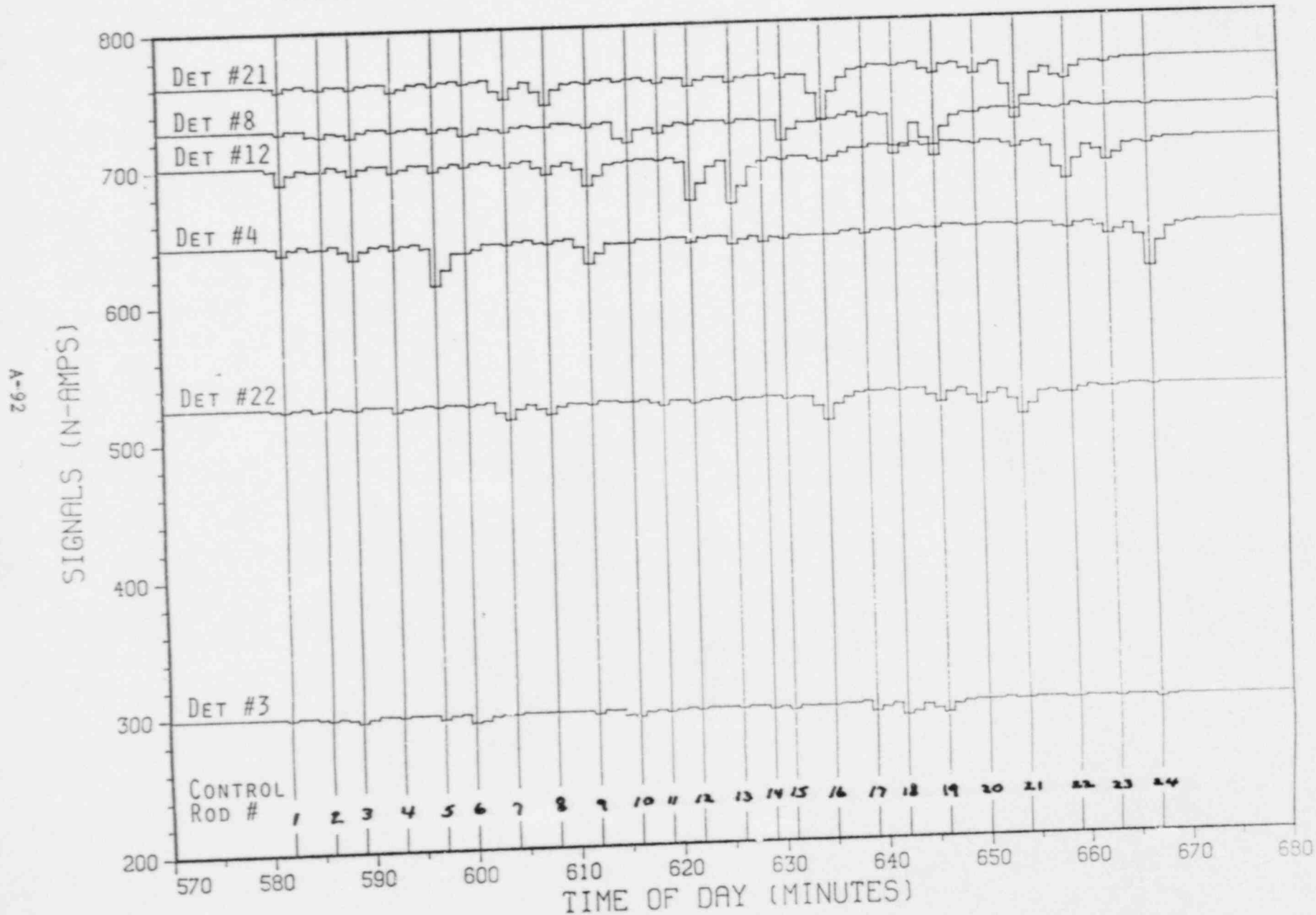
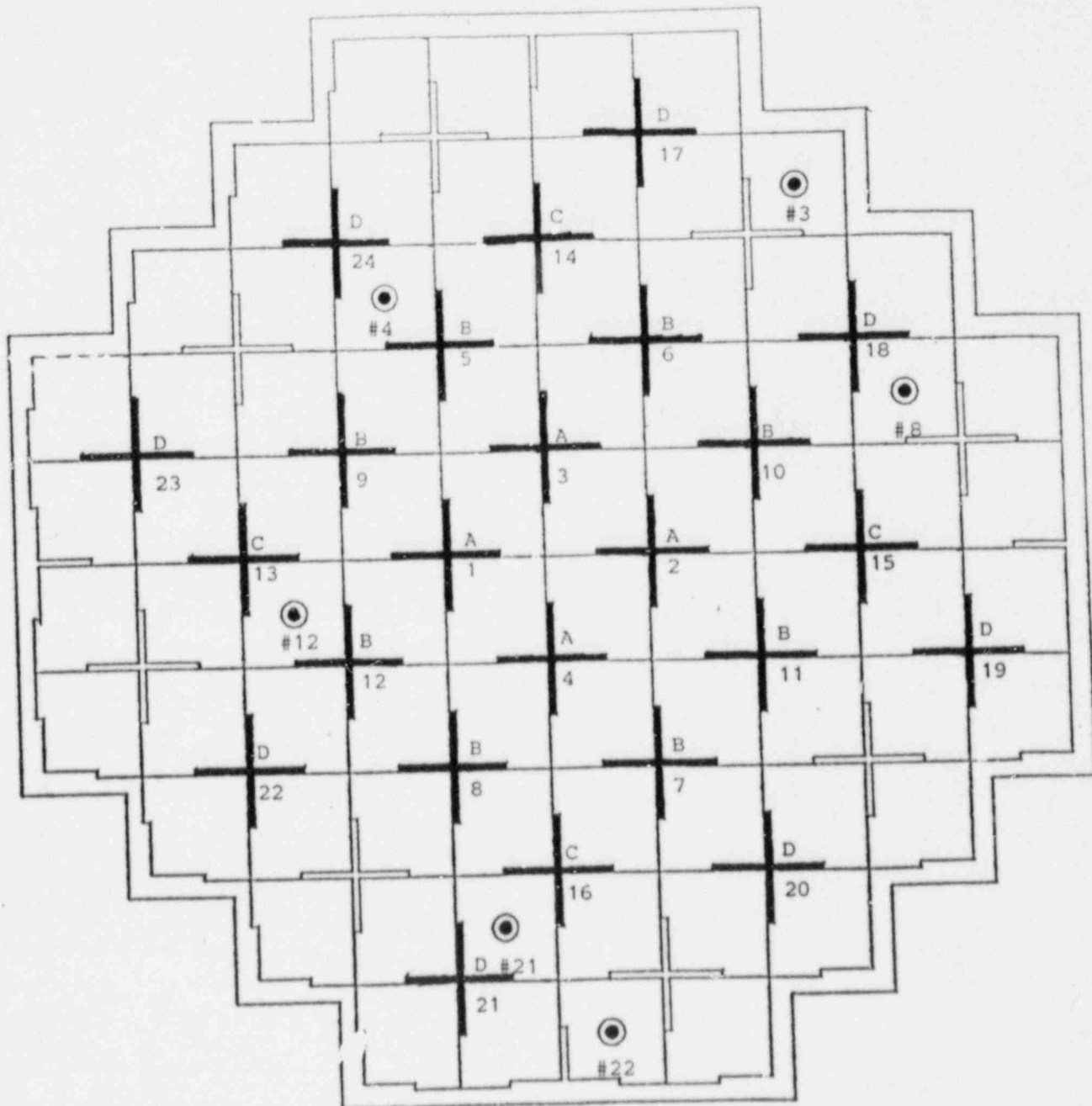


FIGURE 7-1

FIGURE 7-2

CONTROL ROD IDENTIFICATION
AND
FIXED DETECTOR LOCATIONS



8.0 INCORE DETECTION SYSTEM MEASUREMENT UNCERTAINTIES

Present Technica' Specifications require 5.0% system measurement uncertainty for ≥ 17 operable thimbles and 6.8% for < 17 and ≥ 12 operable thimbles. The 17 thimbles represent 75% of the total system of instrument thimbles. Yankee feels that the 5.0% value of measurement uncertainty is valid for the combination system with ≥ 17 operable thimbles. We believe that this value is appropriate based on the following:

1. The fixed detector data has been shown to be equivalent to the movable data, in terms of determination of the core power distribution and peaking factors, and the 5.0% value has been previously justified for ≥ 17 available movable thimbles as 4.23% for assembly powers ≥ 1.0 .
2. An evaluation of the Westinghouse MIDS measurement uncertainty performed by Westinghouse (Reference 9) has shown the overall measurement uncertainty in F_Q to be 4.58% (95/95 confidence) for a system with $\geq 75\%$ of available thimbles.
3. Babcock and Wilcox has shown (Reference 10) the measurement uncertainty for the fixed detectors to be 4.1% (95/95 confidence) even at 65% rhodium depletion (about ten calendar years).

In addition to these arguments, Yankee has other factors which contribute to supporting a 5.0% measurement uncertainty. The Yankee core is much smaller relative to other reactor cores, both axially and radially. The small core is closely coupled and minor perturbations within the core can be detected even by flux redistribution to other core locations. The Yankee core operates at base load exclusively and has no burnable poisons and virtually no control rod insertion. An excellent analytical model of the Yankee core, better than the industry average model which varies about 2.5% (Reference 8), also contributes to less uncertainty in the inferred locations which are not instrumented.

9.0 FIXED DETECTOR OPERABILITY

An analysis was performed to determine an acceptable number of fixed detector failures per string in order to define an operability requirement for the fixed detector strings. This analysis quantified the effect of detector failures on the determination of measured peaking factors. Detector failures are defined via maximum and minimum signal deviation criteria included in the DAS software. Failed detectors are substituted for by an algorithm in the DAS software provided by B&W. Substitution of failed detector data is accomplished by replacement from a preassigned fixed detector string. Substitution for failed detectors is needed to calculate power distribution and provide depletion data for the updating of the failed detector's expended charge.

The sensitivity analysis was performed for numerous failed detector replacement options based on an actual measurement (YR19209) taken during Cycle 19. When a detector signal has been declared erroneous, a replacement signal is calculated using data from another fixed detector string. The replaced signal is derived by ratioing the sum of the remaining signals from both strings and multiplying the replacement string's signal by this ratio. An example of this scheme is shown below:

	<u>Bad String</u>	<u>Replacement String</u>
Signal 1	100	200
Signal 2	-bad-	-400-
Signal 3	300	600
Signal 4	250	500
Signal 5	<u>200</u>	<u>400</u>
Sum of		
Remaining =	850	1,700
Signals		

$$\text{Replaced Signal} = \frac{850}{1,700} \times 400 = 200$$

Since the number of possible combinations of up to two failed detectors per string within the core is large, the analysis was performed on what was believed to be worst-case scenarios. Each detector string has available to it four replacement strings for the substitution algorithm. The four best replacement strings were previously determined for each of the six fixed detector strings by comparison of their measured axial shapes. When an erroneous signal has been found on a string, the B&W software calls for the first choice replacement string. If on this replacement string the replacement signal is also erroneous, the B&W software will call for the second choice replacement string. In the highly unlikely situation that all four replacement string options are rejected, a predetermined analytical axial shape would be used. The possible number of replacement options for the many combinations of failed detectors on a fixed string would lead to an analysis of immense proportions. The analysis performed consisted of finding replacement signals which deviated from the measured signal by the largest amount. The analysis consisted of failing each measured detector signal independently on a string and determining the worst replacement signal obtained from the four replacement string options. It is possible for each string to have 20 unique combinations of replacement signals assuming only one signal on that string fails. Of the possible 120 combinations of replacement signals for the six fixed strings, 24 separate cases containing only the worst replacement signal per string were analyzed with the INCORE code to determine the calculated peaking factors.

A second scenario considered the possibility that a single erroneous signal occurred on each of the six detector strings. Eight combinations were analyzed. Four cases used the worst replacement signal in the center detectors, and four cases used the worst replacement signals that would produce a top-skewed or a bottom-skewed shape with the greatest deviation from the actual shape. A top-skewed shape was created by combining the available replacement signals in such a way that the larger replacement signals were used on the top detector of the string and smaller replacement signals on the bottom detector of the string. The converse was used to produce the worst

bottom-skewed shapes. An example of a top-skewed shape produced by using the worst replacement signal on each of the six detector strings is shown below.

Assumed Failed Signals (Underlined)

<u>String</u>	<u>No. 3</u>	<u>No. 4</u>	<u>No. 8</u>	<u>No. 12</u>	<u>No. 21</u>	<u>No. 22</u>
Top	<u>211</u>	<u>529</u>	<u>618</u>	<u>561</u>	630	<u>411</u>
	627	1066	1122	1197	1094	780
	794	1229	1271	1366	1243	903
	803	1191	1211	1326	1174	867
Bottom	676	919	805	1040	<u>799</u>	586

Replaced Signals (Underlined)

<u>String</u>	<u>No. 3</u>	<u>No. 4</u>	<u>No. 8</u>	<u>No. 12</u>	<u>No. 21</u>	<u>No. 22</u>
Top	<u>424</u>	<u>644</u>	<u>644</u>	<u>721</u>	630	<u>458</u>
	627	1066	1122	1197	1094	780
	794	1229	1271	1366	1243	903
	803	1191	1211	1326	1174	867
Bottom	676	919	805	1040	<u>789</u>	586

The third scenario assumed that two failures occurred on only one of the six strings. Eighteen combinations of this scenario were analyzed. The final scenario considered assumed that two failures occurred on each of the six strings. For both of these scenarios, only the worst replacement signals were considered. The top and bottom-skewed shapes were found to produce the largest peaking factor differences from the actual measured values.

The results of the analysis are summarized in Table 9-1. The maximum deviation in $F_{\Delta H}$, F_Q , and kW/ft were found to be 0.43%, 0.61%, and 0.61%, respectively.

As shown in Figure 9-1, the measured axial shapes are similar for the six detector strings. First choice replacement signals for each detector deviated from the measured value by up to 5% in the top and bottom detectors within a string and by approximately 2% on the three center detectors of the string. The worst cases analyzed assumed top-skewed shapes in which the top replacement signal was 100% higher and the bottom replacement signal was 25% lower than the measured value. As shown in the results, these cases produced the largest deviations in the pin peaking parameters from the base case. In most instances of detector failures, the first choice replacement option would be used. However, the analysis has considered the unlikely situation of multiple detector failures in order to provide for substituted values.

An acceptance criteria of up to two failures per string to define a fixed detector string as operable is justified based on the determination of peaking factor values with up to two failed detectors per string. Any more than two failures per string would be considered unacceptable, and the fixed detector string would then be declared inoperable.

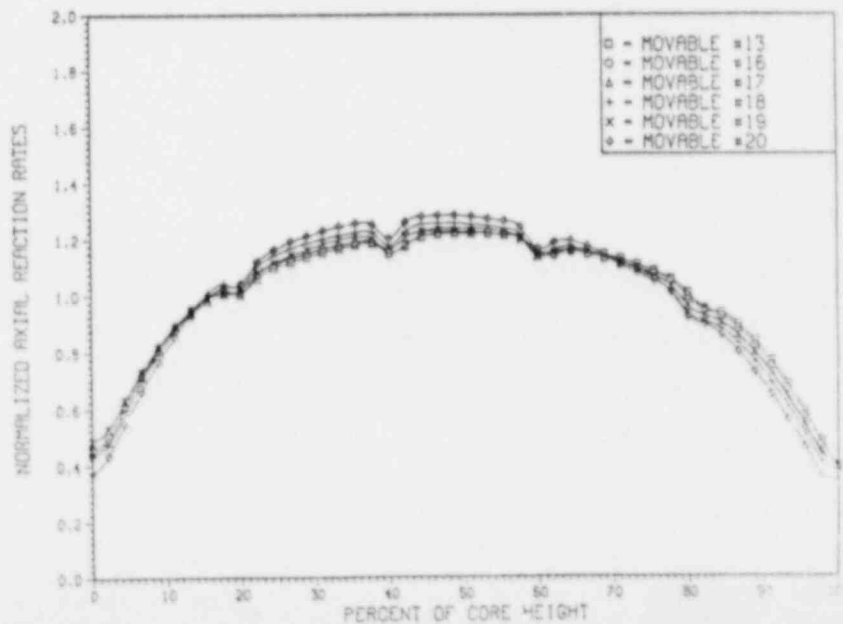
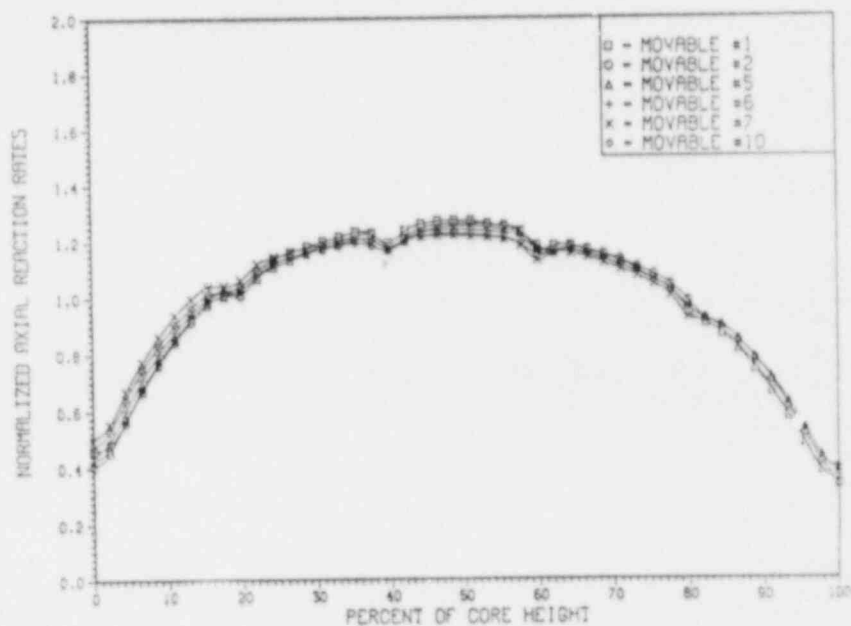
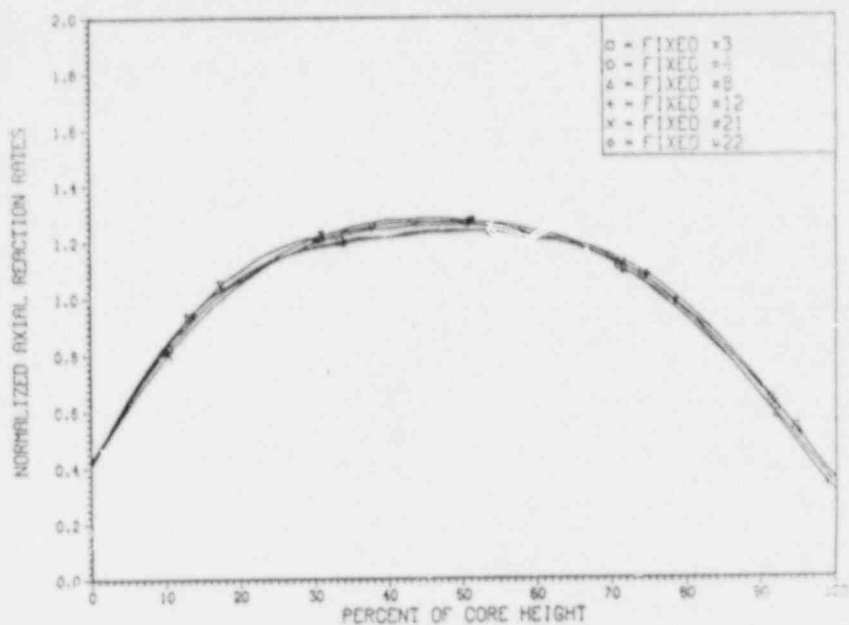
TABLE 9-1
Summary of Pin Peaking Results
Various Signal Replacement Options

	Base Case YR19209	Scenario #1		Scenario #2		Scenario #3		Scenario #4	
		1 Replacement on only 1 String		6 Replacements 1 Per String		2 Replacements on only 1 String		12 Replacements 2 Per String	
		(Min.)	(Max.)	(Min.)	(Max.)	(Min.)	(Max.)	(Min.)	(Max.)
Fresh	1.4497	1.4481	1.4526	1.4483	1.4535	1.4434	1.4540	1.4495	1.4497
FΔH									
Burnt	1.5235	1.5219	1.5248	1.5219	1.5277	1.5211	1.5279	1.5192	1.5289
Fresh	1.9621	1.9600	1.9633	1.9585	1.9684	1.9582	1.9661	1.9584	1.9719
Fq									
Burnt	2.0142	2.0120	2.0154	2.0106	2.0217	2.0102	2.0192	2.0094	2.0264
Fresh	9.514	9.504	9.520	9.496	9.544	9.495	9.538	9.496	9.562
Kw/Ft									
Burnt	9.766	9.756	9.772	9.749	9.803	9.747	9.791	9.743	9.826

Largest Deviation From Base Case (%)

	FΔH		Fq		Kw/Ft	
	Fresh	Burnt	Fresh	Burnt	Fresh	Burnt
(Min.)	-0.43	-0.28	-0.20	-0.24	-0.20	-0.24
(Max.)	0.30	0.35	0.50	0.61	0.50	0.61

FIGURE 9-1
YANKEE CORE 19 NORMALIZED RELATIVE AXIAL SHAPES
FIXED AND MOVABLE DETECTOR LOCATIONS (YH19200)



10.0 CONCLUSIONS

The use of an Incore Detection System consisting of both movable fission chambers and fixed rhodium detectors has been qualified for the Yankee plant. Detailed analysis of the cross correlation of the two detector types has been presented both theoretically and based on measured plant data. It has been shown that the fixed detectors can provide equivalent movable data for the determination of power distribution and peaking factors in the Yankee core. Demonstration of the accuracy of the radial and axial components of measured power distributions has been provided via comparison to the movable data. The combination FIDS and MIDS has been shown to provide greater measurement observability, increased core coverage, and greater effectiveness for detection of core anomalies and mispositioned control rods than the MIDS alone. The operability of the fixed detector strings has also been defined based on the analysis of measured peaking factors with failed detectors. Finally, the combination Incore Detection System provides an enhancement over the MIDS alone due to the continuous monitoring capability of the fixed detectors. The fixed detectors can be used to provide data of previous core operation to establish a reference point for change or may be used to monitor core flux changes on a continuous basis.

11.0 REFERENCES

1. Letter, USNRC to Yankee Atomic Electric Company, "SER for Amendment No. 53," November 24, 1978.
2. Letter, USNRC to Yankee Atomic Electric Company, "SER for Amendment No. 72," March 8, 1982.
3. Letter, USNRC to Yankee Atomic Electric Company, "SER for Amendment No. 100," December 1, 1986.
4. Letter, USNRC to Yankee Atomic Electric Company, "SER for Amendment No. 106," June 26, 1987.
5. WCAP-7149, "The INCORE Code," W. D. LaGett and L. D. Eisenhart, December 1967.
6. "Calibration of Self-Powered Neutron Detectors," M. F. Sulcoski and H. D. Warren, Nuclear Science and Engineering, 85, 245-250 (1983).
7. "CASMO-3, A Fuel Assembly Burnup Program," Malte Edenius, et al., Studsvik Energiteknik A. B., November 1986.
8. Memorandum, P. Neogy and A. Prince (BNL) to J. Carew (BNL), "Impact of Failed Detectors on the Measurement of Anomalous Power Distributions," August 8, 1986.
9. WCAP-7810, "Evaluation of Nuclear Hot Channel Factor Uncertainties," December 1971.
10. Babcock and Wilcox Technical Document 12-1137521, "Fixed Incore System Benefits," October 11, 1982.